1-1-2017

Dynamic Fluctuations From Hydrodynamics And Kinetic Theory In High Energy Collisions

Christopher David Zin
Wayne State University,

DYNAMIC FLUCTUATIONS FROM HYDRODYNAMICS AND KINETIC THEORY IN HIGH ENERGY COLLISIONS

by

CHRISTOPHER ZIN

DISSERTATION

Submitted to the Graduate School

of Wayne State University,

Detroit, Michigan

in partial fulfillment of the requirements

for the degree of

DOCTOR OF PHILOSOPHY

2017

MAJOR: Physics

Approved By:

_____

Advisor Date

_____

_____

_____

_____

DEDICATION

To my family, whose consistent love and support will always form the fundamental constituents of my success.

ACKNOWLEDGMENTS

Education is a lifelong process that begins day one. As with many other facets of life, one gains a significant advantage by having a strong foundation. Therefore, it is first and foremost that I would like to thank my parents. Without their guidance none of this would have been possible. In addition, as one's character is shaped by those who surround him or her, I would also like to extend special thanks to all of my family and friends.

Education is also instruction, motivation, discussion and distraction. I feel lucky to have had an advisor that provides all of these. Sean's commitment to his students goes well beyond that expected of a professor and for this I cannot thank him enough. If my students are fortunate, I will pass his influence and teachings on to them. Apparently education also involves a lot of talk about Star Trek, for which I can also thank Sean.

The members of my committee deserve special thanks for taking the time to help further my career. While this group could have been selected solely on qualifications, I chose them based on the impressions they made on me during my first years in grad school. No less thanks go to Sergei, Joern, Gil and Abhijit who have each played a unique and meaningful role in my advancement. George deserves my utmost recognition for his part in all of this work.

The office staff deserves far more credit than they often receive. Theirs is a job I do not envy - dealing with the rest of us. In particular, I thank De, Shere and Janice for all the help they've given me throughout the years. I also wish to thank our late custodian Kenny whose morning chats helped brighten almost any day, and because those who are gone should not be forgotten.

Along these lines, I extend the deepest gratitude to Jim Veneri. As anyone who knew him is aware, Jim was always looking out for his kids, and Southpaw was no exception. His Mathematics Resource Center was my home during my undergraduate years and, furthermore, it was his love for physics that encouraged me to join the program. One day, I hope that his goal of bringing closer the math and physics departments is realized.

Recognition goes to my friends in physics, who each made the journey a little bit easier. Ehab and Khadije, who have been with me from the start, as well as Doaa who joined shortly thereafter. Chiara, for exchanging one word each day and for lending an ear on days when one word wasn't enough. Jinjin, Victoria, Kolja, and Rachael with whom I've shared many a drink. Abir and Raj for all the lunches and chats. Jocelyn, Mackenzie and a peculiar mention to the NZ rugby team for their haka - a dance whose name is difficult enough to remember that it can provide a laugh. Fortunately, I have met far too many friends and colleagues to list all those who deserve recognition but know that you are all appreciated. More generally, I would like to thank every member of the faculty and staff in the physics department at WSU. I cannot think of a single person who did not help contribute to making my time here a positive experience.

Recently, it seems especially important to make college a positive experience. We should strive to continue making education attainable and desirable, for the lives we impact and the knowledge we impart is not limited to those in our classrooms but spreads throughout our community. Those who disregard science, and higher education in general, seem to have gained a foothold at all levels of society - including the federal government. Notably, the current executive branch is proving daily that nescience is, in fact, an antonym of science. While many generations may feel they can lay claim to this sentiment, recent election results serve as a strong indicator that it is worse than ever.

As scientists and educators, I know that many of us feel inclined to stay away from politics but in recent months we have demonstrated our concern. The March for Science took place on April 22, 2017 with an estimated global attendance of over one million people, including thousands in Detroit alone. These numbers are statistically significant by any meaningful measure! I truly believe this backward era to be short-lived but it is critical that we continue to confront the voices of disregard until we hear nothing but the rain.

$\sim$ *Chris*

TABLE OF CONTENTS

LIST OF FIGURES

CHAPTER 1 INTRODUCTION

The importance of studying correlations and fluctuations in high energy ion collisions has been known for decades. This has never been more apparent than in recent years where these measurements helped mark the discovery of Quark-Gluon Plasma (QGP) [13–15]. The many different types of correlations present in ion collisions can provide us with valuable knowledge regarding microscopic interactions inside this high density medium. In particular, the non-perturbative aspects of the strong interaction are difficult to study experimentally and probing the hot and dense QGP is one of the few avenues we have available.

The general outline of this thesis is as follows. We begin with a discussion motivating the study of the thermalization process in heavy ion collisions and, more importantly, pA and high multiplicity pp collisions. In Chapter 2 we review some theoretical background concepts useful to our work. Chapter 3 details the application of Langevin noise to problems relevant in ion physics and serves as an example of the more intricate usage of noise in the following chapters. We extend these examples in Chapters 4 and 5 where we incorporate noise into relativistic hydrodynamics and kinetic theory, respectively. In these chapters we define functions that measure correlations above equilibrium in order to study the thermalization process. In Chapter 6 we introduce fluctuation observables that probe targeted aspects of ion collisions and provide a connection to the correlation functions from previous chapters. Chapter 7 is a phenomenological illustration of our partial thermalization model. We compare to experiment and make predictions surrounding the observable consequences of equilibration.

1.1 Motivation

Heavy ion collision systems contain a range of effects that can be attributed to a QGP undergoing hydrodynamic expansion. Measurements of the azimuthal anisotropy of particle distributions provide broad support for the hydrodynamic description of these large systems [16]. One studies this anisotropy using the harmonic coefficients v_n defined in the Fourier

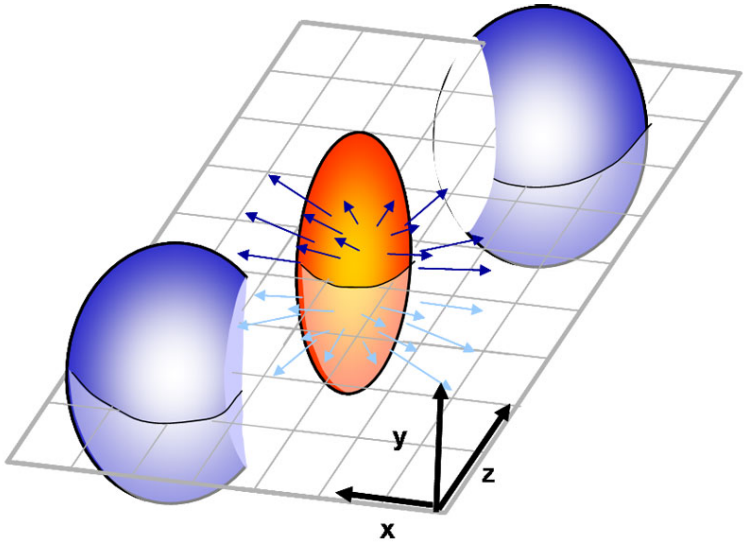

Figure 1.1: A cartoon depicting the production of anisotropic flow in a peripheral heavy ion collision. The x-z plane defines the reaction plane. The centrality of the collision is a measure of how much the ions overlap in the x-direction. Source: ioppweb

expansion of the particle distribution

$$\frac{1}{N}\frac{dN}{d\phi} = 1 + 2v_1\cos(\phi - \Psi_{RP}) + 2v_2\cos[2(\phi - \Psi_{RP})] + \cdots \tag{1.1}$$

for the angle azimuthal with respect to the beam direction ϕ, and the angle determining the reaction plane Ψ_{RP} as defined in Fig. 1.1. The coefficients are given by

$$v_n = \langle\cos[n(\phi - \Psi_{RP})]\rangle, \tag{1.2}$$

where $\langle\cdots\rangle$ represents an average of an ensemble of events. Altogether, these coefficients describe the transverse shape of the collision volume and, in particular, elliptic flow is measured with v_2. The ellipsoidal anisotropy typical of v_2 is shown by the almond shape in Fig. 1.1.

Experimental measurements of v_2 are shown in Fig. 1.2. The left figure depicts elliptic flow over a wide range of collisional energies, showing a consistent increase in v_2 with increasing energy. The figure on the right shows v_2 as a function of centrality (as defined in Fig. 1.1)

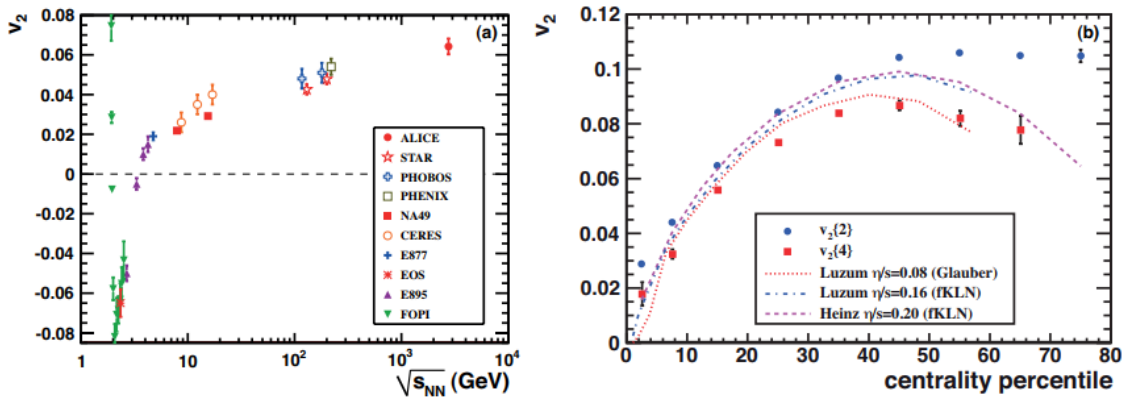

Figure 1.2: a) Integrated elliptic flow compared at a wide range of energies, from Ref. [1]. b) Elliptic flow as a function of centrality compared to viscous hydrodynamic model calculations, from Ref. [2].

as measured by the ALICE experiment[1]. Also shown are theory curves from hydrodynamic calculations. The closeness of these curves to data in the central region demonstrates the applicability of hydrodynamics to these collisions. Notably, the hydrodynamic models differ from data in the most peripheral region.

Figure 1.3 shows more examples of hydrodynamical models compared to data, this time to particle spectra. The top left figure shows the models fitting quite well to data in the most central bin over the entire range of transverse momentum. The other figures include more peripheral bins. Again, we see model deviation from data in the most peripheral region.

One of the goals of this thesis is to offer an explanation of this behavior. Hydrodynamics is applicable when the system under consideration is in local equilibrium. Data indicates that the large central collision systems have enough time for particle scattering to thermalize the system. Peripheral collisions result in less dense and shorter lived systems that may not be able to reach a state of complete equilibration. Evidence of incomplete thermalization of data motivates our work.

More intriguing, however, are the recent measurements of similar anisotropy in pA and high multiplicity pp collisions [6, 17–21]. An example of one such measurement is shown

[1]The data points are cumulants of v_2, measured using two (circles) and four (squares) particle correlations.

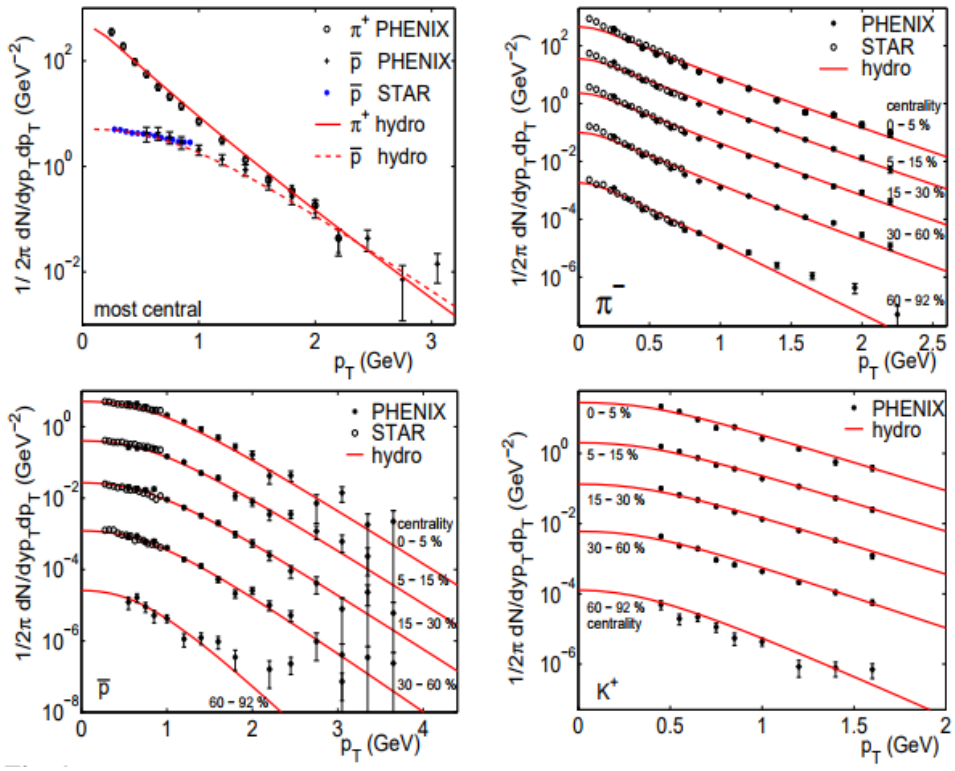

Figure 1.3: Symbols show single particle p_t-spectra measured in Au+Au collisions at RHIC. Curves show hydrodynamic model calculations. PHENIX and STAR data are from Refs. [3] and [4], respectively. Curves and figure are from Ref. [5].

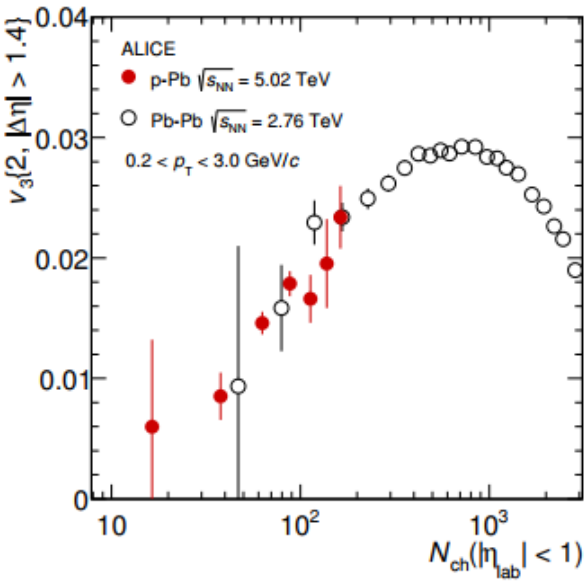

Figure 1.4: Third harmonic flow coefficient in p-Pb and Pb-Pb collisions. From Ref. [6].

in Fig. 1.4, comparing the third harmonic v_3 in p-Pb to Pb-Pb collisions using the same kinematic cuts. The similar magnitudes reported lead one to believe that these azimuthal correlations are, indeed, flow-like. This implies that there is, at least, some degree of thermalization present in these small systems. This raises profound questions about the onset of collective flow and its relation to hydrodynamics.

As an illustrative application, we study transverse momentum fluctuations, long argued to be a probe of thermalization [22]. These fluctuations now have a wide body of data available for comparison. Data distinctly depart from equilibrium expectations in peripheral heavy ion collisions at RHIC and LHC [23]. We argue that measurements of pA collisions can help determine whether these systems are indeed thermal.

CHAPTER 2 BACKGROUND

In this chapter we review some background information that will be useful throughout the rest of this text. We start with a simple description of an ion collision to help define a few terms. The two ions approach each other along the beam direction, also called the longitudinal direction, which defines the z-axis. The directions transverse to the beam are then the x- and y-axes. One ion is designated the projectile and the other the target (for non-fixed target colliders, the choice can be done arbitrarily). When the two ions collide, it is actually the constituent nucleons of the ions colliding. Those nucleons that do collide are called participants, while those that do not are called spectators. Participants contribute to the formation of the collision system and spectators continue on while leaving little trace of their existence. The impact parameter $\mathbf{b}$ is the transverse distance between the centers of the two nuclei. Figure 2.1 demonstrates this for peripheral ($b \approx R_A$) and central ($b \approx 0$) collisions.

Throughout the rest of this work we will be using natural units such that $c = \hbar = k_B = 1$. Furthermore, Greek letters denote space and time components ($\mu, \nu, \ldots = 0, 1, 2, 3$), while Latin letters denote only spatial components ($i, j, \ldots = 1, 2, 3$). Four-vectors are always given a Greek index, while three-vectors either have a Latin index or are written in bold text. We also make use of Einstein summation notation.

2.1 Kinematic variables

In this section we review some kinematic variables useful to the study of relativistic ion collision. They are designed in such a way that they transform simply under Lorentz boosts. Furthermore, they provide a number of convenient identities that allow for easier calculations. We make use of the position and momentum four-vectors given as

$$x^\mu = (t, x, y, z) \qquad \text{and} \qquad p^\mu = (E, p_x, p_y, p_z)\,, \tag{2.1}$$

and we use the spacetime metric $g^{\mu\nu} = \mathrm{diag}(1, -1, -1, -1)$.

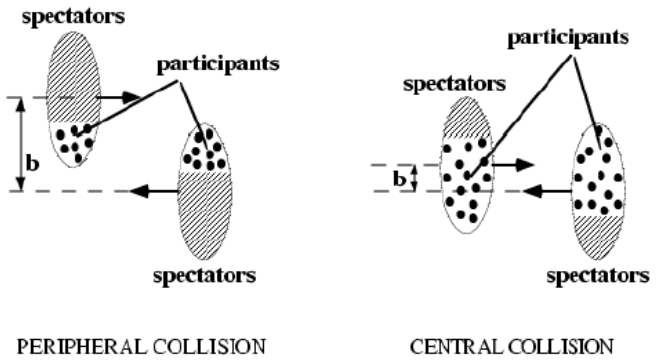

Figure 2.1: A schematic diagram of a heavy ion collision in the transverse plane. Participants and spectators are shown in peripheral and central collisions.

The rapidity of a particle is defined as

$$y = \frac{1}{2} \ln \frac{E + p_z}{E - p_z} = \frac{1}{2} \ln \frac{1 + v_z}{1 - v_z}, \tag{2.2}$$

where the second equality follows from $v_z = p_z/E$. Rapidity can be thought of as another expression of the longitudinal velocity of a particle. In some ways, it behaves more naturally than velocity at relativistic speeds. Firstly, rapidity can take on values from $-\infty$ to ∞, as one expects of the velocity in a non-relativistic context. Secondly, rapidity is additive under boosts of the coordinate system as, again, is familiar at non-relativistic speeds. The inverse transformations to (2.2) are given by

$$E = m_t \cosh y \qquad \text{and} \qquad p_z = m_t \sinh y, \tag{2.3}$$

where the transverse mass is $m_t = \sqrt{E^2 - p_z^2} = \sqrt{m^2 + p_t^2}$ for the transverse momentum $p_t = \sqrt{p_x^2 + p_y^2}$.

The usefulness of rapidity to describe velocity makes one desire a similar variable for

spacetime. Thus, we are led to define the spatial rapidity[1]

$$\eta = \frac{1}{2} \ln \frac{t+z}{t-z}. \tag{2.4}$$

Spatial rapidity is often paired with the proper time

$$\tau = \sqrt{t^2 - z^2}. \tag{2.5}$$

Together, these two allow us to define a new coordinate system via the transformation

$$(t, x, y, z) \to (\tau, x, y, \eta)\,. \tag{2.6}$$

This coordinate system is often called Milne coordinates or, simply, proper time and rapidity coordinates. A volume element transforms to the new system as

$$d^4x = \tau d\tau d\eta d^2x_\perp, \tag{2.7}$$

which can be easily verified by calculating the Jacobian of the transformation using (2.4) and (2.5). The inverse transformation is given by

$$t = \tau \cosh \eta \qquad \text{and} \qquad z = \tau \sinh \eta. \tag{2.8}$$

In a spacetime diagram, as in Fig. 2.2, contours of constant spatial rapidity are lines through the origin with slope $t/z = \coth \eta$. Contours of constant proper time are hyperbolas asymptotic to the forward and backward light cones defined by the equation $t = \pm\sqrt{z^2 + \tau^2}$. This diagram allows us a deeper understanding of the Milne coordinate system. In Cartesian coordinates, suppose we choose two points on the z-axis. After any amount of time t has

[1]We wish to try to preempt any confusion regarding the two rapidities while moving forward in the text. When referring to the spatial rapidity we sometimes just say "rapidity", however, the spatial rapidity is always denoted by η.

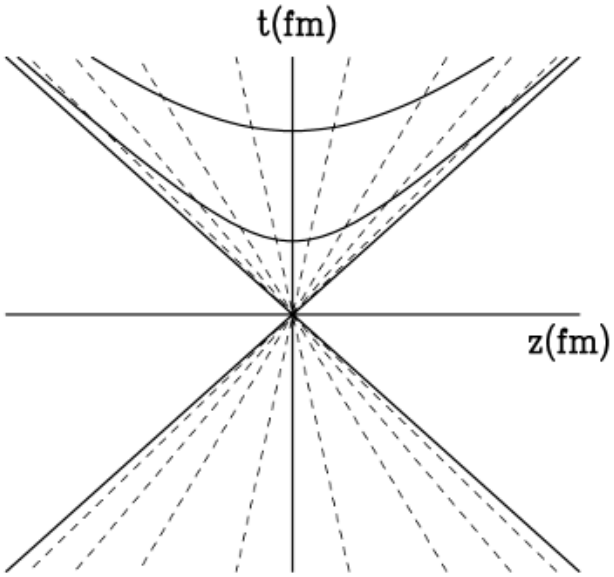

Figure 2.2: A spacetime diagram depicting hyperbolas of constant proper time and lines of constant rapidity. The light cone is located at $\eta = \pm\infty$.

elapsed the distance between these points remains unchanged. Now we repeat this for the spatial rapidity by choosing two contours in Fig. 2.2. At early times t_1, these contours are close together (in Cartesian terms). However, at later times t_2 they grow distant, even though we have followed the same "points" through time. It is in this way that Milne coordinates describe an expanding spacetime, an idea closely related to the material in the next section.

In general there need not be any relation between rapidity and spatial rapidity. However, in the case that particles are moving at speed $v_z = z/t$, the two rapidities are equal:

$$\eta = \frac{1}{2}\ln\frac{1+z/t}{1-z/t} = \frac{1}{2}\ln\frac{1+v_z}{1-v_z} = y. \tag{2.9}$$

Note that rapidity describes the velocity of a particle, while the spatial rapidity describes the position of the particle. Thus, we see that in this curious case, there is a significant correlation between velocity and position. This idea is also closely related to the material in the next section. We shall also make use of the following Lorentz factor identity applicable

to this situation:

$$\gamma = \frac{1}{\sqrt{1 - z^2/t^2}} = \frac{1}{\sqrt{1 - \sinh^2\eta/\cosh^2\eta}} = \cosh\eta, \tag{2.10}$$

found using $\cosh^2\eta - \sinh^2\eta = 1$.

We note that in experiment it is comparatively easy to measure the momentum rather than the energy of a particle. A more useful variable for experimentalists is the pseudorapidity given by

$$\eta_p = -\ln[\tan(\theta/2)] \tag{2.11}$$

where θ is the angle with which a particle emerges from the collision measured relative to the beam axis. One can also write the pseudorapidity as

$$\eta_p = \frac{1}{2}\ln\frac{|\mathbf{p}| + p_z}{|\mathbf{p}| - p_z} \tag{2.12}$$

which clarifies its relation to the rapidity. The relation is even more obvious at large p_z where the two quantities are nearly identical $y \approx \eta_p$. Pseudorapidity is often denoted with the symbol η in the literature, however, for our purposes it is more convenient to allow the spatial rapidity to have its own distinct letter.

Finally, a quick word on the center of mass energy of a collision. For two scattered particles with incoming momenta $\mathbf{p}_1$ and $\mathbf{p}_2$ and outgoing momenta $\mathbf{p}_3$ and $\mathbf{p}_4$, the Mandelstam variable s is defined as

$$s = (\mathbf{p}_1 + \mathbf{p}_2)^2 = (\mathbf{p}_3 + \mathbf{p}_4)^2. \tag{2.13}$$

The total collision energy is then given by $\sqrt{s}$ and this value is often used to denote the strength of a collision – e.g. a Pb+Pb collision at $\sqrt{s} = 2760$ GeV.

2.2 Longitudinal invariance and Bjorken expansion

Theoretical calculations in heavy ion physics can be difficult and often implausible without making some simplifying assumptions. To describe the hydrodynamic expansion of the

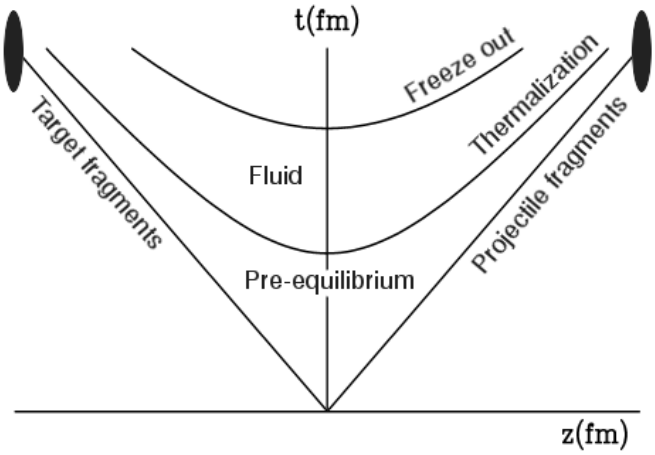

Figure 2.3: The stages of a nuclear collision undergoing Bjorken expansion. Hyperbolas are curves of constant proper time that indicate when the system moves to a new stage.

fluid following a collision, for instance, one needs to specify the equation of state, energy density, pressure, fluid four-velocity and any transport coefficients under consideration. None of these quantities are known from first principles so we generally employ a variety of models to allow for a deeper understanding of the underlying physics. We make a number of our own simplifying assumptions in the following chapters but an especially common model is Bjorken's approach to longitudinal boost-invariance, which we describe here.

One starts by assuming the following description of a nucleus-nucleus collision, as shown in Fig. 2.3. Due to their high speeds, the two approaching nuclei are Lorentz contracted into two-dimensional nuclear pancakes. After the pancakes collide they pass through each other, depositing energy in the region near $z = 0$ at time $t = 0$. Particle production for the entire system begins at an initial proper time τ_0 (hyperbola not depicted). The system is in a state of pre-equilibrium until thermalization occurs and the quark-gluon plasma is formed. Finally, after a period of hydrodynamic expansion and cooling (during which hadronization occurs), all interactions between particles cease and the system freezes out at a final proper time τ_F. Bjorken's basic assumption of longitudinal invariance is that "throughout the 'central-plateau' region[2] the initial conditions – imposed a proper time ~ 1 fm/c after the collision

[2]The central-plateau region refers to the flat region near the center of the particle distribution viewed as a function of rapidity. This is seen fairly well in experiment, see Refs. [24, 25].

time – are invariant with respect to Lorentz transformations" [26].

The initial expansion of the fluid is assumed to be only in the longitudinal direction so that particles have transverse velocity $v_t = 0$. The longitudinal velocity of particles is assumed to have a specific scaling profile: after a time t, particles at a distance z from the point of collision have velocity $v_z = z/t$. One-dimensional expansion is expected to be a good approximation for a short time after the collision and we expect three-dimensional expansion to occur once the time elapsed is approximately equal to the radius of the nuclei $t \approx 1.2A^{1/3} \approx 7$ fm. This approximation is most appropriate at high energies ($\sqrt{s} > 100$ GeV), near central rapidity ($\eta \approx 0$) and near the transverse center of the collision system.

By changing to the proper time $\tau = \sqrt{t^2 - z^2}$ and spatial rapidity $\eta = (1/2)\ln[(t+z)/(t-z)]$ we see the benefit of this model. In this coordinate system, the four-velocity of particles becomes

$$u^\mu = \gamma\left(1, 0, 0, \frac{z}{t}\right) \qquad \Rightarrow \qquad u^\mu = \left(\frac{t}{\tau}, 0, 0, \frac{z}{\tau}\right), \tag{2.14}$$

using the identities in Sec. 2.1. Then,

$$u^\eta = \frac{\partial \eta}{\partial \tau} = \frac{\partial t}{\partial \tau}\frac{\partial \eta}{\partial t} + \frac{\partial z}{\partial \tau}\frac{\partial \eta}{\partial z} = u^t\left(\frac{-z}{\tau^2}\right) + u^z\left(\frac{t}{\tau^2}\right) = 0, \tag{2.15}$$

using u^t and u^z from (2.14). Since the velocity on the η-axis vanishes and the initial conditions are assumed to be independent of η (from Bjorken's assumption), all quantities – e, p, etc. – are independent of η and unchanged under Lorentz boosts. Thus, a fluid undergoing Bjorken expansion is longitudinally invariant.

As an example of the simplicity offered by this model, we use it to quickly find a few equations for the evolution of some of the thermodynamic variables of an expanding Bjorken system. To do this, we use two convenient identities,

$$\partial_\mu u^\mu = 1/\tau \qquad \text{and} \qquad u^\mu \partial_\mu = \partial/\partial\tau \tag{2.16}$$

which one can easily verify. Then using conservation of energy-momentum $\partial_\mu T^{\mu\nu}_{id} = 0$ for the stress-energy tensor of an ideal gas $T^{\mu\nu}_{id} = (e+p)u^\mu u^\nu - pg^{\mu\nu}$ we have

$$\begin{aligned} 0 &= u_\nu \partial_\mu T^{\mu\nu}_{id} \\ &= \left[\partial_\mu (e+p)\right] u^\mu + (e+p)\left[\partial_\mu u^\mu\right] + (e+p)u^\mu \left[u_\nu \partial_\mu u^\nu\right] - u^\mu \partial_\mu p \\ &= \frac{\partial}{\partial\tau}(e+p) + \frac{e+p}{\tau} + 0 - \frac{\partial}{\partial\tau}p \\ &= \frac{\partial e}{\partial\tau} + \frac{e+p}{\tau}, \end{aligned} \tag{2.17}$$

where we used the identity $u_\nu \partial_\mu u^\nu = \frac{1}{2}\partial_\mu (u_\nu u^\nu) = \frac{1}{2}\partial_\mu 1 = 0$. Taking this one step further, we can apply the first law of thermodynamics in the form $de = Tds + \mu dn$ and the enthalpy relation $e + p = Ts + \mu n$ we find

$$\begin{aligned} 0 &= T\left(\frac{\partial s}{\partial\tau} + \frac{s}{\tau}\right) + \mu\left(\frac{\partial n}{\partial\tau} + \frac{n}{\tau}\right) \\ &= T\partial_\nu s^\nu + \mu\partial_\nu n^\nu, \end{aligned} \tag{2.18}$$

where we have identified the entropy and particle currents as $s^\nu = su^\nu$ and $n^\nu = nu^\nu$, respectively. Conservation of the particle current implies $\partial_\nu n^\nu = 0$, so that (2.18) implies $\partial_\nu s^\nu = 0$, and we have

$$\frac{\partial s}{\partial\tau} + \frac{s}{\tau} = 0 \qquad \text{and} \qquad \frac{\partial n}{\partial\tau} + \frac{n}{\tau} = 0. \tag{2.19}$$

Thus, we see that in the Bjorken model both entropy and particle density decrease as the inverse of the proper time via $s = s_0\tau_0/\tau$ and $n = n_0\tau_0/\tau$. While these equations only hold for an ideal fluid undergoing Bjorken expansion, we will find them to be adequate for approximations later on.

2.3 Blast wave model

The transverse expansion of the collision volume is one of the most widely studied aspects of heavy ion collisions. Experimental measurements of the azimuthal anisotropy have provided conclusive evidence that the expansion of the thermalized system can by described

hydrodynamically [16]. While a full hydrodynamic description would be ideal, it is also often intractable. In addition to the reasons mentioned in Sec. 2.2, hydrodynamical simulations need to run many (perhaps millions) of events in order to gain the statistics needed to answer the questions we address in this thesis. We therefore turn to a simplified model of transverse expansion known as the blast wave model.

The basic idea of the blast wave model is as follows. After the formation time, the collision volume consists of a dense medium of particles with random transverse motion. Outgoing particles on the outermost layer of this volume will move away from the center, while ingoing particles will scatter off the particles in subsequent layers. This results in the surface layer expanding outward into the vacuum with an average velocity in the transverse direction. Initially, the second outermost layer of particles will scatter off the particles in subsequent layers as well as off the particles in the outermost layer. However, as the surface layer expands it becomes more diffuse allowing the second layer to expand. Evolution of the system continues on in this manner until freeze out.

The blast wave model is convenient for its simplicity. It makes the assumptions that particles are locally thermalized at a freeze out temperature and that they are moving outward with a collective transverse velocity gradient. In this way, it describes transverse expansion with two parameters: β the blast wave surface velocity, and T the freeze out temperature. Despite its simplicity it decently describes elliptic flow and transverse momentum spectra [23, 27, 28]. However, it also suffers from its simplicity. The blast wave model contains no information about the underlying particle production mechanism, perturbative QCD processes, hadronization, resonance decay, etc. As such, jet effects are beyond its reach and instead, the blast wave model seeks to describe soft processes. Final multiplicity, too, cannot be predicted and the magnitude of the particle distribution is normalized to data. Nevertheless, it remains a convenient tool in our studies. The version of the blast wave we apply here was used in Ref. [23]. It is summarized in the following paragraphs.

The pressure gradient due to the anisotropy in density cause the outward expansion of

the system. It is largest near the surface of the system so particles on the outermost layer receive the largest boost. The gradient decreases as we move inward so that particles near the center of the system receive a smaller push. Thus, we assume a Hubble-like expansion wherein the velocity of particles depends on their initial radial position

$$\gamma_t \mathbf{v}_t = \lambda \mathbf{r} \tag{2.20}$$

where $\mathbf{r}$ is the radial vector pointing to the location of the particle, γ_t is a transverse boost factor and λ is a constant dictating the rate of expansion.

We assume particles freeze out at a constant proper time τ_F, defined in (5.11), as in the Bjorken model. Particles with larger rapidity will then freeze out at a later time t than those with a smaller rapidity, as determined by the slopes of the lines in Fig. 2.2. The blast wave model seeks to describe the momentum distribution of particles on the freeze out surface σ determined by τ_F. To accomplish this we use the Cooper-Frye formula [29] given as

$$E\frac{dN}{d^3p} = \int_\sigma f(\mathbf{x}, \mathbf{p}) p^\mu d\sigma_\mu. \tag{2.21}$$

The differential surface element $d\sigma_\mu$ is defined as an outward pointing four-vector perpendicular to the surface σ, f is the phase-space density of particles, and the integral is taken over the freeze out surface. We choose f, following [30], to be a Boltzmann distribution boosted by the fluid velocity u^μ:

$$f(\mathbf{x}, \mathbf{p}) = ae^{-u^\mu p_\mu / T}, \tag{2.22}$$

where a is set by normalization. That we may use a Boltzmann distribution in place of a Fermi-Dirac or Bose-Einstein distribution is due to the fact that most hadrons are heavy enough to be treated as classical particles. Experimental results backing up this claim can be found in Refs. [31, 32]. We can then use this distribution to calculate observable quantities

such as

$$\frac{dN}{dy} = \int E \frac{dN}{d^3p} p_t dp_t d\phi \tag{2.23}$$

$$\langle p_t \rangle = \frac{1}{\langle N \rangle} \int p_t E \frac{dN}{d^3p} d^3p. \tag{2.24}$$

Our interest in the blast wave model is mainly to calculate the value of observables in local equilibrium, done in Chapter 7. We use it in place of more sophisticated models for its accessibility but we also find it very suitable to our needs. Full details and features of this model can be found in Ref. [33].

CHAPTER 3 STOCHASTIC PROCESSES

The concept of Brownian motion was first studied by the botanist Robert Brown in 1827 while observing pollen grains suspended in water. Brown noticed the pollen underwent erratic motion but, as our knowledge of the substructure of matter was not as substantial as it is today, he could not explain this behavior. An explanation came from Albert Einstein in 1905[1] where he detailed that the motion was due to water molecules frequently colliding with the pollen. While Einstein's solution was entirely valid, in 1908 Paul Langevin proposed a separate explanation by introducing the concept of stochastic noise. This jump-started a branch of mathematics via the notions of stochastic differential equations and stochastic processes.

While the theory of stochastic processes has been rigorously developed mathematically, physics provides some very natural examples of stochastic behavior, some famous examples being particle decay, the quantum world and, of course, Brownian motion. Outside of physics, stochastic processes have wide reaching applications from the field of finance with the Black-Scholes equation, to Markov chain models in ecology and even as far as neuroscience with noisy neurons. In recent years, stochastic methods have been applied to hydrodynamics and heavy flavor propagation in quark gluon plasma [35–37]. One of the goals in this work is to apply stochastic methods to the study of correlation functions. We begin with a demonstration of Brownian motion from the perspective of Langevin's theory. Although this example is objectively simpler than the Boltzmann and hydrodynamic implementations we are working towards, it will serve as a nice introduction to the concepts and methods we will need.

3.1 Brownian motion

Consider a non-relativistic system consisting of a fluid at rest, under no external forces, and make note of your favorite particle in the fluid. As this particle of mass m moves through the fluid there are two forces on it that we must consider. The first is the frictional force due to the fluid viscosity, $\mathbf{f}_f = -m\gamma\mathbf{v}$, for the coefficient of friction γ. The second is the

[1] Shortly after, in 1906, Marian Smoluchowski independently came across the same explanation [34].

force from the collisions of the fluid particles on the test particle, ξ. In one dimension for simplicity, Newton's laws give the equation of motion of the test particle as

$$m\dot{v} = -m\gamma v + \xi. \tag{3.1}$$

This equation is known as a Langevin equation due to the stochastic nature of the force ξ. Keeping track of all the individual collisions which contribute to ξ would be cumbersome, and in many cases impossible, so our first step in solving Eq. (3.1) will be to describe what we want and need in regards to a stochastic force.

To facilitate this discussion we partition time into a series of discrete steps Δt. We will not concern ourselves with the details of the partition so long as, at the end of the day, we can take $\Delta t \to 0$ to recover continuous time and full differential equations. This allows us to write Eq. (3.1) as a difference equation.

$$v(t + \Delta t) - v(t) = -\gamma v(t)\Delta t + \Delta W(t) \tag{3.2}$$

where we have made the substitution $(\xi/m)\Delta t = \Delta W$. The stochastic term ΔW now represents the change in velocity due to collisions during the time interval from t to $t + \Delta t$. We make this notational change to make explicit the nature of ΔW. The Wiener process $W(t)$ is described in detail in appendix A.1.

In order to work with the Langevin equation we make two assumptions on ΔW. First, we assume that the collisions are random in direction and magnitude and, thus, we require the average contribution of ΔW to vanish. Second, we will assume a specific form for noise-noise correlation, which is typical for diffusion type problems. We write these assumptions as

$$\langle \Delta W \rangle = 0 \qquad \text{and} \qquad \langle \Delta W^2 \rangle = \Gamma \Delta t, \tag{3.3}$$

where the brackets refer to an average over an ensemble of identically prepared systems

allowed to evolve under the same conditions. Due to the random interactions between the fluid particles, the systems in this ensemble can deviate from each other wildly despite having the same initial conditions. We refer to this as the "thermal average" or the "noise average" and note it must be distinguished from a full event average that we will use later which must also take into consideration an average over the differing initial conditions.

In the second half of Eq. (3.3), Γ represents the "strength" of the noise as we will see later on. Implied in the relation $\Delta W^2 \propto \Delta t$ is the idea that we can consider ΔW to be a differential on the order of $\Delta t^{1/2}$. Half-order differentials are one of the features of stochastic calculus that sets it apart greatly from regular calculus.

Taking the thermal average of Eq. (3.2) and then taking $\Delta t \to 0$ gives

$$\frac{d\langle v\rangle}{dt} = -\gamma\langle v\rangle, \tag{3.4}$$

which has the solution $\langle v\rangle = v_0 e^{-\gamma}$. We see the noise vanishes and the result is a completely deterministic equation for the velocity of the test particle. Notice how the noise does not contribute to the single particle average.

Next we calculate the variance in the velocity $\langle\Delta(v^2)\rangle$. To do this we need to make use of the Itô product rule from stochastic calculus. This is a variation of the usual product rule which is required when using stochastic variables in order to keep all terms of order Δt – in particular ΔW^2. In this case it takes the form:

$$\begin{aligned}\Delta(v^2) &= 2v\Delta v + \Delta v\Delta v \\ &= 2v\left(-\gamma v\Delta t + \Delta W\right) + \left(\gamma^2 v^2\Delta t^2 - 2\gamma v\Delta t\Delta W + \Delta W^2\right) \\ &= -2v^2\gamma\Delta t + \Delta W^2 + \gamma^2 v^2\Delta t^2 + 2v(1-\gamma\Delta t)\Delta W \end{aligned} \tag{3.5}$$

The Δt^2 term vanishes to order Δt and the ΔW term will vanish upon taking the average.

Thus, we find

$$\begin{aligned}\langle \Delta(v^2) \rangle &= -2\gamma \langle v^2 \rangle \Delta t + \langle \Delta W^2 \rangle \\ &= \left(-2\gamma \langle v^2 \rangle + \Gamma \right) \Delta t. \end{aligned} \tag{3.6}$$

Finally, taking $\Delta t \to 0$ we have an equation for the variance in the velocity

$$\frac{d\langle v^2 \rangle}{dt} = -2\gamma \langle v^2 \rangle + \Gamma. \tag{3.7}$$

Notice that here the noise term remains. In general, we will see that for two-particle observables – and, hence, correlations – the noise makes an important contribution.

Up to this point, Γ is an unknown quantity. We can calculate a specific value for this strength term using the fluctuation-dissipation theorem from statistical mechanics. Aptly named, the fluctuation-dissipation theorem relates thermal fluctuations in a system to the dissipative processes acting in the system. Brownian motion provides a simple example. Particles moving through the system dissipate energy due to viscosity. This energy is added to the system, causing the particles to fluctuate more rapidly. In systems that obey detailed balance these two processes must equal each other.

To apply this to Eq. (3.7) note that in equilibrium the system exhibits steady state behavior so the time derivative on the left-hand side must vanish. Thus, we are left with $\Gamma = 2\gamma \langle v^2 \rangle_{eq}$. In this case we can further simplify the result by invoking the equipartition theorem $\langle v^2 \rangle_{eq} = T/m$ for the temperature T and, therefore,

$$\Gamma = 2\gamma T/m. \tag{3.8}$$

It is also interesting to find the variance in the position of the Brownian particle. We

assume $\Delta x = v(t)\Delta t$ is independent of the noise so the usual product rule gives

$$\Delta(x^2) = 2x(t)\Delta x = 2xv\Delta t \qquad \Rightarrow \qquad \frac{d\langle x^2\rangle}{dt} = 2\langle xv\rangle. \tag{3.9}$$

To find $\langle xv\rangle$ we again employ the Itô product rule to accomodate the noisy velocity term:

$$\begin{aligned}\Delta(xv) &= x\Delta v + v\Delta x + \Delta x\Delta v \\ &= x(-\gamma v\Delta t + \Delta W) + v^2\Delta t + v\Delta t(-\gamma v\Delta t + \Delta W) \\ &= (-\gamma xv + v^2)\Delta t + -\gamma v^2(\Delta t)^2 + (x + v\Delta t)\Delta W. \end{aligned} \tag{3.10}$$

We drop the term proportional to Δt^2 when taking the limit $\Delta t \to 0$ and the terms proportional to ΔW vanish upon taking the noise average. Thus, we are left with the equation

$$\frac{d\langle xv\rangle}{dt} = -\gamma\langle xv\rangle + \langle v^2\rangle \tag{3.11}$$

In equilibrium the time derivative again vanishes and we have

$$\langle xv\rangle_{eq} = \langle v^2\rangle_{eq}/\gamma = T/\gamma m \tag{3.12}$$

Plugging this into Eq. (3.9) we find $d\langle x^2\rangle_{eq}/dt = 2\langle v^2\rangle_{eq}/\gamma = 2T/\gamma m$ which we can immediately integrate to get

$$\langle x^2\rangle_{eq} = \frac{2T}{\gamma m}t. \tag{3.13}$$

Identifying $D = T/\gamma m$ as the diffusion coefficient we reproduce Einstein's random walk formula $\langle x^2\rangle_{eq} = 2Dt$

Had we not included noise we would have arrived at contradictory results. To better understand the noise contribution we can reanalyze the problem without noise by taking $\Delta W = 0$ in Eq. (3.2). Now, upon calculating $\Delta(v^2)$ we use the regular product rule or, alternatively, simply set $\Gamma = 0$. As a result, the average $\langle v^2\rangle$ experiences exponential decay

and, in particular, tends to zero in the long time limit – i.e. equilibrium. Immediately this violates the equipartition theorem and, further, leads to the strange result that $\langle x^2 \rangle_{eq} = 0$.

We define the variance of the velocity as $r_v = \langle v^2 \rangle - \langle v \rangle^2$ (here $\langle v \rangle = 0$ but this need not always be the case). Our interest will be in the deviation of r_v from its value in equilibrium $\Delta r_v = r_v - r_{v,eq}$ as this quantity is related to the correlation functions we will study later. This quantity measures the degree to which the particles of the system have thermalized. We wish to obtain an equation of motion for Δr_v:

$$\begin{aligned}
\frac{d\Delta r_v}{dt} &= \frac{dr_v}{dt} - \frac{dr_{v,eq}}{dt} \\
&= \frac{d\langle v^2 \rangle}{dt} - \frac{d\langle v \rangle^2}{dt} - \left(\frac{d\langle v^2 \rangle_{eq}}{dt} - \frac{d\langle v \rangle_{eq}^2}{dt} \right) \\
&= \left(-2\gamma \langle v^2 \rangle + \Gamma \right) - \left(-2\gamma \langle v^2 \rangle \right) - (0 - 0) \\
&= -2\gamma r_v + \Gamma. \qquad (3.14)
\end{aligned}$$

Making the identification $\Gamma = 2\gamma \langle v^2 \rangle_{eq} = 2\gamma \left(\langle v^2 \rangle_{eq} - \langle v \rangle_{eq}^2 \right) = 2\gamma r_{v,eq}$ we have

$$\frac{d\Delta r_v}{dt} = -2\gamma \Delta r_v. \qquad (3.15)$$

Equation (3.15) has two interesting features. First, unlike the closely related Eq. (3.7), it is entirely deterministic. Indeed, the noise Γ has been absorbed into the equilibrium term. Second, the lifetime of Δr_v is $1/2\gamma$, precisely half the value for the lifetime of the mean $\langle v \rangle$ as seen in Eq. (3.4). This factor will be important when we study hydrodynamic transport in Chapter 4.

3.2 Stochastic particle diffusion

In the previous example we introduced stochastic variables to describe the velocity of Brownian particles. One can also describe the density of these particles by treating the diffusion equation in a similar manner. Let $n(\mathbf{x}, t)d\mathbf{x}$ represent the number of particles in the volume $d\mathbf{x}$ at time t and let $\mathbf{J}(\mathbf{x}, t)$ represent the particle current. Due to particle number

conservation these are related via the conservation equation:

$$\frac{\partial n}{\partial t} = -\nabla \cdot \mathbf{J}. \tag{3.16}$$

Fick's law for particle diffusion says that particles will tend to flow from higher density regions to lower density regions. As an equation it is written

$$\mathbf{J} = -D\nabla n \tag{3.17}$$

where the diffusion coefficient D gives the strength of the flow. In general D may depend on position or time but we will take it as constant for simplicity.

In this section we will take conservation of particle number to be exact so Eq. (3.16) cannot be treated stochastically. This assumption is not strictly necessary and does not change the following results much but it will be useful when we deal with momentum later on. However, one can imagine that particle flow can be treated stochastically as it is due to collisions. To add "randomness" to this problem we, therefore, introduce it into Fick's law. Thus, we write

$$\mathbf{J} = -D\nabla n + \mathbf{j} \tag{3.18}$$

where $\mathbf{j}$ represents the stochastic contribution to the particle current. Combining Eqs. (3.16) and (3.18) in the usual way to get the diffusion equation gives

$$\frac{\partial n}{\partial t} = D\nabla^2 n - \nabla \cdot \mathbf{j}. \tag{3.19}$$

In this case, our "stochastic variable" has become "the derivative of a stochastic variable". One can take care and maintain this distinction but for our purposes we need only note that the derivative of a stochastic variable is still stochastic. As such, we treat $\nabla \cdot \mathbf{j}$ in the same manner as we treated ξ in Eq. (3.1).

As before, we write this as a difference equation

$$n(\mathbf{x}, t + \Delta t) - n(\mathbf{x}, t) \equiv \Delta n = D\nabla^2 n(\mathbf{x}, t)\Delta t + \Delta W(\mathbf{x}, t) \tag{3.20}$$

where we have written the stochastic contribution as a Wiener process, now depending on position and time. Our assumptions on ΔW are the same as in the previous section:

$$\langle \Delta W \rangle = 0 \qquad \text{and} \qquad \langle \Delta W_1 \Delta W_2 \rangle = \Gamma_{12}\Delta t \tag{3.21}$$

where $W_i = W(\mathbf{x}_i, t)$. Due to dependence of ΔW on position, the noise term Γ_{12} now also depends on the coordinates $\mathbf{x}_1$ and $\mathbf{x}_2$. However, we should not have same time noise correlations between separated spatial points so we expect Γ_{12} to have the δ-function dependence $\delta(\mathbf{x}_1 - \mathbf{x}_2)$.

Taking the thermal average of Eq. (3.20) shows that – as expected – the average value of the density satisfies the usual diffusion equation:

$$\frac{\partial \langle n \rangle}{\partial t} = D\nabla^2 \langle n \rangle. \tag{3.22}$$

Once again we see that the single particle average is unaffected by noise. The noise is relevant, however, to the correlator $\langle n(\mathbf{x}_1, t)n(\mathbf{x}_2, t)\rangle$. To see this, we apply the Itô product rule to $\Delta(n_1 n_2) \equiv n(\mathbf{x}_1, t + \Delta t)n(\mathbf{x}_2, t + \Delta t) - n(\mathbf{x}_1, t)n(\mathbf{x}_2, t)$:

$$\begin{aligned}
\Delta(n_1 n_2) &= n_1 \Delta n_2 + n_2 \Delta n_1 + \Delta n_1 \Delta n_2 \\
&= n_1 \left(D\nabla_2^2 n_2 \Delta t + \Delta W_2 \right) + n_2 \left(D\nabla_1^2 n_1 \Delta t + \Delta W_1 \right) \\
&\quad + \left(D\nabla_1^2 n_1 \Delta t + \Delta W_1 \right) \left(D\nabla_2^2 n_2 \Delta t + \Delta W_2 \right) \\
&= D\left(\nabla_1^2 + \nabla_2^2 \right) n_1 n_2 \Delta t + \Delta W_1 \Delta W_2 \\
&\quad + \left(n_1 + D\nabla_1^2 n_1 \Delta t \right) \Delta W_2 + \left(n_2 + D\nabla_2^2 n_2 \Delta t \right) \Delta W_1 + D^2 \nabla_1^2 \nabla_2^2 n_1 n_2 \Delta t^2
\end{aligned} \tag{3.23}$$

On taking the thermal average and dropping the second order term the last line vanishes. After using Eq. (3.21) for the noise-noise correlator, dividing by Δt and taking its limit to 0 and then rearranging we arrive at a differential equation for the density correlator:

$$\left[\frac{\partial}{\partial t} - D\left(\nabla_1^2 + \nabla_2^2\right)\right]\langle n_1 n_2\rangle = \Gamma_{12}. \tag{3.24}$$

The calculation for $\Delta\left(\langle n_1\rangle\langle n_2\rangle\right)$ is similar to above, or alternatively since there is no noise on the single particle averages we can take $\Gamma_{12} = 0$. As a result we get

$$\left[\frac{\partial}{\partial t} - D\left(\nabla_1^2 + \nabla_2^2\right)\right]\langle n_1\rangle\langle n_2\rangle = 0. \tag{3.25}$$

Combining these equations and defining the correlation function $r_n \equiv \langle n_1 n_2\rangle - \langle n_1\rangle\langle n_2\rangle$ we find

$$\left[\frac{\partial}{\partial t} - D\left(\nabla_1^2 + \nabla_2^2\right)\right] r_n = \Gamma_{12}. \tag{3.26}$$

We can find the value of Γ_{12} by applying the fluctuation-dissipation theorem. As before, we will require that fluctuations in equilibrium have the appropriate thermodynamic limit. In local equilibrium the time derivative $\partial r_n/\partial t$ vanishes since we have assumed a stationary background. Thus,

$$\Gamma_{12} = -D\left(\nabla_1^2 + \nabla_2^2\right) r_{n,le} \tag{3.27}$$

where $r_{n,le}$ denotes the value of the covariance in local equilibrium. In systems that can be described using the grand canonical ensemble, particle number fluctuations satisfy Poisson statistics. For the Poisson distribution, the variance equals the average so that $\langle N^2\rangle - \langle N\rangle^2 = \langle N\rangle$. Furthermore, local equilibrium erases all correlations at distinct points $\mathbf{x}_1 \neq \mathbf{x}_2$. Therefore, in local equilibrium we have $r_{n,le} = \langle n_1\rangle\delta(\mathbf{x}_1 - \mathbf{x}_2)$. Finally, the noise term is given by

$$\Gamma_{12} = -D\left(\nabla_1^2 + \nabla_2^2\right)\langle n_1\rangle\delta\left(\mathbf{x}_1 - \mathbf{x}_2\right). \tag{3.28}$$

Notice that if we had not considered noise then Eq. (3.26) would have $\Gamma_{12} = 0$. As a result we would find that $r_n \to 0$ as $t \to \infty$, which contradicts that particle number obeys Poisson statistics in equilibrium.

The presence of the delta function in the noise term makes Eq. (3.26) difficult to work with in practice. We can find a more preferable equation by introducing $\Delta r_n \equiv r_n - r_{n,le}$, which measures r_n relative to its value in equilibrium. Combining Eqs. (3.26) and (3.28) we obtain

$$\left[\frac{\partial}{\partial t} - D\left(\nabla_1^2 + \nabla_2^2\right)\right] \Delta r_n = 0. \tag{3.29}$$

Now notice that as $t \to \infty$ we find that $\Delta r_n \to 0$.

This describes the effect of diffusion on the particles in an event. The initial distribution of particles after a collision may have regions where particles are densly clumped together along with regions of lower density. This gives initial correlations r_n which are very different from those in local equilibrium $r_{n,le}$. As the system evolves over time, the initial correlations tend to their value in local equilibrium $r_n \to r_{n,le}$ which describes a smoother distribution of particles throughout the volume. In a real collision, however, the rapid expansion of the system can interfere with this process. If interactions between particles ceases before the system has time to fully thermalize, some of the initial correlations are frozen into the final distribution.

3.3 Stochastic momentum diffusion

The case of first order momentum diffusion is very similar to that of particle diffusion. In this section, we use $\mathbf{g}(\mathbf{x}, t)$ to represent the shear contribution to the momentum current $M^i = T^{0i} - \langle T^{0i} \rangle$. For now, the details of this relationship are unimportant – they will be explained in Chapter 4 – and we are only interested in the equations satisfied by $\mathbf{g}$. Thus, if we briefly look forward to Eq. (4.21) we see that each component of $\mathbf{g}$ individually satisfies the diffusion equation

$$\frac{\partial \langle g^i \rangle}{\partial t} = \nu \nabla^2 \langle g^i \rangle, \tag{3.30}$$

for the kinematic viscosity ν. As in Eq. (3.20), we write this as a difference equation with noise

$$\Delta g^i = \nu \nabla^2 g^i \Delta t + \Delta W^i. \tag{3.31}$$

We make similar assumptions on these ΔW as in previous sections with the caveat that W now depends on the components of $\mathbf{g}$. The defining relations are then given by

$$\langle \Delta W^i \rangle = 0 \qquad \text{and} \qquad \langle \Delta W_1^i \Delta W_2^j \rangle = \Gamma_{12}^{ij} \Delta t \tag{3.32}$$

where $W_k^i = W^i(\mathbf{x}_k, t)$ is the Wiener process that describes the noise affecting the i^{th} component of $\mathbf{g}$ and Γ_{12}^{ij} determines the strength of the noise.

We define the momentum correlation function $r_g^{ij} \equiv \langle g_1^i g_2^j \rangle - \langle g_1^i \rangle \langle g_2^j \rangle$ and the difference $\Delta r_g^{ij} \equiv r_g^{ij} - r_{g,le}^{ij}$ for the local equilibrium correlation function $r_{g,le}^{ij}$. Note that although $\langle g^i \rangle = 0$, we keep these in for generality.

The method and results mimic those in Sec. 3.2. The momentum correlation function satisfies the equation

$$\left[\frac{\partial}{\partial t} - \nu \left(\nabla_1^2 + \nabla_2^2 \right) \right] r_g^{ij} = \Gamma_{12}^{ij}. \tag{3.33}$$

while the deviation of r_g^{ij} from equilibrium satisfies the noise-free diffusion equation

$$\left[\frac{\partial}{\partial t} - \nu \left(\nabla_1^2 + \nabla_2^2 \right) \right] \Delta r_g^{ij} = 0. \tag{3.34}$$

with

$$\Gamma_{12}^{ij} = -\nu \left(\nabla_1^2 + \nabla_2^2 \right) r_{g,le}^{ij} \tag{3.35}$$

In this case we again find that, due to the consideration of stochastic noise, $r_g^{ij} \to r_{g,le}^{ij}$ as the system evolves. We can interpret these results similarly to the case with the particle density. We may have an initially clumpy momentum distribution which results in anisotropic transverse flow. The kinematic viscosity ν tends to diminish the anisotropy bringing the

system closer to local equilibrium.

First order hydrodynamics fails in situations where causality must be considered. In first order diffusion, for example, a δ-function initial condition will instantaneously form a Gaussian, spreading its tails out to infinity. Second order hydrodynamics restores causality to diffusion and, therefore, will be important in our study of nuclear collisions. In moving to second order we pick up new transport coefficients, in particular the relaxation time for the shear stress τ_π. We now apply our methods to second order hydrodynamics.

Looking forward again, the shear modes of the momentum density evolve via second order diffusion and satisfy the Maxwell-Cattaneo equation (4.34)

$$\left(\tau_\pi \frac{\partial^2}{\partial t^2} + \frac{\partial}{\partial t}\right) \langle g^i \rangle = \nu \nabla^2 \langle g^i \rangle. \tag{3.36}$$

To write this as a difference equation we convert it into two first order equations by defining $h^i = \partial g^i / \partial t$. For simplicity of notation we will also define $L = \nu \nabla^2$ and temporarily suppress the vector indices. We can then write the non-averaged version of Eq. (3.36) as

$$\tau_\pi \frac{\partial h}{\partial t} = -h + Lg. \tag{3.37}$$

We take the definition of h as exact and, thus, only apply noise to Eq. (3.37). Then our stochastic system of difference equations is

$$\Delta g = h \Delta t \tag{3.38}$$

$$\Delta h = -\gamma \left(h - Lg\right) \Delta t + \gamma \Delta W \tag{3.39}$$

where $\gamma = 1/\tau_\pi$ and ΔW satisfies Eq. (3.32).

To find an equation for Δr_g, as defined previously, we start with

$$\begin{aligned}\Delta\langle g_1 g_2\rangle &= \langle g_1 \Delta g_2\rangle + \langle g_2 \Delta g_1\rangle \\ &= \left(\langle g_1 h_2\rangle + \langle h_1 g_2\rangle\right)\Delta t.\end{aligned} \tag{3.40}$$

We now define the covariances

$$r_{gh} = \langle g_1 h_2\rangle - \langle g_1\rangle\langle h_2\rangle \qquad \text{and} \qquad r_{hg} = \langle h_1 g_2\rangle - \langle h_1\rangle\langle g_2\rangle. \tag{3.41}$$

As before, note that although $\langle g\rangle = \langle h\rangle = 0$, we keep these quantities in for generality. As a result, the next equation follows trivially, however, one could also repeat the steps in Eq. (3.40) with $\Delta\left(\langle g_1\rangle\langle g_2\rangle\right)$ and combine the two equations. In either case, Eq. (3.40) gives

$$\frac{\partial\, r_g}{\partial t} = r_{gh} + r_{hg}. \tag{3.42}$$

We do the same for r_{gh} and r_{hg}. Notice that only Δh is affected by noise. As a result the quantity $\Delta g \Delta h$ will not contain a term proportional to ΔW^2 and the regular product rule will suffice.

$$\begin{aligned}\Delta\langle g_1 h_2\rangle &= \langle g_1 \Delta h_2\rangle + \langle h_2 \Delta g_1\rangle \\ &= \langle g_1\left[-\gamma\left(h_2 - L_2 g_2\right)\Delta t + \gamma \Delta W_2\right]\rangle + \langle h_2 h_1 \Delta t\rangle \\ &= \left[\langle h_1 h_2\rangle - \gamma\langle g_1 h_2\rangle + \gamma L_2\langle g_1 g_2\rangle\right]\Delta t + \gamma\langle g_1 \Delta W_2\rangle\end{aligned} \tag{3.43}$$

The last term vanishes due to ΔW_2 so that

$$\left(\frac{\partial}{\partial t} + \gamma\right) r_{gh} = r_h + \gamma L_2 r_g \tag{3.44}$$

where $r_h = \langle h_1 h_2 \rangle - \langle h_1 \rangle \langle h_2 \rangle$. The equation for r_{hg} is similar with L_1 replacing L_2

$$\left(\frac{\partial}{\partial t} + \gamma \right) r_{hg} = r_h + \gamma L_1 r_g. \tag{3.45}$$

It will be useful in the future to combine these two equations to obtain

$$\left(\frac{\partial}{\partial t} + \gamma \right) (r_{gh} + r_{hg}) = 2r_h + \gamma \left(L_1 + L_2 \right) r_g. \tag{3.46}$$

To obtain a corresponding equation for r_h we note that $\Delta h_1 \Delta h_2$ will contain ΔW^2 and, as such, we must employ the Itô product rule

$$\begin{aligned} \Delta \langle h_1 h_2 \rangle &= \langle h_1 \Delta h_2 \rangle + \langle h_2 \Delta h_1 \rangle + \langle \Delta h_1 \Delta h_2 \rangle \\ &= -\gamma \langle h_1 \left(h_2 - L_2 g_2 \right) \rangle \Delta t - \gamma \langle h_2 \left(h_1 - L_1 g_1 \right) \rangle \Delta t + \gamma^2 \langle \Delta W_1 \Delta W_2 \rangle \\ &= \gamma \left(-2 \langle h_1 h_2 \rangle + L_1 \langle g_1 h_2 \rangle + L_2 \langle h_1 g_2 \rangle \right) \Delta t + \gamma^2 \Gamma_{12} \Delta t. \end{aligned} \tag{3.47}$$

Thus, the evolution of r_h is given by

$$\left(\frac{\partial}{\partial t} + 2\gamma \right) r_h = \gamma L_1 r_{gh} + \gamma L_2 r_{hg} + \gamma^2 \Gamma_{12}. \tag{3.48}$$

We intend to eliminate the noise by finding final equations for $\Delta r_g = r_g - r_{g,le}$ and $\Delta r_h = r_h - r_{h,le}$, however as an aside, it can be interesting to study the noise itself. To do so, note that in equilibrium in an infinite system the time derivatives in Eqs. (3.42), (3.44), (3.45) and (3.48) all vanish. Equation (3.42) implies $r_{gh,le} = -r_{hg,le}$, however as the equilibrium system is translationally invariant we must have $r_{gh,le} = r_{hg,le}$, and as a result $r_{gh,le} = r_{hg,le} = 0$. Equation (3.46) then gives $2r_{h,le} = -\gamma \left(L_1 + L_2 \right) r_{g,le}$ and Eq. (3.48) gives $2r_{h,le} = \gamma \Gamma_{12}$. Combining these equations we find

$$\Gamma_{12} = -\left(L_1 + L_2 \right) r_{g,le}, \tag{3.49}$$

which matches the form of the noise in Eq. (3.35).

Continuing on, the Δ-forms of the above equations all follow straightforwardly and the method is similar to the previous sections. We find

$$\frac{\partial}{\partial t}\Delta r_g = \Delta r_{gh} + \Delta r_{hg}, \tag{3.50}$$

$$\left(\frac{\partial}{\partial t} + \gamma\right)\left(\Delta r_{gh} + \Delta r_{hg}\right) = 2\Delta r_h + \gamma\left(L_1 + L_2\right)\Delta r_g, \tag{3.51}$$

$$\left(\frac{\partial}{\partial t} + 2\gamma\right)\Delta r_h = \gamma L_1 \Delta r_{gh} + \gamma L_2 \Delta r_{hg}. \tag{3.52}$$

This gives three coupled equations absent of noise, however we need more desirable forms in order to make approximations. First, for Eq. (3.52) we add and subtract the quantities $\frac{1}{2}L_1\Delta r_{hg}$ and $\frac{1}{2}L_2\Delta r_{gh}$ and then use Eq. (3.50). This allows us to write

$$\begin{aligned}\left(\frac{\partial}{\partial t} + 2\gamma\right)\Delta r_h &= \frac{1}{2}\gamma\left(L_1 + L_2\right)\left(\Delta r_{gh} + \Delta r_{hg}\right) + \frac{1}{2}\gamma\left(L_1 - L_2\right)\left(\Delta r_{gh} - \Delta r_{hg}\right) \\ &= \frac{1}{2}\gamma\left(L_1 + L_2\right)\frac{\partial}{\partial t}\Delta r_g + \frac{1}{2}\gamma\left(L_1 - L_2\right)\left(\Delta r_{gh} - \Delta r_{hg}\right).\end{aligned} \tag{3.53}$$

Using Eq. (3.50) in Eq. (3.51) we have

$$\left(\frac{\partial}{\partial t} + \gamma\right)\frac{\partial}{\partial t}\Delta r_g = 2\Delta r_h + \gamma\left(L_1 + L_2\right)\Delta r_g. \tag{3.54}$$

Applying $\partial/\partial t + 2\gamma$ to this equation and using Eq. (3.53) gives

$$\begin{aligned}\left(\frac{\partial}{\partial t} + \gamma\right)\left(\frac{\partial^2}{\partial t^2} + 2\gamma\frac{\partial}{\partial t}\right)\Delta r_g &= 2\left(\frac{\partial}{\partial t} + 2\gamma\right)\Delta r_h \\ &\quad + \gamma\left(L_1 + L_2\right)\frac{\partial}{\partial t}\Delta r_g + 2\gamma^2\left(L_1 + L_2\right)\Delta r_g \\ &= 2\gamma\left(L_1 + L_2\right)\left(\frac{\partial}{\partial t} + \gamma\right)\Delta r_g \\ &\quad + \gamma\left(L_1 - L_2\right)\left(\Delta r_{gh} - \Delta r_{hg}\right).\end{aligned} \tag{3.55}$$

Rearranging this gives the final result for the full evolution of Δr_g

$$\left(\frac{\partial}{\partial t}+\gamma\right)\left[\frac{\partial^2}{\partial t^2}+2\gamma\frac{\partial}{\partial t}-2\gamma\left(L_1+L_2\right)\right]\Delta r_g=\gamma\left(L_1-L_2\right)\left(\Delta r_{gh}-\Delta r_{hg}\right). \tag{3.56}$$

Equation (3.51) we instead wish to write in terms of $\Delta r_{gh}-\Delta r_{hg}$, so using Eqs. (3.44) and (3.45) we find

$$\left(\frac{\partial}{\partial t}+\gamma\right)\left(\Delta r_{gh}-\Delta r_{hg}\right)=-\gamma\left(L_1-L_2\right)\Delta r_g. \tag{3.57}$$

In Eqs. (3.56) and (3.57) we have reduced our system to two coupled equations, free of noise. Furthermore, Eq. (3.56) simplifies appreciably when $\Delta r_{gh}\approx\Delta r_{hg}$, as is the case when the right hand side of Eq. (3.57) is negligible. To see when this occurs, we write the operators L_1 and L_2 in terms of the relative and average coordinates, $\mathbf{x}_r=\mathbf{x}_1-\mathbf{x}_2$ and $\mathbf{x}_a=(\mathbf{x}_1+\mathbf{x}_2)/2$. We then have

$$L_1+L_2=2\nu\nabla_r^2+\frac{\nu}{2}\nabla_a^2 \qquad \text{and} \qquad L_1-L_2=2\nu\nabla_a\cdot\nabla_r. \tag{3.58}$$

The right hand side of Eq. (3.57) is then $-2\gamma\nu\nabla_a\cdot\nabla_r\,\Delta r_g$. If the correlations in Δr_g are translationally invariant and, thus, depend only on $\mathbf{x}_r$, then $\nabla_a\,\Delta r_g=0$ and the right hand side vanishes. If Δr_g is symmetric with respect to $\mathbf{x}_a$ and slowly varying, then the right hand side is negligible near $\mathbf{x}_a=0$ so long as ∇_r does not blow up. This situation is true for an expanding Bjorken system, the type we consider.

In light of this, we choose to study the approximate evolution equation

$$\left[\frac{\tau_\pi}{2}\frac{\partial^2}{\partial t^2}+\frac{\partial}{\partial t}-\nu\left(\nabla_1^2+\nabla_2^2\right)\right]\Delta r_g^{ij}=0 \tag{3.59}$$

where we have returned to the original notation. Equation (3.59) is a solution to Eq. (3.56) for the types of systems we are interested in studying in this work.

Equation (3.59) alleviates causality concerns since it is hyperbolic due to the $\partial^2/\partial t^2$ term. As such, the solutions are wave-like and an initial perturbation will propagate out at a finite

speed determined by ν and τ_π. At very early times, $t \ll \tau_\pi/2$, the wave part of Eq. (3.59) dominates and initial pulses propagate out at speeds up to $\sqrt{2\nu/\tau_\pi}$. At much later times, $t \gg \tau_\pi/2$, the diffusive part dominates and the first order Navier-Stokes result (3.34) holds. To see this we can view Eq. (3.59) as a relaxation equation

$$\frac{\partial}{\partial t}\Psi = -\frac{2}{\tau_\pi}\left[\Psi - \nu\left(\nabla_1^2 + \nabla_2^2\right)\Delta r_g\right], \tag{3.60}$$

where at long times $\Psi = \partial(\Delta r_g)/\partial t$ relaxes to $\nu\left(\nabla_1^2 + \nabla_2^2\right)\Delta r_g$. Note the relaxation time $\tau_\pi/2$ is half the value compared to the relaxation of the mean in Eq. (3.36). This is the same halving we saw in Brownian motion, Eq. (3.15). Note also that for $\tau_\pi = 0$, Eq. (3.59) reduces to the first order equation (3.34).

There are two situations where we may wish to solve the coupled equations (3.56) and (3.57) instead of Eq. (3.59). In pA collisions we do not expect the rapidity dependence to be symmetric in $\mathbf{x}_a$. However, it would be possible to remove the asymmetry by averaging over $\mathbf{x}_a$. Also, if the correlations are strongly dependent on position or time we cannot simplify to Eq. (3.59).

CHAPTER 4 RELATIVISTIC HYDRODYNAMICS

Hydrodynamics typically involves studying a set of equations derived from conservation laws. In general, these conservation laws are absolute and lead to completely deterministic equations of motion for fluid systems. As a result of stochastic microscopic behavior, real fluids experience fluctuations in their flow which can be accounted for by using hydrodynamic noise [38–40]. In Sec 3.3 we added noise to hydrodynamic equations to obtain differential equations for correlation functions. In this chapter we seek to derive these hydrodynamic equations.

Our goal with hydrodynamics is to describe the rapidity dependence of transverse momentum correlations. We begin by observing that these fluctuations are spread along the beam direction by shear hydrodynamic modes. In general, shear modes account for the linear response of a fluid in directions perpendicular to an initial impulse. Viscous diffusion spreads this response throughout the fluid, tending to make the velocity distribution as uniform as possible. On the other hand, sound modes are compression waves that propagate in the same direction as the initial impulse and will generally be less important in determining the overall response to low frequency fluctuations. We discuss this further after Eqs. (4.21) and (4.22) but start with a general discussion of the hydrodynamic equations we require.

4.1 First-order relativistic hydrodynamics

We begin with notation. The local energy density we denote as $e(t, \mathbf{x})$, the pressure as $p(t, \mathbf{x})$ and the four-velocity as $u^\mu = \gamma(1, \mathbf{v})$ where the Lorentz factor is $\gamma = (1 - v^2)^{1/2}$. We note that $u^\mu u_\mu = 1$ by definition and in the frame where the fluid is locally at rest we have $u^\mu = (1, 0, 0, 0)$. The stress-energy tensor for an ideal fluid is given as

$$T^{\mu\nu}_{id} = (e + p)u^\mu u^\nu - p g^{\mu\nu} \tag{4.1}$$

where for the metric tensor we use the convention $g^{\mu\nu} = \mathrm{diag}(+, -, -, -)$. To include viscosity and other dissipative processes we write $T^{\mu\nu} = T^{\mu\nu}_{id} + \Pi^{\mu\nu}$ where $\Pi^{\mu\nu}$ is the viscous stress tensor representing the deviation from ideal fluid behavior. We define the projection

operator

$$\Delta^{\mu\nu} = g^{\mu\nu} - u^\mu u^\nu \tag{4.2}$$

which satisfies $\Delta^{\mu\alpha}\Delta_{\alpha\nu} = \Delta^\mu_\nu$ and $\Delta^{\mu\nu}u_\nu = 0$. As such, it acts to project onto the space orthogonal to the fluid velocity. It is convenient to use the derivatives

$$D = u^\mu\partial_\mu \qquad \text{and} \qquad \nabla^\mu = \partial^\mu - u^\mu u^\nu\partial_\nu = \Delta^{\mu\nu}\partial_\nu \tag{4.3}$$

which are the projections of ∂_μ onto the space parallel and perpendicular to u^μ, respectively. In the local rest frame D reduces to a time derivative and ∇^μ to the gradient operator.

One can derive the equations of motion for hydrodynamics from conservation of the stress-energy tensor $\partial_\mu T^{\mu\nu} = 0$. In the case of an ideal fluid this is straightforward. Introducing the enthalpy density $w = e + p$ we have

$$0 = \partial_\mu T^{\mu\nu}_{id} = (Dw)\,u^\nu + w\,(\partial_\mu u^\mu)\,u^\nu + wDu^\nu - \partial^\nu p. \tag{4.4}$$

This first equation is obtained by contracting this equation with u_ν

$$\begin{aligned} u_\nu\partial_\mu T^{\mu\nu}_{id} &= Dw + w\partial_\mu u^\mu + wu^\mu u_\nu\partial_\mu u^\nu - Dp \\ &= De + w\partial_\mu u^\mu = 0, \end{aligned} \tag{4.5}$$

where, on the second line, we used the identity $u_\nu\partial_\mu u^\nu = 0$ mentioned in Chapter 2. This is known as the continuity equation. Another equation is obtained by contracting with $\Delta_{\nu\alpha}$

$$\begin{aligned} \Delta_{\nu\alpha}\partial_\mu T^{\mu\nu}_{id} &= (Dw)\,\Delta_{\nu\alpha}u^\nu + w\,(\partial_\mu u^\mu)\,\Delta_{\nu\alpha}u^\nu + w\Delta_{\nu\alpha}Du^\nu - \Delta_{\nu\alpha}\partial^\nu p \\ &= w\,(g_{\nu\alpha} - u_\nu u_\alpha)\,u^\mu\partial_\mu u^\nu - \nabla_\alpha p \\ &= wDu_\alpha - \nabla_\alpha p = 0. \end{aligned} \tag{4.6}$$

This is the relativistic version of the Euler equation for an ideal fluid.

Turning now to the viscous case, we need only add the projections of $\partial_\mu \Pi^{\mu\nu}$ to the ideal equations. One finds

$$De + w\partial_\mu u^\mu + u_\nu \partial_\mu \Pi^{\mu\nu} = 0, \tag{4.7}$$

$$wDu_\alpha - \nabla_\alpha p + \Delta_{\nu\alpha}\partial_\mu \Pi^{\mu\nu} = 0. \tag{4.8}$$

While the problem of specifying $\Pi^{\mu\nu}$ in general is by no means a simple task, we can find a convenient form to first order in the mean free path without too much trouble. First we rewrite the last term of Eq. (4.7) using the product rule

$$u_\nu \partial_\mu \Pi^{\mu\nu} = \partial_\mu \left(u_\nu \Pi^{\mu\nu}\right) - \Pi^{\mu\nu}\partial_\mu u_\nu. \tag{4.9}$$

We now choose to use the Landau-Lifshitz definition of the four velocity

$$u^\mu = \frac{u_\nu T^{\nu\mu}}{u_\alpha T^{\alpha\beta} u_\beta} \tag{4.10}$$

which defines the local rest frame of the fluid as the frame in which the energy flow vanishes. In this frame $u_\nu T^{\mu\nu} = e u^\mu$ which implies $u_\nu \Pi^{\mu\nu} = 0$ from our definition of the stress-energy tensor. Using this and the definition of the operator ∇_μ we have

$$u_\nu \partial_\mu \Pi^{\mu\nu} = -\Pi^{\mu\nu} \nabla_{(\mu} u_{\nu)} \tag{4.11}$$

where we have temporarily introduced the symmetrization notation

$$A_{(\mu} B_{\nu)} = \frac{1}{2}\left(A_\mu B_\nu + A_\nu B_\mu\right). \tag{4.12}$$

Now, to find a specific form for $\Pi^{\mu\nu}$, we invoke the second law of thermodynamics. In equilibrium the entropy four flow s^μ can be written as $s^\mu = s u^\mu$ for the entropy density s.

The second law, in covariant form, then says

$$\partial_\mu s^\mu \geq 0. \tag{4.13}$$

In equilibrium and with zero chemical potential we can apply the thermodynamic relations

$$e + p = Ts \qquad \text{and} \qquad Tds = de. \tag{4.14}$$

Expanding Eq. (4.13) while using Eq. (4.7) and these relations we have

$$\begin{aligned}
\partial_\mu s^\mu &= Ds + s\partial_\mu u^\mu \\
&= \frac{De}{T} + \frac{e+p}{T}\partial_\mu u^\mu \\
&= \frac{1}{T}\left[-w\partial_\mu u^\mu + \Pi^{\mu\nu}\nabla_{(\mu}u_{\nu)} + (e+p)\,\partial_\mu u^\mu\right] \\
&= \frac{1}{T}\Pi^{\mu\nu}\nabla_{(\mu}u_{\nu)} \geq 0.
\end{aligned} \tag{4.15}$$

We can write any symmetric tensor $A_{\mu\nu}$ as the sum of a traceless tensor and a remainder via the identity

$$A_{\mu\nu} = \left(A_{\mu\nu} - \frac{1}{3}\Delta_{\mu\nu}A^\mu_\mu\right) + \frac{1}{3}\Delta_{\mu\nu}A^\mu_\mu. \tag{4.16}$$

Note the term in parentheses is traceless as $\Delta^\mu_\mu = 3$. We apply this to both symmetric tensors $\Pi^{\mu\nu}$ and $\nabla_{(\mu}u_{\nu)}$ and write

$$\Pi^{\mu\nu} = S^{\mu\nu} + \Delta_{\mu\nu}\Pi \qquad \text{and} \qquad \nabla_{(\mu}u_{\nu)} = \left(\nabla_{(\mu}u_{\nu)} - \frac{1}{3}\Delta_{\mu\nu}\partial_\alpha u^\alpha\right) + \frac{1}{3}\Delta_{\mu\nu}\partial_\alpha u^\alpha. \tag{4.17}$$

For $\Pi^{\mu\nu}$ we denote the traceless part as $S^{\mu\nu}$ for later use. The factor of $1/3$ is absorbed into the scalar Π. For $\nabla_{(\mu}u_{\nu)}$ we note that it has trace $\partial_\alpha u^\alpha$.

Using these decompositions in Eq. (4.15) and simplifying we have

$$\frac{1}{T}S^{\mu\nu}\left(\nabla_{(\mu}u_{\nu)}-\frac{1}{3}\Delta_{\mu\nu}\partial_\alpha u^\alpha\right)+\frac{1}{T}\Pi\partial_\alpha u^\alpha\geq 0. \tag{4.18}$$

The simplest way to guarantee this inequality is satisfied is by setting $S^{\mu\nu}\propto\nabla^{(\mu}u^{\nu)}-\frac{1}{3}\Delta^{\mu\nu}\partial_\alpha u^\alpha$ and $\Pi\propto\partial_\alpha u^\alpha$ so that the left hand side is a sum of squares. The proportionality constants are determined by looking at the non-relativistic limit and comparing with the Navier-Stokes equations. They turn out to be $\eta/2$ and ζ, respectively, for the shear viscosity coefficient η and bulk viscosity coefficient ζ. In full we write

$$S^{\mu\nu}=\eta\left(\nabla^\mu u^\nu+\nabla^\nu u^\mu-\frac{2}{3}\Delta^{\mu\nu}\partial_\alpha u^\alpha\right)\qquad\text{and}\qquad\Pi=\zeta\partial_\alpha u^\alpha. \tag{4.19}$$

Equations (4.7) and (4.8) along with the identifications in Eqs. (4.17) and (4.19) are known as the relativistic Navier-Stokes equations.

Our interest is primarily in the shear modes, as we explain in a moment. To separate out these modes we perform a Helmholtz decomposition of the momentum current $M^i=T^{0i}-\langle T^{0i}\rangle$. Small fluctuations produce a small velocity $\mathbf{v}$ corresponding to $\mathbf{M}\approx(e+p)\mathbf{v}$. We then break $\mathbf{M}$ into transverse shear modes $\mathbf{g}$ and longitudinal sound modes $\mathbf{g}_l$ via $\mathbf{M}=\mathbf{g}+\mathbf{g}_l$. The shear modes are divergence-free, $\nabla\cdot\mathbf{g}=0$, while the longitudinal modes are curl-free, $\nabla\times\mathbf{g}_l=0$. To see the immediate usefulness of this decomposition we write, to linear order in the fluctuations of $\mathbf{v}$, the conservation form of the Navier-Stokes equation for a fluid at rest

$$\frac{\partial}{\partial t}\mathbf{M}+\nabla p=\frac{\zeta+\frac{1}{3}\eta}{w}\nabla\left(\nabla\cdot\mathbf{M}\right)+\frac{\eta}{w}\nabla^2\mathbf{M}. \tag{4.20}$$

Taking the curl of this equation leads to

$$\frac{\partial}{\partial t}\mathbf{g}=\nu\nabla^2\mathbf{g}, \tag{4.21}$$

for the kinematic viscosity $\nu=\eta/w$, and we immediately see that the shear modes satisfy a

diffusion equation to first order. Similarly, if we takes the divergence we find

$$\frac{\partial}{\partial t}\mathbf{g}_l + \nabla p = \frac{\zeta + \frac{4}{3}\eta}{w}\nabla\left(\nabla \cdot \mathbf{g}_l\right). \tag{4.22}$$

This equation alone shows that sound modes are more complex than shear modes as pressure must be kept into consideration. Moreover, both shear and bulk viscosities are involved in the damping of these sound modes. For low frequency perturbations, however, one can focus on the shear modes.

To see why, we analyze the mode structure of these equations. For (4.21) we simply assume $\mathbf{g} \sim e^{i(\mathbf{k}\cdot\mathbf{x}-\omega t)}$ for modes of frequency ω and wavenumber $\mathbf{k}$. We find the shear modes are damped with

$$\omega = -i\nu k^2. \tag{4.23}$$

Conversely, sound modes propagate at the sound speed $c_s = (\partial p/\partial e)^{1/2}$ and have

$$\omega = \pm c_s k - \frac{i}{2}\left(\frac{\zeta + \frac{4}{3}\eta}{w}\right)k^2 \approx \pm c_s k. \tag{4.24}$$

A general perturbation will excite both shear and longitudinal modes at a range of frequencies, however, this becomes simpler in the limit of high or low frequencies. A low frequency perturbation satisfying

$$\omega \sim \nu k^2 \ll c_s k, \tag{4.25}$$

will predominantly excite shear modes, while perturbations at higher frequencies

$$\omega \sim c_s k \gg \nu k^2 \tag{4.26}$$

excite sound waves. Note that in the hydrodynamic regime, $\nu k \ll c_s$ is always true because macroscopic length scales $\sim k^{-1}$ must greatly exceed the mean free path $\sim \nu$. In an ion collision, Bjorken expansion stretches the longitudinal distance scale k^{-1} for rapidity correla-

tions with proper time. This scales becomes large so that the low frequency regime applies. For more detailed discussion on this topic, see Refs. [41–43].

4.2 Second-order relativistic hydrodynamics

The relativistic Navier-Stokes theory is inherently flawed in that it is not causal. Indeed, small perturbations of frequency ω and wavenumber k about an equilibrium fluid disperse via the relation $\omega \approx (\eta/w)k^2$, reaching speeds up to $v(k) = d\omega/dk = 2(\eta/w)k$. For large k these speeds can exceed the speed of light, violating causality [44]. Our goal is to find a hydrodynamic equation describing the evolution of correlations in a fluid. Allowing a localized perturbation to instantaneously affect the entire fluid – and, thus, correlations in the fluid – can lead to results that do not accurately describe a real collision. To restore causality to the theory we must move to second order hydrodynamics.

In order to find an expression for $\Pi^{\mu\nu}$ during the derivation of the Navier-Stokes equations, we assumed the entropy four flow was equal to its equilibrium value $s^\mu = su^\mu$. This is the root of the problem with causality. For a dissipative fluid which need not be in equilibrium s^μ can depend on higher order terms, in particular terms proportional to the relaxation time τ_π, a second order transport coefficient. Second order hydrodynamics includes several new transport coefficients to account for the shear stress, bulk stress and heat current. Our interest lies mainly in the shear stress, described by τ_π, therefore in this section we only include the shear contribution.

The Müller-Israel-Stewart equation describing the relaxation of the shear stress is our starting point for second order hydrodynamics. This relaxation equation is

$$\Delta^\mu_\alpha \Delta^\nu_\beta D\Pi^{\alpha\beta} = -\frac{1}{\tau_\pi}\left(\Pi^{\mu\nu} - S^{\mu\nu}\right) - \kappa \nabla_\alpha u^\alpha \Pi^{\mu\nu}. \tag{4.27}$$

where the coefficient κ is given by

$$\kappa = \frac{1}{2}\left[1 + \frac{d\ln(\tau_\pi/\eta T)}{d\ln\tau}\right]. \tag{4.28}$$

To describe the evolution of the shear modes we consider fluctuations of a fluid mostly at rest. The momentum current $M^i = T^{0i} - \langle T^{0i} \rangle$ is then small and in the rest frame of the fluid we can write $M^i \approx (e+p)v^i$ for perturbations of the fluid velocity $v^i \ll 1$. Conservation of momentum $\partial_\mu T^{\mu i} = 0$ then gives

$$\frac{\partial}{\partial t} M^i - \partial^i p = -\partial_\mu \Pi^{\mu i} \tag{4.29}$$

to linear order in v^i and M^i. Note, in particular, that for small velocities we can make the identifications $D \to \partial/\partial t + v^i \partial_i$ and $\nabla^i \to \partial^i$. Doing the same for Eq. (4.27) we find

$$\frac{\partial}{\partial t} \Pi^{\mu i} = -\frac{1}{\tau_\pi} \left(\Pi^{\mu i} - S^{\mu i} \right). \tag{4.30}$$

To proceed we write the momentum current as $M^i = g^i + g^i_l$ as in Sec. 4.1. In Eqs. (4.29) and (4.30), g^i only receives contributions from divergence-free terms. Similarly, g^i_l only receives contributions from curl-free terms. As g^i_l is curl-free, it can be expressed as the gradient of a potential $\partial^i \phi$ and, thus, only benefits from terms that can be expressed as such – i.e. terms proportional to ∂^i. We discard these terms to focus on g^i and use the symbols $\Pi^{\mu i}_T$ and $S^{\mu i}_T$ to denote the shear contributions of these terms. This results in

$$\frac{\partial}{\partial t} g^i = -\partial_\mu \Pi^{\mu i}_T \qquad \text{and} \qquad \frac{\partial}{\partial t} \Pi^{\mu i}_T = -\frac{1}{\tau_\pi} \left(\Pi^{\mu i}_T - S^{\mu i}_T \right). \tag{4.31}$$

We can eliminate $\Pi^{\mu i}_T$ to reduce these to one equation by taking $\partial/\partial t$ of the left equation and ∂_μ of the right. Combining them we find

$$\left(\tau_\pi \frac{\partial^2}{\partial t^2} + \frac{\partial}{\partial t} \right) g^i = -\partial_\mu S^{\mu i}_T. \tag{4.32}$$

The first order form of $S^{\mu\nu}$ found in Eq. (4.19) leads to causality violations. However, for small perturbations of a stationary fluid it is a useful approximation and we apply it to

our second order theory. Linearizing Eq. (4.19) for these perturbations and considering only the shear contribution we find

$$\partial_\mu S_T^{\mu i} = -\nu \nabla^2 g^i \tag{4.33}$$

Writing it out in full, we find the evolution of the shear modes satisfies

$$\left(\tau_\pi \frac{\partial^2}{\partial t^2} + \frac{\partial}{\partial t}\right) g^i = \nu \nabla^2 g^i. \tag{4.34}$$

The form of this equation is that of a Maxwell-Cattaneo equation. It is a second order, causal diffusion equation for the modes g^i that holds for small fluctuations of a quiescent fluid. Notice that for $\tau_\pi = 0$ it reduces to first order theory – Eq. (4.21).

4.3 Ion collisions in hydrodynamics

After a nuclear collision, the momentum current M^i in each collision event varies slightly from its average value over an ensemble of events due to hydrodynamic fluctuations of the background fluid. Equation (4.29) and, consequently, Eq. (4.34) were derived by considering fluctuations of a mostly static background. To generalize these results to ion collisions we will now linearize about a fluid undergoing Bjorken expansion. We assume the event-averaged flow velocity has the form $u^\mu = (t/\tau, 0, 0, z/\tau)$ for longitudinal proper time $\tau = \sqrt{t^2 - z^2}$ and spacetime rapidity $\eta = (1/2)\log[(t+z)/(t-z)]$. Here we summarize the calculation, leaving the full details to Ref. [41].

Using $\partial_\mu(\delta T_{id}^{\mu i} + \delta\Pi^{\mu i}) = 0$, we generalize Eq. (4.29) including the underlying expansion in the first term to obtain

$$\left(\frac{\partial}{\partial \tau} + \frac{1}{\tau}\right) M^i - \partial^i p = -\partial_\mu \delta\Pi^{\mu i}, \tag{4.35}$$

where we take $M^i = \delta T_{id}^{0i}$ for the Cartesian transverse coordinates $i = x, y$. The extra term proportional to $1/\tau$ arises in a manner similar to the calculation of the energy density in Eq.

(2.17). We also linearize the relaxation Eq. (4.27) following Ref. [45] to find

$$D\delta\Pi^{\mu i} = -\frac{1}{\tau_\pi}\left(\delta\Pi^{\mu i} - \delta S^{\mu i}\right) - \frac{\kappa}{\tau}\delta\Pi^{\mu i} \tag{4.36}$$

We generalize Eq. (4.31) by again only considering the shear contribution to obtain

$$\left(\frac{\partial}{\partial\tau} + \frac{1}{\tau}\right) g^i = -\partial_\mu \delta\Pi_T^{\mu i}, \tag{4.37}$$

where the divergence-free contribution $\delta\Pi_T^{\mu i}$ satisfies (4.36) with $\delta S^{\mu i}$ replaced by $\delta S_T^{\mu i}$. Similar to the derivation of the static background Eqs. (4.29) and (4.30) we use (4.36) and (4.37) to eliminate $\delta\Pi_T^{\mu i}$ and obtain an equation for g^i:

$$\left[\tau_\pi \frac{\partial^2}{\partial\tau^2} + \left(1 + \frac{\kappa\tau_\pi}{\tau}\right)\frac{\partial}{\partial\tau}\right]\left(g^i\tau\right) = -\nu\tilde{\nabla}^2\left(g^i\tau\right), \tag{4.38}$$

where the tilde indicates the derivative comoving with the Bjorken flow.

To find an equation analogous to (4.34) for the expanding system we define the rapidity density of total momentum $\mathcal{G}^i \equiv \int g^i\tau d^2x_\perp$ where the integral is taken over the transverse area of the two colliding nuclei. Integrating (4.38) we find

$$\left[\tau_\pi \frac{\partial^2}{\partial\tau^2} + \left(1 + \frac{\kappa\tau_\pi}{\tau}\right)\frac{\partial}{\partial\tau}\right]\mathcal{G}^i = \frac{\nu}{\tau^2}\frac{\partial^2\mathcal{G}^i}{\partial\eta^2}. \tag{4.39}$$

Having found a Maxwell-Cattaneo type equation for fluctuations above a Bjorken background, we repeat the derivation in Sec. 3.3 to obtain an evolution equation for the correlation function

$$r_{\mathcal{G}}^{ij} = \langle\mathcal{G}_1^i\mathcal{G}_2^j\rangle - \langle\mathcal{G}_1^i\rangle\langle\mathcal{G}_2^j\rangle \tag{4.40}$$

and then eliminate the noise by defining $\Delta r_{\mathcal{G}}^{ij}$, the difference of $r_{\mathcal{G}}^{ij}$ from its value in equilibrium $r_{\mathcal{G},le}^{ij}$ as in (3.59). Finally, we obtain the second order viscous diffusion equation for

transverse momentum correlations in rapidity

$$\left[\frac{\tau_\pi^*}{2}\frac{\partial^2}{\partial\tau^2}+\frac{\partial}{\partial\tau}-\frac{\nu^*}{\tau^2}\left(2\frac{\partial^2}{\partial\eta_r^2}+\frac{1}{2}\frac{\partial}{\partial\eta_a^2}\right)\right]\Delta r_{\mathcal{G}}^{ij}=0. \tag{4.41}$$

where we have changed to the relative and average rapidity coordinates $\eta_r = \eta_2 - \eta_1$ and $\eta_a = (\eta_1+\eta_2)/2$, respectively. The new starred coefficients are defined as $\tau_\pi^* = \tau_\pi/(1+\kappa\tau_\pi/\tau)$ and $\nu^* = \nu/(1+\kappa\tau_\pi/\tau)$. In deriving (4.41), we make assumptions similar to those used in the derivation of (3.59), namely that the collision system under consideration is symmetric and that the coefficients τ_π^* and ν^* vary slowly with time. For full generality we would have to solve equations analogous to (3.56) and (3.57) but this will be relegated to future work.

As noted in the discussion of (3.59), this is a hyperbolic equation that removes any concerns of causality violation. At early times, the wave-like nature of (4.41) dominates through the second-order derivative, while for $\tau \gg \tau_\pi/2$ it relaxes to the diffusion equation

$$\frac{\partial}{\partial\tau}\Delta r_{\mathcal{G}}^{ij}\approx\frac{\nu^*}{\tau^2}\left(2\frac{\partial^2}{\partial\eta_r^2}+\frac{1}{2}\frac{\partial^2}{\partial\eta_a^2}\right)\Delta r_{\mathcal{G}}^{ij}, \tag{4.42}$$

except near the wave front where the second time derivative is always important. The time variation of the coefficients as well as the explicit τ dependence affect the relaxation rate. Furthermore, the halving of the relaxation time compared to the mean behavior described by (4.34) is precisely the same behavior we saw in Brownian motion; see Eq. (3.15).

4.4 Rapidity width of $\Delta r_{\mathcal{G}}$

To conclude this chapter, we demonstrate the utility of Eq. (4.41) by using it to explore the behavior of $\Delta r_{\mathcal{G}}$, the counterpart of $\Delta r_{\mathcal{G}}^{ij}$ with i and j taken as the radial component. To keep the discussion simple, we assume the coefficients τ_π^* and ν^* to be constant. In general, one would have to solve (4.41) coupled with equations determining the behavior of the temperature T. The temperature influences the evolution of $\Delta r_{\mathcal{G}}$ through the kinematic

viscosity $\nu = \eta/Ts$, the relaxation time[1] $\tau_\pi = \beta\nu$ and the coefficient κ given by (4.28). While this behavior is important for a general analysis, it makes understanding the equations very difficult. Taking τ_π^* and ν^* constant decouples (4.41) from the temperature allowing a qualitative, although limited, analysis. We will study more realistic transport coefficients in future work.

The most important feature of $\Delta r_{\mathcal{G}}$ is its width in relative rapidity as this is sensitive to the viscosity [46]. The width has also been measured in Ref. [7]. We first define the moments of the correlation function via

$$\langle \eta_r^n \rangle = A^{-1} \int \eta_r^n \Delta r_{\mathcal{G}} d\eta_r d\eta_a \tag{4.43}$$

where A is simply used for normalization. We multiply (4.41) by η_r^n and then integrate over both η_r and η_a. To simplify, we use the identity

$$\int \eta_r^n \frac{\partial^2 \Delta r_{\mathcal{G}}}{\partial \eta_r^2} d\eta_r = n(n-1) \int \eta_r^{n-2} \Delta r_{\mathcal{G}} d\eta_r, \tag{4.44}$$

which one can show by integrating by parts and canceling the surface terms. This quantity is only nonzero for $n \geq 2$. We find

$$\left(\frac{\tau_\pi^*}{2} \frac{d^2}{d\tau^2} + \frac{d}{d\tau} \right) A \langle \eta_r^n \rangle = \frac{2\nu^*}{\tau^2} n(n-1) A \langle \eta_r^{n-1} \rangle. \tag{4.45}$$

Setting $n = 0, 1$ shows that A and $\langle \eta_r \rangle$ satisfy this equation with the right side equal to zero. Thus, we take these as constants and, furthermore, we take $\langle \eta_r \rangle = 0$ assuming a symmetric system. The rapidity width is then given by the second moment $\sigma^2 = \langle \eta_r^2 \rangle$, which satisfies

$$\left(\frac{\tau_\pi^*}{2} \frac{d^2}{d\tau^2} + \frac{d}{d\tau} \right) \sigma^2 = \frac{4\nu^*}{\tau^2}. \tag{4.46}$$

[1]This form of τ_π is inspired by kinetic theory. By varying β, we can vary τ_π while keeping the other coefficients fixed.

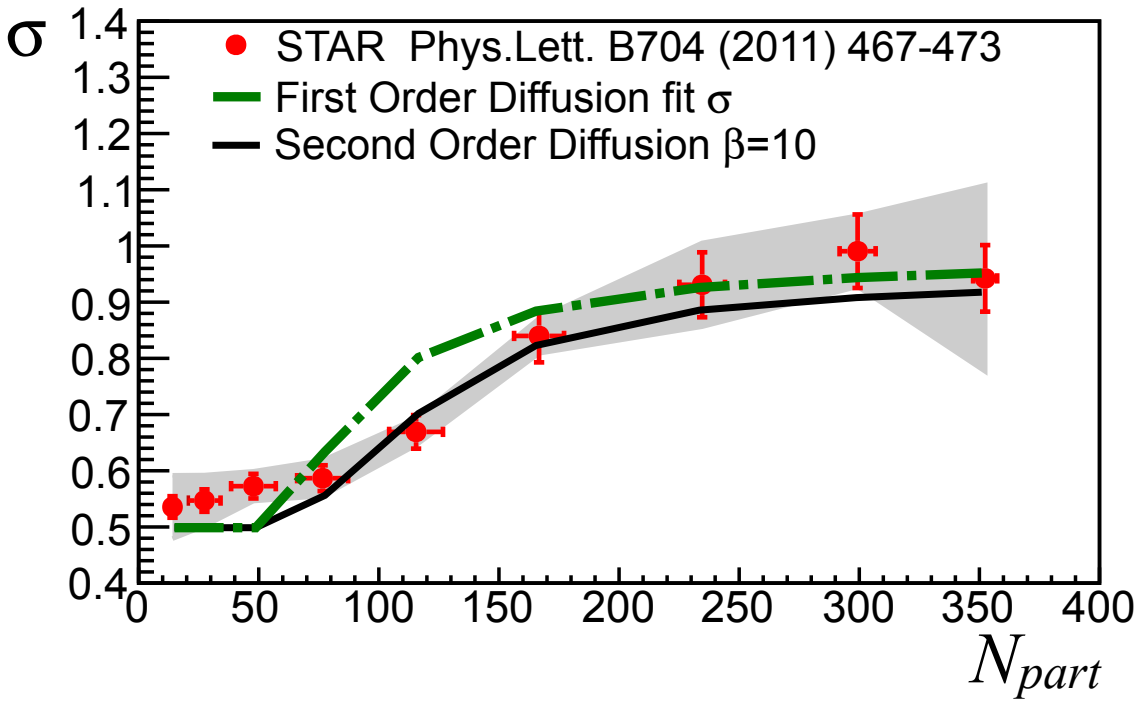

Figure 4.1: Rapidity width as a function of the number of participants for second order momentum diffusion calculations compared to first order results. Data from STAR include shaded area to denote the systematic uncertainty in the fit procedure [7].

This equation also holds for temperature and time dependent τ_π^* and ν^*, however, by taking the values constant we see that the width is a function of the lifetime of the system alone.

Equation (4.46) describes first order diffusion when $\tau_\pi^* = 0$ and $\nu^* = \nu$. In this case, we can solve (4.46) to find

$$\sigma^2 = \sigma_0^2 + \frac{4\nu}{\tau_0}\left(1 - \frac{\tau_0}{\tau}\right), \tag{4.47}$$

which reproduces the result from [46]. The width increases quickly and acausally at early times, reaching the value

$$\sigma_\infty^2 = \sigma_0^2 + \frac{4\nu}{\tau_0}. \tag{4.48}$$

That this asymptotic value depends only on the initial conditions is a consequence of the underlying Bjorken flow. In a stationary fluid, a spike in momentum diffuses with width $\sim (2\nu t)^{1/2}$. Bjorken expansion stretches the longitudinal scale $\propto t$, overtaking diffusion and freezing in the initial inhomogeneity.

In order to plot (4.47) as a function of centrality, we identify τ as the freeze out time τ_F and relate it to the number of participants N_{part}. Hydrodynamic calculations agree with τ_F increasing like the square of the rms radius of participants R [47]. To approximate this behavior we use

$$\tau_F - \tau_0 = K \left[R(N_{part}) - R_0 \right]^2 \tag{4.49}$$

where τ_0 is the formation time and R_0 is roughly the radius of a proton. We compute $R(N_{part})$ using a Glauber model. The constant K we fix so that freeze out in the most central collisions has a specified value τ_{Fc}.

First order results[2] are presented in Fig. 4.1 along with experimental measurements from [7]. The dot-dash curve represents out best fit to the data using (4.47) evaluated at τ_F, Eq. (4.49). For the kinematic viscosity $\nu = \eta/Ts$ we use the lower limit $\eta/s = 0.08$ and a freeze out temperature of $T = 140$ MeV for all centralities. We take $\tau_0 = 0.65$ fm to fix (4.48) and $\tau_F = 12$ fm to specify K in (4.49). The rapidity width in first order diffusion rises roughly with data although it is consistently above the data in the region where it grows most rapidly. This is a result of the rapid increase of (4.47) in first order diffusion.

To obtain results for second order diffusion we must solve (4.46) in full, where we take $\tau_\pi^* = \tau_\pi$ and $\nu^* = \nu$ to be constant. To do this we must specify an initial condition for $d\sigma^2/d\tau \equiv \theta_0^2$ at $\tau = \tau_0$, the value of which is unknown. In accord with the discussion surrounding (4.42) we take the initial correlation function to satisfy

$$\left.\frac{\partial \Delta r_{\mathcal{G}}}{\partial \tau}\right|_{\tau=\tau_0} = \frac{\nu_0}{\tau_0^2}\left(2\frac{\partial^2}{\partial \eta_r^2} + \frac{1}{2}\frac{\partial^2}{\partial \eta_a^2}\right)\Delta r_{\mathcal{G}}. \tag{4.50}$$

The corresponds to a value of $\theta_0^2 = 4\nu/\tau_0^2$. We then integrate (4.46) twice to find

$$\sigma^2 = \sigma_0^2 + \frac{\theta_0^2 \tau_\pi}{2}\left(1 - e^{-2(\tau-\tau_0)/\tau_\pi}\right) + \frac{8\nu}{\tau_\pi}\int_{\tau_0}^{\tau} du \int_{\tau_0}^{u} \frac{ds}{s^2} e^{2(s-u)/\tau_\pi}. \tag{4.51}$$

[2]In order to demonstrate the usefulness of Eq. (4.41), I present our results from [41]. However, I wish to acknowledge that Fig. 4.1 was created by the coauthors.

The solid black curve in Fig. 4.1 shows this value at the freeze out time (4.49). We again use the limiting value of $\eta/s = 0.08$ but now choose the freeze out temperature $T = 150$ MeV for all centralities. Best fit occurs for $\tau_0 = 1.0$ fm and $\tau_{Fc} = 10$ fm. For the relaxation time $\tau_\pi = \beta\nu$ we find excellent agreement with data by taking $\beta = 10$.

We hesitate to draw any solid conclusions from this prediction on account of the strong approximations we have made, in particular regarding the variation of the coefficients τ_π^* and ν^*. However, this schematic calculation offers insight into the role that momentum correlations play in the physics of ion collisions. After the introduction of the observable $\mathcal{C}$, we will return briefly to Eq. (4.41), in Sec. 6.5, to further discuss transverse momentum correlations.

CHAPTER 5 KINETIC THEORY

The Boltzmann equation describes the evolution of a thermodynamic system toward an equilibrium state due to a combination of diffusion and scattering processes as well as any outside forces applied to the system. Applications are numerous and span many fields from particle transport in plasmas and superfluids to radiative transfer in planetary atmospheres. As the initial state is not assumed to be in local equilibrium, it is also one of the few tools available for studying the non-equilibrium aspects of ion collisions [48–62]. Nevertheless, it is not ideal for two reasons we tackle in this chapter.

Firstly, as a nonlinear integro-differential equation, the full Boltzmann equation can be quite difficult to solve, even numerically. To overcome this obstacle we make assumptions on the types of solutions allowed as well as on the effect collisions have on the system. Care must be taken when making these assumptions to not break desirable system properties, in particular the conservation laws. While many of the assumptions we make are common when dealing with the Boltzmann equation, we introduce a novel way to enforce the conservation laws. Furthermore, while these approximate methods may not describe an evolving system in as much detail as the full equation, they do allow for exact solutions to be found and offer physical insight into the processes involved.

Secondly, the standard form of the Boltzmann equation has no mechanism for describing correlations. The molecular chaos ansatz, or Stosszahlansatz, assumes that particles are uncorrelated prior to collision. As our entire end goal is to describe two-particle correlations, due in part to collisions, we are compelled to introduce such a mechanism. Our method is to add Langevin noise to the Boltzmann equation, consistent with the conservation laws obeyed by the microscopic scattering processes [63–65]. Our result, Eq. (5.60), is a new relativistic transport equation for the two-body distribution function.

5.1 Boltzmann equation

The evolution of the QGP system is characterized by the single particle phase space distribution function $f(\mathbf{x}, \mathbf{p}, t)$, which gives the density of partons in the system at time t

and phase space position $(\mathbf{x}, \mathbf{p})$:

$$f(\mathbf{x}, \mathbf{p}, t) = \frac{dN}{d^3\mathbf{x}d^3\mathbf{p}} \tag{5.1}$$

To describe an expanding QGP we need to use the covariant form of the Boltzmann equation but for the time being we focus on the local rest frame where, using the Landau-Lifschitz velocity, the momentum density vanishes. In this frame the evolution of $f(\mathbf{x}, \mathbf{p}, t)$ is described by the kinetic equation

$$\frac{\partial}{\partial t} f(\mathbf{x}, \mathbf{p}, t) + \mathbf{v}_\mathbf{p} \cdot \nabla f(\mathbf{x}, \mathbf{p}, t) = I\{f\}, \tag{5.2}$$

where $\mathbf{v}_\mathbf{p} = \mathbf{p}/E$ is the single particle particle velocity. The left side of Eq. (5.2) describes the free streaming (collision-free) evolution of the system. One can write the left side as df/dt, describing the drift of particles at constant velocity $\mathbf{v}_\mathbf{p}$ between collisions.

Collisions cause f to evolve to the local thermal equilibrium form f^e. The collision term on the right side of Eq. (5.2) describes the effect of collisions on the evolution of $f(\mathbf{x}, \mathbf{p}, t)$. In principle it must contain the effect of all possible $m \rightleftharpoons n$ body scattering processes. For $2 \to 2$ elastic scattering of a single parton species we have

$$I\{f\} = \int W_{12\to34} \left(f_3 f_4 - f_1 f_2\right) d\mathbf{p}_2 d\mathbf{p}_3 d\mathbf{p}_4, \tag{5.3}$$

where $f_i = f(\mathbf{x}, \mathbf{p}_i, t)$, $d\mathbf{p} = d^3p/(2\pi)^3$ and the scattering rate $W_{12\to34} \propto \delta(p_1^\mu + p_2^\mu - p_3^\mu - p_4^\mu)$. This form of the collision integral relies on the molecular chaos assumption. As such, particles are assumed to be uncorrelated prior to their collisions. To more accurately describe correlations, one could replace the products $f_i f_j$ with two-particle distributions. Our approach in Sec. 5.4 will be to add Langevin noise in order to introduce correlations, similar to the previous chapters.

Energy and momentum conservation during collisions forces the moments of $I\{f\}$ with

respect to E and $\mathbf{p}$ to vanish. Furthermore, since elastic collisions conserve particle number, the momentum integral of $I\{f\}$ also vanishes. We write these conservation conditions succinctly as

$$\int d\mathbf{p} \begin{Bmatrix} 1 \\ \mathbf{p} \\ E \end{Bmatrix} I\{f\} = 0. \tag{5.4}$$

Equation (5.3) also determines the local equilibrium distribution which, assuming Boltzmann statistics, has the form

$$f^e = e^{-\gamma(E-\mathbf{p}\cdot\mathbf{v}-\mu)/T}, \tag{5.5}$$

where $\gamma = (1-v^2)^{-1/2}$. The temperature T, fluid velocity $\mathbf{v}$ and chemical potential μ can vary in space and time. We note that the Boltzmann distribution is an appropriate choice for an equilibrium distribution in the context of ion collisions as a result of most hadrons having a large enough mass to be treated as classical particles – experimental support for this claim can be found in Refs. [31, 32].

5.2 Relaxation time approximation

To simplify calculations we employ the relaxation time approximation. In this approximation we estimate the collision term as

$$I\{f\} \approx -\nu(f - f^e) \tag{5.6}$$

and write the Boltzmann equation as

$$\frac{\partial}{\partial t} f(\mathbf{x},\mathbf{p},t) + \mathbf{v}_\mathbf{p} \cdot \nabla f(\mathbf{x},\mathbf{p},t) = -\nu \left(f(\mathbf{x},\mathbf{p},t) - f^e(\mathbf{x},\mathbf{p},t) \right). \tag{5.7}$$

This approximation assumes that collisions always serve to restore f to its local equilibrium form. Ignoring the streaming terms for a moment and noticing that f^e solves the equation we see

$$\frac{\partial}{\partial t}(f - f^e) = -\nu(f - f^e) \qquad \Rightarrow \qquad (f - f^e) = (f - f^e)_0 e^{-\nu t}, \tag{5.8}$$

so that the relaxation time ν^{-1} sets the scale for this process[1]. In general ν^{-1} is determined by the microscopic scattering processes and can be momentum dependent.

The conservation laws, previously enforced by the scattering rate W_{12}, no longer hold true in this equation. For example, the number of particles determined by f is not forced to be equal to that of f^e and, in fact, $\langle N \rangle$ would relax to the equilibrium value $\langle N \rangle_e$ on the time scale ν^{-1}. To be consistent with these laws we must explicitly require that Eq. (5.4) hold:

$$\int d\mathbf{p} \begin{Bmatrix} 1 \\ \mathbf{p} \\ E \end{Bmatrix} f = \int d\mathbf{p} \begin{Bmatrix} 1 \\ \mathbf{p} \\ E \end{Bmatrix} f^e. \tag{5.9}$$

The effect of this condition is to constrain the values of T, μ and $\mathbf{v}$ in f^e at each space-time point. Note that Eq. (5.9) contains a set of highly non-linear constraints which, in general, can be quite difficult to enforce.

The covariant form of Eq. (5.7) can be written as

$$p^\mu \partial_\mu f = -\nu p \cdot u \left(f - f^e \right), \tag{5.10}$$

where the fluid four-velocity is $u^\mu = \gamma(1, \mathbf{v})$ and $p \cdot u \equiv p^\mu u_\mu$ with the metric $g^\mu = \mathrm{diag}(1, -1, -1, -1)$. In the local rest frame, where $u^\mu = (1, 0, 0, 0)$, this reduces to Eq. (5.7) and ν^{-1} corresponds to the mean free time between parton collisions.

To find a solution of Eq. (5.10) we will use the method of characteristics, commonly used to solve the nonrelativistic Boltzmann equation [66, 67]. To start we simplify the equation by introducing a proper time parameter τ defined via

$$\frac{dx^\mu}{d\tau} = \frac{p^\mu}{p \cdot u}. \tag{5.11}$$

In the rest frame of the fluid it is clear that $p \cdot u = E$, so the time component of Eq. (5.11) is simply $dt/d\tau = 1$ in this frame. This implies that τ is the time in the rest frame – i.e.

[1] In our equations we prefer to use the collision frequency ν rather than the eponymous relaxation time, commonly written $\tau = 1/\nu$, mostly for aesthetic purposes.

the proper time. Equation (5.11) is a characteristic equation for the original equation and defines characteristic curves $x^\mu(\tau)$. Along these curves we can write the Boltzmann equation as

$$\frac{d}{d\tau} f(\mathbf{x}(\tau), \mathbf{p}, \tau) = -\nu(f - f^e), \tag{5.12}$$

where we have divided by $p \cdot u$ and used Eq. (5.11).

Reducing the Boltzmann equation to a first order ODE allows us to find solutions for f. In the free streaming case, where we take $\nu = 0$, we find $f(\mathbf{x}(\tau), \mathbf{p}, \tau) = f_0(\mathbf{x}_0, \mathbf{p})$, for the initial distribution f_0. Moreover, the spatial components of Eq. (5.11) imply that partons in a cell initially at $\mathbf{x}_0$ drift unchanged along the path $\mathbf{x} = \mathbf{x}_0 + \mathbf{v}_\mathbf{p} t$. Thus, we find

$$f(\mathbf{x}(\tau), \mathbf{p}, \tau) = f_0(\mathbf{x} - \mathbf{v}_\mathbf{p} t, \mathbf{p}), \qquad \text{free streaming} \tag{5.13}$$

where t can be found as a function of τ using $dt/d\tau = E/p \cdot u$. Note that Eq. (5.13) is a solution of Eq. (5.2) with $I\{f\} = 0$.

Allowing collisions, we now consider Eq. (5.12) in full. To simplify calculations we define the survival probability

$$S(\tau, \tau_0) = \exp\left\{ -\int_{\tau_0}^{\tau} \nu(\tau') d\tau' \right\}, \tag{5.14}$$

which gives the probability partons suffer no collisions as they travel along their characteristic paths – see Sec. A.3. Multiplying (5.12) by the integrating factor $\theta = \theta_0 S^{-1}$ we have

$$\begin{aligned} \theta \frac{df}{d\tau} + \theta \nu f &= \nu \theta f^e \\ \frac{d}{d\tau}(\theta f) &= \nu \theta f^e \\ \theta f &= \theta_0 f_0 + \int_{\tau_0}^{\tau} \nu(\tau') \theta(\tau') f^e d\tau'. \end{aligned} \tag{5.15}$$

The full solution can then be written as

$$f(\mathbf{x},\mathbf{p},\tau) = f_0(\mathbf{p},\mathbf{x}-\mathbf{v}_p t)S(\tau,\tau_0) + \int_{\tau_0}^{\tau} \nu(\tau')S(\tau,\tau')f^e(\mathbf{p},\mathbf{x}-\mathbf{v}_p t')d\tau', \tag{5.16}$$

where $t = t(\tau)$ and $t' = t(\tau')$ are determined via Eq. (5.11). Computing (5.16) can be difficult in practice as we must specify the parameters T, $\mathbf{v}$ and μ as a function of time by enforcing the nonlinear constraints in Eq. (5.9). Note that Baym approached this single particle distribution problem in a different manner but obtained equivalent results [48]. In particular, Eq. (5.16) matches Baym's Eq. (17).

5.3 Linearized Boltzmann equation

To further simplify this calculation we will use the linearized versions of these equations. We expand $f \approx f^e(1+h)$ for a small perturbation $h \ll 1$. The distribution functions in the collision term, Eq. (5.3), then satisfy

$$\begin{aligned} f_3 f_4 - f_1 f_2 &\approx f_3^e f_4^e (1+h_3)(1+h_4) - f_1^e f_2^e (1+h_1)(1+h_2) \\ &= f_1^e f_2^e (h_3 + h_4 - h_1 - h_2) + \mathcal{O}(h^2), \end{aligned} \tag{5.17}$$

where $h_i = h(\mathbf{x},\mathbf{p}_i,\tau)$. In the second line we use $f_3^e f_4^e = f_1^e f_2^e$, which is true of the equilibrium distributions as they satisfy detailed balance. The full collision term, to linear order in h, is given by

$$I\{f\} = \int W_{12\to 34} f_1^e f_2^e (h_3 + h_4 - h_1 - h_2) d\mathbf{p}_2 d\mathbf{p}_3 d\mathbf{p}_4 = f_1^e L h \tag{5.18}$$

and, thus, the full linearized Boltzmann equation is

$$\frac{dh}{d\tau} = Lh. \tag{5.19}$$

The operator L is linear on h and satisfies the eigenequations

$$L\phi_\alpha = -\nu_\alpha \phi_\alpha \tag{5.20}$$

for eigenfunctions $\phi_\alpha(\mathbf{p})$ and eigenvalues ν_α. We associate the first five eigenfunctions with the collisional invariants 1, $\mathbf{p}$ and E. These eigenfunctions have eigenvalue zero as a result of the conservation laws and are linear in the conserved quantities. The other eigenvalues must be positive in order for f to relax to f^e. We may also choose an orthonormal set of ϕ_α, the first five of which can be written

$$\phi_1 = 1, \qquad \phi_{2,3,4} = \sqrt{\frac{n}{wT}}\mathbf{p}, \qquad \phi_5 = \sqrt{\frac{n}{c_v T}}\left(E - \frac{e}{n}\right), \tag{5.21}$$

where n is particle density, w is enthalpy density, e is energy density and c_v is specific heat. They are orthonormal in the sense that

$$\int d\mathbf{p}\frac{f^e}{n}\phi_\alpha\phi_\beta = \delta_{\alpha\beta}. \tag{5.22}$$

As an example for ϕ_1 and ϕ_2, one can check

$$\int d\mathbf{p}\frac{f^e}{n}\left(1\cdot\sqrt{\frac{n}{wT}}p_x\right) = \sqrt{\frac{n}{wT}}\langle p_x\rangle = 0 \qquad \text{and} \tag{5.23}$$

$$\frac{n}{wT}\int d\mathbf{p}\frac{f^e}{n}\left(p_x\cdot p_x\right) = \frac{n}{wT}\langle p_x^2\rangle = 1. \tag{5.24}$$

Equation (5.23) follows from conservation of momentum, while Eq. (5.24) can be calculated using (5.5) as in [68].

For the linearization $f - f^e \approx f^e h$, the conservation conditions for the relaxation time approximation – Eq. (5.9) – becomes

$$\int d\mathbf{p}\phi_\alpha f^e h = 0 \qquad \text{for} \qquad \alpha = 1, ..., 5, \tag{5.25}$$

so that the collisional invariants are orthogonal to the perturbation h. Note that, as was the case in the relaxation time approximation, Eq. (5.25) is required to enforce the conservation laws. Notice, also, that the linearized way of enforcing the conservation conditions does not

specify values of T, $\mathbf{v}$ and μ as was the case with the original Eq. (5.4) but in contrast to the relaxation time approximation Eq. (5.9). We can specify values for the local equilibrium parameters in (5.5) by requiring that f^e satisfy the free streaming equation

$$\frac{df^e}{d\tau} = 0, \tag{5.26}$$

where T, $\mathbf{v}$ and μ will depend on position along the curve $\mathbf{x}^\mu(\tau)$ from Eq. (5.11).

The linearized evolution of f^e describes the flow of a dissipation-free fluid. Starting with the covariant version of Eq. (5.2) we integrate over momentum and enforce Eq. (5.4) to get

$$\int d\mathbf{p} p^\mu \partial_\mu f = \int d\mathbf{p} I\{f\} \qquad \Rightarrow \qquad \partial_\mu j^\mu = 0, \tag{5.27}$$

where the parton current is $j^\mu = \int d\mathbf{p} f p^\mu / E = n u^\mu$ for parton density n. Multiplying (5.2) by p^ν and integrating over momentum gives

$$\int d\mathbf{p} p^\nu p^\mu \partial_\mu f = \int d\mathbf{p} p^\nu I\{f\} \qquad \Rightarrow \qquad \partial_\mu T^{\mu\nu} = 0, \tag{5.28}$$

where we have enforced Eq. (5.4) and $T^{\mu\nu} = \int d\mathbf{p} f p^\mu p^\nu / E$ is the stress-energy tensor. When $f = f^e$, $T^{\mu\nu}$ is the stress-energy tensor for an ideal dissipation-free fluid

$$T^{\mu\nu}_{id} = (e + P) u^\mu u^\nu - P g^{\mu\nu}, \tag{5.29}$$

where P is the pressure of an ideal Boltzmann gas. Equations (5.27) and (5.28) thus match the Euler equations for relativistic dissipation-free flow. Note that this is not the case for the full distribution f which includes dissipation at linear order.

In the relaxation time approximation we assume that all the quantities relevant to the distribution function f relax at the same rate ν^{-1}. The eigenvalues of L describe the relaxation of the modes. One can see this most simply by noticing that Eq. (5.19) implies we

can write h generally as

$$h(\mathbf{x}, \mathbf{p}, \tau) = \sum_{\alpha>5} c_\alpha(\mathbf{x})\phi_\alpha(\mathbf{p})e^{-\nu_\alpha \tau}. \tag{5.30}$$

If we assume all the eigenfunctions of L with nonzero eigenvalue relax at the same rate – i.e. $\nu_\alpha = \nu$ for $\alpha > 5$ – we find that

$$\frac{df}{d\tau} = f^e L h = -\nu f^e h = -\nu(f - f^e). \tag{5.31}$$

Therefore, this assumption reproduces the relaxation time approximation.

As previously mentioned, the conservation conditions are not explicitly enforced in the relaxation time approximation or for the linearized Boltzmann equation since there is no guarantee, a priori, that f and f^e will produce the same quantities – e.g. particle number, energy density. To explicitly enforce these conditions we write the collision term as

$$I\{f\} \approx -\nu(1 - P)f(\mathbf{x}, \mathbf{p}, t), \tag{5.32}$$

where P is a projection operator that projects f into the corresponding local equilibrium distribution f^e. We define

$$P\psi(\mathbf{p}) = \frac{f^e(\mathbf{p})}{n} \sum_{\alpha=1}^{5} \phi_\alpha(\mathbf{p}) \int d\mathbf{p}' \phi_\alpha(\mathbf{p}')\psi(\mathbf{p}'), \tag{5.33}$$

where ψ is an arbitrary function of momentum. To prove P is a projection operator we show

$P^2 = P$:

$$\begin{aligned}
P^2\psi(\mathbf{p}) &= \frac{f^e(\mathbf{p})}{n}\sum_{\alpha=1}^{5}\phi_\alpha(\mathbf{p})\int d\mathbf{p}'\phi_\alpha(\mathbf{p}')P\psi(\mathbf{p}') \\
&= \frac{f^e(\mathbf{p})}{n}\sum_{\alpha=1}^{5}\phi_\alpha(\mathbf{p})\int d\mathbf{p}'\phi_\alpha(\mathbf{p}')\left(\frac{f^e(\mathbf{p}')}{n}\sum_{\beta=1}^{5}\phi_\beta(\mathbf{p}')\int d\mathbf{p}''\phi_\beta(\mathbf{p}'')\psi(\mathbf{p}'')\right) \\
&= \frac{f^e(\mathbf{p})}{n}\sum_{\alpha=1}^{5}\phi_\alpha(\mathbf{p})\left(\sum_{\beta=1}^{5}\int d\mathbf{p}'\frac{f^e(\mathbf{p}')}{n}\phi_\alpha(\mathbf{p}')\phi_\beta(\mathbf{p}')\right)\int d\mathbf{p}''\phi_\beta(\mathbf{p}'')\psi(\mathbf{p}'') \\
&= \frac{f^e(\mathbf{p})}{n}\sum_{\alpha=1}^{5}\phi_\alpha(\mathbf{p})\left(\sum_{\beta=1}^{5}\delta_{\alpha\beta}\right)\int d\mathbf{p}''\phi_\beta(\mathbf{p}'')\psi(\mathbf{p}'') \\
&= \frac{f^e(\mathbf{p})}{n}\sum_{\alpha=1}^{5}\phi_\alpha(\mathbf{p})\int d\mathbf{p}''\phi_\alpha(\mathbf{p}'')\psi(\mathbf{p}'') \\
&= P\psi(\mathbf{p}),
\end{aligned} \tag{5.34}$$

where we use the orthonormality condition (5.22) to go from line 3 to line 4. Note that as a projection operator P also satisfies $P(1-P) = 0$ and $(1-P)^2 = 1-P$.

In light of Eq. (5.32) one would expect $Pf = f^e$. This is true to linear order as we now show. Note that Eq. (5.25) implies $\int \phi f = \int \phi f^e$ for the first five eigenfunctions and we use $\phi_1 = 1$. Then,

$$\begin{aligned}
Pf(\mathbf{p}) &= \frac{f^e(\mathbf{p})}{n}\sum_{\alpha=1}^{5}\phi_\alpha(\mathbf{p})\int d\mathbf{p}'\phi_\alpha(\mathbf{p}')f(\mathbf{p}') \\
&= \frac{f^e(\mathbf{p})}{n}\sum_{\alpha=1}^{5}\phi_\alpha(\mathbf{p})\int d\mathbf{p}'\phi_\alpha(\mathbf{p}')f^e(\mathbf{p}') \\
&= f^e(\mathbf{p})\sum_{\alpha=1}^{5}\phi_\alpha(\mathbf{p})\int d\mathbf{p}'\frac{f^e(\mathbf{p}')}{n}\phi_\alpha(\mathbf{p}')\phi_1(\mathbf{p}') \\
&= f^e(\mathbf{p})\sum_{\alpha=1}^{5}\phi_\alpha(\mathbf{p})\delta_{\alpha 1} \\
&= f^e(\mathbf{p})\phi_1(\mathbf{p}) = f^e(\mathbf{p}).
\end{aligned} \tag{5.35}$$

Thus, $Pf = f^e$ with corrections beyond linear order. We then write the linearized Boltzmann

equation in the relaxation time approximation as

$$\frac{df}{d\tau} = -\nu(1-P)f \tag{5.36}$$

The power of P lies in enforcement of the conservation conditions. The usefulness of P is that it allows for convenience in calculations as we now demonstrate with another proof that $Pf = f^e$. First we note that as an operator P commutes with $d/d\tau$ because of (5.33) with (5.26). Specifically, Eq. (5.26) shows that f^e is constant with respect to τ. Thus, outside of ψ, Eq. (5.33) has no τ dependence and we have

$$\begin{aligned} P\frac{d}{d\tau}\psi(\mathbf{p}) &= \frac{f^e(\mathbf{p})}{n}\sum_{\alpha=1}^{5}\phi_\alpha(\mathbf{p})\int d\mathbf{p}'\phi_\alpha(\mathbf{p}')\frac{d}{d\tau}\psi(\mathbf{p}') \\ &= \frac{d}{d\tau}\frac{f^e(\mathbf{p})}{n}\sum_{\alpha=1}^{5}\phi_\alpha(\mathbf{p})\int d\mathbf{p}'\phi_\alpha(\mathbf{p}')\psi(\mathbf{p}') \\ &= \frac{d}{d\tau}P\psi(\mathbf{p}). \end{aligned} \tag{5.37}$$

Using Eq. (5.32) we approximate the linearized Boltzmann equation as $df/d\tau = -\nu(1-P)f$ (which matches (5.36) but we have yet to prove $Pf = f^e$ on the second go around!). Multiplying both sides by P and using $P(1-P) = 0$ gives

$$P\frac{d}{d\tau}f = -\nu P(1-P)f \qquad \Rightarrow \qquad \frac{d}{d\tau}Pf = 0. \tag{5.38}$$

Thus, Pf is constant with respect to τ and using (5.26) we can identify it with f^e which, again, holds to linear order.

Another example of the convenience afforded by P in seen when multiplying Eq. (5.36) by $1-P$. On the left hand side we commute $1-P$ with $d/d\tau$ and on the right hand side we use $(1-P)^2 = 1-P$. We find

$$\frac{d}{d\tau}(1-P)f = -\nu(1-P)f \qquad \Rightarrow \qquad (1-P)f = (1-P)f_0 S(\tau,\tau_0), \tag{5.39}$$

where S is given by (5.14). This solution assumes ν is independent of $\mathbf{p}$ which need not always be true. Rearranging (5.39) we find a solution to the Boltzmann equation:

$$f = f_0(\mathbf{x} - \mathbf{v_p}t, \mathbf{p})S(\tau, \tau_0) + f^e(\mathbf{x} - \mathbf{v_p}t, \mathbf{p})(1 - S(\tau, \tau_0)), \tag{5.40}$$

where $t = t(\tau)$ as in Eq. (5.16). We note that we can check the legitimacy of this result by comparing with a solution found without using P, specifically Eq. (5.16). Equation (5.26) implies the linearized f^e is constant in τ so integrating (5.16) by parts gives (5.40).

We use the linearized relaxation time approximation moving forward because it provides a simple description of transport that incorporates the conservation laws effectively. While it might not describe the first instants of pre-equilibrium evolution as effectively as the full relaxation time approximation or the full Boltzmann equation, none of these approaches is fully reliable at that stage.

5.4 Considering correlations

Scattering causes the relaxation processes described by the collision terms in Eqs. (5.3) and (5.6). Additionally, scattering causes stochastic fluctuations of the phase space distribution which give rise to correlations aside from those already present in the initial conditions. The Boltzmann equation is insufficient to describe these correlations because the assumption of molecular chaos presupposes that particles are uncorrelated prior to their collisions. Our goal in this section will be to describe these additional correlations using a Langevin model as in previous chapters. We characterize these correlations with the function

$$C_{12} \equiv C(\mathbf{x}_1, \mathbf{p}_1, \mathbf{x}_2, \mathbf{p}_2, t) = \langle f_1 f_2 \rangle - \langle f_1 \rangle \langle f_2 \rangle \tag{5.41}$$

where $f_i = f(\mathbf{x}_i, \mathbf{p}_i, t)$ and the brackets refer to the noise average from Chapter 3.

To add Langevin noise to the linearized Boltzmann equation we divide phase space into discrete cells. The action of collisions randomly transfers momentum between particles in these cells and, thus, causes the phase space distribution to fluctuate. To describe this

process we write Eq. (5.36) as a difference equation

$$f(\tau + \Delta\tau) - f(\tau) \equiv \Delta f = -\nu(1 - P)f(\tau)\Delta\tau + \Delta W, \tag{5.42}$$

where ΔW is the stochastic increment to the distribution f at the phase space point $(\mathbf{x}, \mathbf{p})$ in the time from τ to $\tau + \Delta\tau$. As before, these increments vanish upon noise averaging and are correlated via the relation

$$\langle \Delta W(\mathbf{x}_1, \mathbf{p}_1)\Delta W(\mathbf{x}_2, \mathbf{p}_2)\rangle = \Gamma_{12}\Delta\tau. \tag{5.43}$$

To obtain the equation for the linearized phase space distribution $\langle f\rangle$ we average Eq. (5.42) over the noise to find

$$\langle f(\tau + \Delta\tau)\rangle - \langle f(\tau)\rangle = -\nu(1 - P)\langle f(\tau)\rangle\Delta\tau \tag{5.44}$$

which, in the limit $\Delta\tau \to 0$, can be written

$$\frac{d}{d\tau}\langle f\rangle = -\nu(1 - P)\langle f\rangle. \tag{5.45}$$

This reproduces Eq. (5.36) for the one-body distribution. Thus, while the stochastic contribution alters f, in the long time limit, $\langle f\rangle$ follows the solution (5.40). In particular, the noise term has no effect on the mean. Later we will briefly consider the more general situation that $\langle f\rangle$ satisfies the nonlinear equation.

We emphasize that, due to its definition, each linearized f in the noise averaged $\langle f\rangle$ has the same initial conditions. Thus, each f corresponds to the same local equilibrium f^e and for each f we have $Pf = f^e$. The linearized evolution of f^e follows from the Euler equations as shown in Eqs. (5.27) and (5.28). Similarly, drift follows the deterministic curves $x^\mu(\tau)$ of the method of characteristics. Both f^e and the curves can differ from event to event.

We now follow the procedure of Chapter 3 to construct an equation for the correlation function (5.41). We take the product of f's at two phase space points and use the Itô product rule with (5.42) and (5.43) to find

$$\begin{aligned}\Delta\langle f_1 f_2\rangle &= \langle f_2 \Delta f_1\rangle + \langle f_1 \Delta f_2\rangle + \langle \Delta f_1 \Delta f_2\rangle \\ &= \langle f_2[-\nu(1-P_1)f_1\Delta\tau + \Delta W_1]\rangle + \langle f_1[-\nu(1-P_2)f_2\Delta\tau + \Delta W_2]\rangle + \langle \Delta W_1 \Delta W_2\rangle \\ &= -\nu\left[(1-P_1)+(1-P_2)\right]\langle f_1 f_2\rangle\Delta\tau + \Gamma_{12}\Delta\tau, \end{aligned} \tag{5.46}$$

where the projection P_i acts on the corresponding distribution f_i. The product $\Delta(\langle f_1\rangle\langle f_2\rangle)$ averages out any noise contribution and we have

$$\Delta(\langle f_1\rangle\langle f_2\rangle) = -\nu\left[(1-P_1)+(1-P_2)\right]\langle f_1\rangle\langle f_2\rangle\Delta\tau \tag{5.47}$$

We combine these equations and take $\Delta\tau \to 0$ to find a differential equation for C_{12}:

$$\left(\frac{d}{d\tau} + \nu(1-P_1) + \nu(1-P_2)\right) C_{12} = \Gamma_{12}. \tag{5.48}$$

The flaw with the correlation function C_{12} is that the pair of particles described by f_1 and f_2 may, in fact, be the same particle. To describe distinct particle pairs we subtract off this possibility and write

$$G_{12} = C_{12} - \langle f_1\rangle\delta(1-2) \tag{5.49}$$

where we abbreviate $\delta(1-2) = \delta(\mathbf{x}_1 - \mathbf{x}_2)\delta(\mathbf{p}_1 - \mathbf{p}_2)$. The quantity G_{12} compares the phase space density of distinct pairs, $\langle f_1 f_2\rangle - \langle f_1\rangle\delta(1-2)$, to the Poisson expectation, $\langle f_1\rangle\langle f_2\rangle$, in the absence of correlations. In principle, one can measure G_{12} by just counting pairs of particles. To find an equation for G_{12} we simply subtract the same particle contribution from (5.48)

$$\left(\frac{d}{d\tau} + \nu(1-P_1) + \nu(1-P_2)\right) G_{12} = \Gamma'_{12}. \tag{5.50}$$

where the noise terms Γ'_{12} and Γ_{12} are related by

$$\Gamma'_{12} = \Gamma_{12} - \left(\frac{d}{d\tau} + 2\nu(1-P_1)\right)\langle f_1\rangle\delta(1-2). \tag{5.51}$$

In practice we prefer to study the pair correlation function G_{12} as it vanishes in local equilibrium for sufficiently large systems. In the grand canonical ensemble, the number of particles in equilibrium fluctuates following Poisson statistics, i.e. the variance in number of particles equals the mean, $\langle N^2\rangle - \langle N\rangle^2 = \langle N\rangle$. Correspondingly the equilibrium phase space correlations $(\langle f_1 f_2\rangle - \langle f_1\rangle\langle f_2\rangle)^e$ tend to the Poissonian expectation $\langle f_1\rangle\delta(1-2)$ and G_{12} vanishes.

The projection operators allow us a convenient method to study the noise terms Γ_{12} and Γ'_{12}. We can infer the form of Γ_{12} from first principles. First, the local nature of the stochastic fluctuations implies that ΔW_1 and ΔW_2 are uncorrelated for different phase space cells. As a result, we expect Γ_{12} to be singular at points $(\mathbf{x}_1, \mathbf{p}_1) = (\mathbf{x}_2, \mathbf{p}_2)$ as the cell size tends to zero and to vanish otherwise. Second, Eq. (5.48) shows that Γ_{12} is a source of correlations due to collisions. Since detailed balance applies to the equilibrium state, the contribution to the evolution of f due to scattering should be zero, $(\partial f/\partial t)_{coll} \equiv 0$, and thus Γ_{12} should vanish in equilibrium. Therefore, we can explicitly include the two orthogonal projections $(1-P_1)(1-P_2)$ when writing Γ_{12}. In full we should have

$$\Gamma_{12} = (1-P_1)(1-P_2)a_1\delta(1-2), \tag{5.52}$$

where a_1 is a function yet to be determined. In particular, notice this form implies $P_i\Gamma_{12} = 0$ and $(1-P_i)\Gamma_{12} = \Gamma_{12}$. Thus, we can combine this with (5.48) and multiply by P_1P_2 to find

$$\frac{d}{d\tau}P_1P_2C_{12} = 0 \equiv \frac{d}{d\tau}C^e_{12}, \tag{5.53}$$

where we define the equilibrium correlation function $C^e_{12} \equiv P_1P_2C_{12}$ and use the property

$P(1-P)=0$.

We can use the fluctuation-dissipation theorem, as in Chapter 3, to determine Γ_{12}. We give two examples. First, we start by considering a uniform system close to equilibrium, such that $\langle f\rangle \approx f^e$. In equilibrium, the time derivative in (5.48) must vanish, so we can write

$$\Gamma_{12} \approx [\nu(1-P_1)+\nu(1-P_2)]C^e_{12}. \tag{5.54}$$

We now multiply both sides by $(1-P_1)(1-P_2)$. The form (5.52) shows the left side is unaffected. For the right side we have

$$[\nu(1-P_2)(1-P_1)^2+\nu(1-P_1)(1-P_2)^2]C^e_{12} = 2\nu(1-P_1)(1-P_2)C^e_{12}. \tag{5.55}$$

The discussion after Eq. (5.51) shows $C^e_{12} = \langle f_1\rangle\delta(1-2)$ so altogether we write

$$\Gamma_{12} = 2\nu(1-P_1)(1-P_2)\langle f_1\rangle\delta(1-2). \tag{5.56}$$

In this example we find $a_1 = 2\nu\langle f_1\rangle$. In the case where this system is in equilibrium, $\langle f_1\rangle = f^e$, and this quantity vanishes by virtue of the projections. However, this is the correct general structure.

For the second example we look at the other end of the spectrum. Consider the steady state behavior of a system that cannot equilibrate due to large gradients caused by, for example, fixed boundary conditions. Here, the τ derivatives in (5.48) and (5.50) do not vanish since they contain contributions from the gradients, $d/d\tau = \partial/\partial\tau + \mathbf{v}_1\cdot\nabla_1 + \mathbf{v}_2\cdot\nabla_2$. Furthermore, the large gradients conflict with the assumptions of the linearized approach so we must use the non-linearized relaxation time approximation (5.12). In this case $Pf \neq f^e$. We multiply Eq. (5.51) by P_1P_2 and use (5.52) to find

$$P_1P_2\Gamma'_{12} = \frac{d}{d\tau}P_1P_2\Gamma_{12} - P_1P_2\frac{d}{d\tau}\langle f_1\rangle\delta(1-2) = \nu P_1P_2(\langle f_1\rangle - f^e)\delta(1-2) \tag{5.57}$$

For the last equality we must use the full (5.12) to evaluate the derivative because the constrained system is never close to equilibrium. In accord with the fluctuation-dissipation theorem we equate these equilibrium fluctuations to the non-equilibrium fluctuations and write

$$\Gamma'_{12} = \nu P_1 P_2(\langle f_1\rangle - f^e)\delta(1-2) \tag{5.58}$$

We then multiply Eq. (5.51) by $1 - P_1$ to obtain

$$\begin{aligned}\Gamma_{12} &= (1-P_1)\Gamma'_{12} - \nu(1-P_1)(\langle f_1\rangle - f^e)\delta(1-2) + 2\nu(1-P_1)\langle f_1\rangle\delta(1-2)\\ &= \nu(1-P_1)(\langle f_1\rangle + f^e)\delta(1-2)\\ &= \nu(1-P_1)(1-P_2)(\langle f_1\rangle + f^e)\delta(1-2)\end{aligned} \tag{5.59}$$

For the last line we exploited the delta function to write $P_1\delta(1-2) = P_2\delta(1-2)$. In this example we find $a_1 = \nu(\langle f_1\rangle + f^e)$. Note that if we remove the boundary conditions and apply the constraints of the first example then we recover the result (5.56).

Using the results of the second example as our most general case we write the evolution equation for the two-body correlation function

$$\left(\frac{d}{d\tau} + \nu(1-P_1) + \nu(1-P_2)\right) G_{12} = \nu P_1 P_2(\langle f_1\rangle - f^e)\delta(1-2), \tag{5.60}$$

where the presence of the projection operators enforces energy, momentum and number conservation. Equation (5.60) is our main result for this section. In the next section we use it to construct solutions for the evolution of G_{12}, which we then integrate in Chapter 7 to study partially thermalized systems. In the local rest frame of the fluid we can expand $d/d\tau$ and write

$$\left(\frac{\partial}{\partial t} + \mathbf{v}_{\mathbf{p}_1}\cdot\nabla_1 + \mathbf{v}_{\mathbf{p}_2}\cdot\nabla_2 + \nu(2-P_1-P_2)\right) G_{12} = \nu P_1 P_2(\langle f_1\rangle - f^e)\delta(1-2), \tag{5.61}$$

where the relaxation rate and projection operators depend on the average one-body distribution $\langle f(\mathbf{x}, \mathbf{p}, t)\rangle$ and the local equilibrium distribution f^e. Equation (5.61) was derived earlier using similar methods by Dufty, Lee and Brey in Ref. [69] for non-relativistic fluids from a general analysis of the BBGKY hierarchy.

In order to use these equations for phenomenological purposes, we would start by solving Eq. (5.60) with the initial condition corresponding to a single collision event. We would then use the full non-linear solution (5.16) to solve for $\langle f(\mathbf{x}, \mathbf{p}, t)\rangle$ together with the conservation conditions (5.9) to fix the parameters T, $\mathbf{v}$ and μ in the local equilibrium distribution f^e. We can then use these to solve (5.60) for the correlation function. Finally we must remember to average over an ensemble of initial conditions. Physically, the difference between $\langle f\rangle$ and f^e may by arbitrarily large, as in our second example. In fact, such general solutions need not ever reach equilibrium [50].

In the next section we use these results to illustrate how this method can be applied to heavy ion collisions. We assume the deviation of the phase space distribution from its equilibrium value to always be small enough so that the linearized solution (5.40) for $\langle f\rangle$ is applicable. In this case, one can use the conservation conditions (5.25), or solve dissipation-free Euler equations, to determine effective T, $\mathbf{v}$ and μ parameters for the initial conditions in each event. For our purposes, this will not need to be done explicitly. For this work, the source term in (5.60) exactly vanishes.

In Ref. [70], Calzetta and Hu take on an early effort to study a fully relativistic version of the Boltzmann-Langevin equation. Our work here follows the path laid out in [22] to address thermalization using these equations. The effects of critical phenomena were introduced by Stephanov [71] but spatial inhomogeneity was not considered.

5.5 Ion collisions in kinetic theory

We now construct formal solutions for the evolution of G_{12}. We solve Eq. (5.60) in a manner similar to the derivation of (5.40). The four following equations will, respectively, use the definitions $G^e_{12} \equiv P_1 P_2 G_{12}$, $X_{12} \equiv (1 - P_1) P_2 G_{12}$, $X_{21} \equiv P_1 (1 - P_2) G_{12}$ and $\Delta G_{12} \equiv$

$(1-P_1)(1-P_2)G_{12}$. We multiply (5.60) by the combinations P_1P_2, $P_1(1-P_2)$, $(1-P_1)P_2$ and $(1-P_1)(1-P_2)$ and use properties of the projectors to find:

$$\frac{d}{d\tau}G^e_{12} = \nu P_1P_2(\langle f_1\rangle - f^e)\delta(1-2), \tag{5.62}$$

$$\frac{d}{d\tau}X_{12} = -\nu X_{12}, \tag{5.63}$$

$$\frac{d}{d\tau}X_{21} = -\nu X_{21}, \tag{5.64}$$

$$\frac{d}{d\tau}\Delta G_{12} = -2\nu\Delta G_{12}. \tag{5.65}$$

To relate these new variables to the original correlation function we note the identity

$$1 = P_1P_2 + P_1(1-P_2) + (1-P_1)P_2 + (1-P_1)(1-P_2) \tag{5.66}$$

and thus we have

$$G_{12} = G^e_{12} + X_{12} + X_{21} + \Delta G_{12}. \tag{5.67}$$

The equilibrium correlation function G^e_{12} is defined in the same sense as C^e_{12} and thus we have $G^e_{12} = C^e_{12} - P_1\langle f_1\rangle\delta(1-2)$. In the case that the fully linearized solution (5.40) holds then $P_1\langle f_1\rangle = f^e$ and we can apply Eq. (5.26). Then using (5.53) we have $dG^e_{12}/d\tau = 0$ so that G^e_{12}, as well as C^e_{12} and f^e, are constant along the characteristic curves defined in (5.11). We will assume this to be true in Sec. 6.4 but a more general non-linear description of the underlying flow described by Eq. (5.10) would allow G^e_{12} to vary with τ. We do point out, however, that in this case one can still extract (5.53) from (5.60) by applying P_1P_2 to find

$$\frac{d}{d\tau}G^e_{12} = \nu P_1P_2(\langle f_1\rangle - f^e)\delta(1-2) = -P_1P_2\frac{d}{d\tau}\langle f_1\rangle\delta(1-2), \tag{5.68}$$

where the second equality uses the non-linearized (5.12). This can be rearranged to give (5.53).

If $\delta f = f - f^e$ is the deviation of the phase space distribution from its local equilib-

rium value, then one can interpret ΔG_{12} as the non-equilibrium contribution to correlations $\langle \delta f_1 \delta f_2 \rangle - \langle \delta f_1 \rangle \langle \delta f_2 \rangle - \langle \delta f_1 \rangle \delta(1-2)$. The mixed correlation function X_{12} is the covariance $\langle \delta f_1 f_2^e \rangle - \langle \delta f_1 \rangle f_2^e$. While one might expect the deviation from equilibrium to be uncorrelated with equilibrium, we note that X_{12} need not vanish because δf and f^e correspond to the same T, $\mathbf{v}$ and μ. In this sense, X_{12} enforces the conservation laws.

We construct solutions in step with (5.40) by integrating Eqs. (5.63), (5.64) and (5.65) to find

$$X_{12} = X_{12}^0 S, \qquad X_{21} = X_{21}^0 S, \qquad \Delta G_{12} = \Delta G_{12}^0 S^2 \tag{5.69}$$

for the survival probability $S = S(\tau, \tau_0)$ given by Eq. (5.14). Assembling the pieces via (5.67) we finally obtain the general solution

$$G_{12} = G_{12}^e + (X_{12}^0 + X_{21}^0) S + \Delta G_{12}^0 S^2. \tag{5.70}$$

The two-particle local equilibrium correlation function

$$G_{12}^e = G_{12}^e(\mathbf{x}_1 - \mathbf{v}_{\mathbf{p}_1} t, \mathbf{p}_1, \mathbf{x}_2 - \mathbf{v}_{\mathbf{p}_2} t, \mathbf{p}_2), \tag{5.71}$$

again, accounts for drift following (5.11). The temperature and other local equilibrium parameters in these linearized equations follows the relativistic Euler equation. The initial functions X_{12}^0 and ΔG_{12}^0 follow a similar path dependence. Their values are determined by the initial spatial distribution of nucleon participants and their first few interactions. As a check on this solution we note that, at the initial time τ_0, $S(\tau_0, \tau_0) = 1$ and (5.70) gives $G_{12}^0 = G_{12}^e + X_{12}^0 + X_{21}^0 + \Delta G_{12}^0$, matching (5.67) with initial values. In Sec. 7.1 we will illustrate a method of integrating the solution (5.70) to study the approach to thermalization using p_t fluctuations.

CHAPTER 6 CORRELATIONS AND FLUCTUATIONS

Our results in Chapters 4 and 5 are not sufficient for experimental studies of heavy ion collisions. For one, we have been using the noise average defined in Chapter 3 and the appendix and laboratory conditions are not such that experimentalists can perfectly recreate initial conditions to repeat a collision. Furthermore, in real experiments it is not enough to simply have equations for the evolution of correlations – we need something that we can measure. After a collision experimentalists typically have access to particle information such as charge and momentum. Our goal in this section is to find an observable that connects our theory, in particular Eqs. (4.40) and (5.70), to experimental observables.

All observables are subject to fluctuations, which generally depend on properties of the system and can be used to study these properties. We break these fluctuations up into two classes. At the most basic level each collision event is different because a finite and varying number of particles are produced. The finite size of each event is an inherent cause of fluctuations which we refer to as statistical fluctuations. We evaluate these fluctuations by considering how a system behaves in local equilibrium. The second type of fluctuations are those above equilibrium, which we call dynamical fluctuations, and they encompass all other types of fluctuations. We then write the total fluctuations in a system as

$$\sigma^2_{total} = \sigma^2_{stat} + \sigma^2_{dyn}. \tag{6.1}$$

All of the observables we study in this chapter are dynamical and, thus, can be written in the form $\sigma^2_{dyn} = \sigma^2_{total} - \sigma^2_{stat}$. Dynamical fluctuations necessarily vanish in equilibrium, which we will see as a consequence of how we define our observables.

Also in this section we reconcile the difference between the noise average and an event average. As such, we need to use notation distinguishing between the two. We will denote the event average of a quantity X as $\langle X \rangle$ and the noise average by $\langle X \rangle_n$. A full event average $\langle \langle X \rangle_n \rangle$ consists of averaging over the initial conditions of $\langle X \rangle_n$.

6.1 Observables

The most fundamental quantity that can be observed after a nuclear collision is the number of particles that hit the detector. We call this observable the multiplicity of the event and denote it as N. Repeating this measurement for many collisions – often millions – and averaging the value gives the event averaged multiplicity $\langle N \rangle$. Physicists have concocted a number of ways to make this observable interesting, including measurements of N for specific species of particles [72, 73], measuring it as a function of the direction it emerges from the collision volume [74,75] and comparing the values of $\langle N \rangle$ observed in different types of collisions [15, 76]. As an introduction to the notation we will use, for a single event we write $N_\alpha = \sum_a 1$ where the sum is over the particles a in an event. The event average is then $\langle N \rangle = \frac{1}{N_{ev}} \sum_\alpha N_\alpha$ where this sum goes over all events α and N_{ev} is the total number of events.

Momentum is another basic property of particles we can measure. The event averaged sum total of the i-th component of the momentum of all the particles in an event is denoted $\langle P_i \rangle = \langle \sum_a p_{i,a} \rangle = \frac{1}{N_{ev}} \sum_\alpha \sum_a p_{i,a}$ for the momentum of a single particle $p_{i,a}$. Momentum is interesting in that it is a conserved quantity. One would expect, when summing over all the particles in an event, that $P_i = 0$ but this is not the result we observe experimentally. Particle detectors do not have 100% efficiency and some particles slip past unnoticed. Neutral particles, in particular, are difficult to detect and carry away some of the total momentum undetected. Furthermore, detectors cannot cover the entire region surrounding a collision. Measurements, in fact, are often conducted in a narrow rapidity range and, thus, conserving particles will fall outside of the detection window. Part of our interest lies in understanding the mechanisms that transport particles outside of this region. Initial momentum distributions are spread large in rapidity due to processes such as jets, string fragmentation and Glasma field interactions. Later evolution is restricted by causality to more local processes like scattering and, thus, diffusion. Measurements of the observables is this section can provide insight into these processes.

The average momentum per particle $P_{i,\alpha}/N_\alpha$ in an event α can be studied in two different ways. One may take the event average directly $\langle P_i/N\rangle = \frac{1}{N_{ev}}\sum_\alpha P_{i,\alpha}/N_\alpha$. Alternatively, we can study the ratio $\langle p_i\rangle = \langle P_i\rangle/\langle N\rangle$ – sometimes called the inclusive average. For our purposes, the inclusive average is the more preferable of the two: it can be expressed simply as an integral of distribution functions and it is used by experiment to study the same observables we are interested in. Instead of the individual components, we often study the average transverse momentum $\langle p_t\rangle = \langle P_t\rangle/\langle N\rangle$ for $p_t = \sqrt{p_x^2 + p_y^2}$ where x and y are the directions orthogonal to the beam axis z. This can have a large effect on the observables we measure mainly because p_t is not a conserved quantity – e.g. compare Eqs. (6.10) and (6.12).

It is theoretically convenient to connect these observables to the momentum density of particles $\rho_1(\mathbf{p}) = dN/d^3p$. For example,

$$\langle N\rangle = \int \rho_1(\mathbf{p})d^3p \qquad \text{and} \qquad \langle p_t\rangle = \frac{1}{\langle N\rangle}\int p_t\rho_1(\mathbf{p})d^3p, \tag{6.2}$$

where the integrals are taken over the freeze out surface. To study correlations between different particles we introduce the pair distribution

$$\rho_2(\mathbf{p}_1,\mathbf{p}_2) = \frac{dN}{d^3p_1 d^3p_2}. \tag{6.3}$$

for particle pairs of momentum $\mathbf{p}_1$ and $\mathbf{p}_2$. In an uncorrelated system that behaves according to Poisson statistics, such as during local equilibrium in an ion collision, the pair distribution factors $\rho_2(\mathbf{p}_1,\mathbf{p}_2) \to \rho_1(\mathbf{p}_1)\rho_1(\mathbf{p}_2)$. We note that ρ_1 and ρ_2 are related to the phase-space density f of Chapter 5 via the integrals

$$\rho_1(\mathbf{p}) = \int \langle f(\mathbf{x},\mathbf{p})\rangle d^3x, \tag{6.4}$$

$$\rho_2(\mathbf{p}_1,\mathbf{p}_2) = \int \left[\langle f(\mathbf{x}_1,\mathbf{p}_1)f(\mathbf{x}_2,\mathbf{p}_2)\rangle - \langle f_1(\mathbf{x}_1,\mathbf{p}_1)\rangle\delta(1-2)\right] d^3x_1 d^3x_2 \tag{6.5}$$

where $\delta(1-2) = \delta(\mathbf{x}_1 - \mathbf{x}_2)\delta(\mathbf{p}_1 - \mathbf{p}_2)$ and the integrals are over the Cooper-Frye freeze out surface with $dx = p^\mu d\sigma_\mu / E$. The second equation tells us that ρ_2 only considers distinct particles and, as a result, the integral of ρ_2 gives the number of distinct pairs $\langle N(N-1)\rangle$. Finally, as our primary interest is studying correlations we define the correlation function

$$r(\mathbf{p}_1, \mathbf{p}_2) = \rho_2(\mathbf{p}_1, \mathbf{p}_2) - \rho_1(\mathbf{p}_1)\rho_1(\mathbf{p}_2). \tag{6.6}$$

Due to the factoring of the momentum distributions, r vanishes in local equilibrium.

6.1.1 Multiplicity fluctuations

Having defined the basic correlators we can now build more substantial observables to target specific properties of the collisions we wish to study. In the case of multiplicity we define

$$\mathcal{R} \equiv \frac{\langle N^2\rangle - \langle N\rangle^2 - \langle N\rangle}{\langle N\rangle^2} = \frac{1}{\langle N\rangle^2}\int r(\mathbf{p}_1, \mathbf{p}_2) d^3p_1 d^3p_2. \tag{6.7}$$

Note that in the absence of correlations $r \to 0$ and $\mathcal{R}$ vanishes, making it a measure of the dynamical fluctuations of the system. We will see this is the case with all of the observables we study. While this is directly a result of being able to express them as integrals of r, we can also see this from the definition of $\mathcal{R}$. In the grand canonical ensemble[1], uncorrelated particles obey Poisson statistics. Therefore, in equilibrium, the variance $\sigma_N^2 = \langle N^2\rangle - \langle N\rangle^2$ equals the mean $\sigma_{stat}^2 = \langle N\rangle$ and $\mathcal{R}$ vanishes.

The dynamic multiplicity variance $\mathcal{R}$ can be used to study critical phenomena in heavy ion collisions, e.g. see [72]. A multiplicity fluctuation observable, related to $\mathcal{R}$, was measured by PHENIX [78]:

$$\omega_{ch} = \frac{\langle N_{ch}^2\rangle - \langle N_{ch}\rangle^2}{\langle N_{ch}\rangle}, \tag{6.8}$$

where N_{ch} is the charged particle multiplicity. Although experimenters found no evidence of critical behavior in their dataset it was observed that fluctuations decrease with increasing

[1] As a technical point, we note that the GCE is the most relevant ensemble to ion physics. Measurements usually take place near midrapidity and, thus, energy and conserved quantum numbers can be exchanged with the rest of the system. [77]

collision centrality, offering support to the notion that increasingly central collisions are more thermalized. In [23], it was pointed out that $\mathcal{R}$ is important in comparing measurements in different centrality ranges. To maintain consistency with data from different sources, we use $\mathcal{R}$ as a measure of the scale of correlations.

6.1.2 Momentum fluctuations

Dynamic momentum correlations are characterized by the observable

$$\mathcal{C}_{ij} \equiv \frac{1}{\langle N\rangle^2}\left\langle \sum_{a\neq b} p_{i,a}p_{j,b}\right\rangle - \langle p_i\rangle\langle p_j\rangle = \frac{1}{\langle N\rangle^2}\int p_{i1}p_{j2}r(\mathbf{p}_1,\mathbf{p}_2)d^3p_1d^3p_2, \tag{6.9}$$

where $\sum_{a\neq b} = \sum_a \sum_{b,b\neq a}$ denotes a double sum over pairs a and b such that $a \neq b$. Note that $\mathcal{C}$ is an integral over the correlation function r, causing it to vanish in equilibrium and justifying the moniker "dynamic". Choosing $i, j = x, y$ leads to a special case where conservation of momentum dictates that each component of the total momentum vanishes $P_i = 0$. As mentioned, this is not the case in experiment where technology impairs complete measurement but under ideal conditions fluctuations of conserved quantities are highly constrained. To see this we note that the unrestricted sum $\sum_{a,b} p_{i,a}p_{i,b} = P_iP_j$ also vanishes so that $\sum_{a\neq b} p_{i,a}p_{j,b} = -\sum_a p_{i,a}p_{j,a}$. It then follows that in the full range of measurement

$$\mathcal{C}_{ij} \to -\frac{\langle p_i^2\rangle}{\langle N\rangle}\delta_{ij}. \tag{6.10}$$

Our focus will be on the transverse analogue of $\mathcal{C}_{ij}$:

$$\mathcal{C} \equiv \frac{1}{\langle N\rangle^2}\left\langle \sum_{a\neq b} p_{t,a}p_{t,b}\right\rangle - \langle p_t\rangle^2 = \frac{1}{\langle N\rangle^2}\int p_{t1}p_{t2}r(\mathbf{p}_1,\mathbf{p}_2)d^3p_1d^3p_2. \tag{6.11}$$

As p_t is not a conserved quantity, the total transverse momentum P_t does not vanish and Eq. (6.10) is replaced by

$$\mathcal{C} \to \frac{\langle P_t^2\rangle - \langle P_t\rangle^2}{\langle N\rangle^2} - \frac{\langle p_t^2\rangle}{\langle N\rangle}. \tag{6.12}$$

The extra term in Eq. (6.12) accounting for fluctuations in total p_t from event to event can be quite large and demonstrates the effect that non-conserved quantities can have on the observables. In Ref. [46] it was shown that $\mathcal{C}$ is sensitive to viscosity and we extend this notion in the later chapters. Moreover, azimuthal anisotropy can be studied with $\gamma' \equiv (\mathcal{C}_{yy} - \mathcal{C}_{xx})/(\mathcal{C}_{yy} + \mathcal{C}_{xx})$, as proposed in Ref. [79].

A differential version of $\mathcal{C}$ was measured experimentally by the STAR collaboration [7,8]:

$$\mathcal{C}(\eta_r, \phi_r) = \frac{1}{\langle N \rangle_1 \langle N \rangle_2} \left\langle \sum_{a \neq b} p_{t,a} p_{t,b} \right\rangle_{1,2} - \langle p_t \rangle_1 \langle p_t \rangle_2 \tag{6.13}$$

where the numbers $\langle N \rangle_i$ and $\langle p_t \rangle_i$ refer to the multiplicity and transverse momentum in (η_i, ϕ_i) bins for particles $i = 1, 2$. They found broad, ridge-type structure in $\mathcal{C}(\eta_r, \phi_r)$ familiar from measurements of observables lacking the momentum weights. The near side ($\phi_r = 0$) structure builds to a large symmetric peak at $\eta_r = 0$, $\phi_r = 0$. The rapidity dependence of $\mathcal{C}$ is characterized by the width σ of this peak in η_r. In Au+Au collisions at the top RHIC energy, experimenters find that σ increases from 0.54 ± 0.02(statistical) $\pm\, 0.06$(systematic) in the most peripheral collisions to 0.94 ± 0.06(statistical) $\pm\, 0.17$(systematic) in central collisions. Significantly, STAR also presented the detailed rapidity distributions $\mathcal{C}(\eta_r)$ for three centralities [7] and for several other centralities [8].

Dynamic fluctuations of the transverse momentum can also be studied with the covariance

$$\langle \delta p_{t1} \delta p_{t2} \rangle \equiv \frac{\left\langle \sum_{a \neq b} \delta p_{ta} \delta p_{tb} \right\rangle}{\langle N(N-1) \rangle} = \int \delta p_{t1} \delta p_{t2} \frac{r(\mathbf{p}_1, \mathbf{p}_2)}{\langle N(N-1) \rangle} d^3 p_1 d^3 p_2, \tag{6.14}$$

for $\delta p_{ti} = p_{ti} - \langle p_t \rangle$. It measures the average covariance for all pairs of particles a and b in the same event with respect to the inclusive $\langle p_t \rangle$ calculated over all events. Again, expressing $\langle \delta p_{t1} \delta p_{t2} \rangle$ as a weighted integral over r shows that it is a dynamic measure of fluctuations.

One can also express $\langle \delta p_{t1} \delta p_{t2} \rangle$ as a difference in variances $\sigma^2_{P_t} - \sigma^2_{P_t,stat}$ by identifying

$$\sigma^2_{P_t} = \langle (P_t - N\langle p_t \rangle)^2 \rangle \qquad \text{and} \qquad \sigma^2_{P_t,stat} = \langle N \rangle \left(\langle p_t^2 \rangle - \langle p_t \rangle^2 \right). \tag{6.15}$$

To show that $\sigma^2_{P_t} \to \sigma^2_{P_t,stat}$ in equilibrium, we first show

$$\sigma^2_{P_t} = \int \delta p_{t1} \delta p_{t2} (\langle f_1 f_2 \rangle - \langle f_1 \rangle \langle f_2 \rangle) d^3x_1 d^3x_2 d^3p_1 d^3p_2 \tag{6.16}$$

and

$$\sigma^2_{P_t,stat} = \int \delta p_{t1} \delta p_{t2} \langle f_1 \rangle \delta(1-2) d^3x_1 d^3x_2 d^3p_1 d^3p_2. \tag{6.17}$$

To show (6.16) we note that the integrals over $\langle f \rangle$ vanish by definition of $\langle p_t \rangle$ and then

$$\begin{aligned} \int \delta p_{t1} \delta p_{t2} \langle f_1 f_2 \rangle d^3x_1 d^3x_2 d^3p_1 d^3p_2 &= \left\langle \sum_{a,b} \delta p_{ta} \delta p_{tb} \right\rangle \\ &= \left\langle \sum_{a,b} p_{ta} p_{tb} - 2\langle p_t \rangle \sum_{a,b} p_{ta} + \langle p_t \rangle^2 \sum_{a,b} 1 \right\rangle \\ &= \left\langle P_t^2 - 2\langle p_t \rangle N P_t + \langle p_t \rangle^2 N^2 \right\rangle \\ &= \left\langle (P_t - N\langle p_t \rangle)^2 \right\rangle. \end{aligned} \tag{6.18}$$

For (6.17) we have

$$\begin{aligned} \int \delta p_{t1} \delta p_{t2} \langle f_1 \rangle \delta(1-2) d^3x_1 d^3x_2 d^3p_1 d^3p_2 &= \int (\delta p_t)^2 \langle f \rangle d^3x d^3p \\ &= \langle N \rangle \langle (\delta p_t)^2 \rangle \\ &= \langle N \rangle \left(\langle p_t^2 \rangle - \langle p_t \rangle^2 \right). \end{aligned} \tag{6.19}$$

Since $(\langle f_1 f_2 \rangle - \langle f_1 \rangle \langle f_2 \rangle) \to \langle f_1 \rangle \delta(1-2)$ for equilibrium systems obeying Poisson statistics

we have the result $\sigma^2_{P_t} \to \sigma^2_{P_t,stat}$. Finally, we have

$$\langle N(N-1)\rangle \langle \delta p_{t1}\delta p_{t2}\rangle = \left\langle \sum_{a,b} \delta p_{ta}\delta p_{tb} \right\rangle - \left\langle \sum_a (\delta p_{ta})^2 \right\rangle = \sigma^2_{P_t} - \sigma^2_{P_t,stat}. \tag{6.20}$$

Experimentally $\langle \delta p_{t1}\delta p_{t2}\rangle$ (or related quantities) was measured in [10, 80, 81] where significant non-statistical fluctuations are observed as well as a dilution in the fluctuations with increasing centrality, indicating that $\langle \delta p_{t1}\delta p_{t2}\rangle$ can be used as a signal of thermalization. We compare our theory with this data in Chapter 7. In Ref. [23], $\langle \delta p_{t1}\delta p_{t2}\rangle$ was used to study early-time correlation contributions to flow. In Sec. 7.1 we build on these results to find the effect that incomplete thermalization can have on the observables. As a final note, r in Eq. (6.14) can be replaced with ρ_2 as $\int \delta p_t \rho_1 d^3p = 0$ by definition.

6.1.3 Momentum-multiplicity fluctuations

Up to this point we have discussed observables that measure fluctuations in multiplicity and correlations between the momenta of pairs of particles. We now wish to discuss the relation between multiplicity and momentum. A natural starting point is the covariance $\langle NP_t\rangle - \langle N\rangle\langle P_t\rangle$. To see how this quantity should behave in equilibrium we turn to the grand canonical ensemble. The grand canonical partition function describes systems in equilibrium and is given by

$$\mathcal{Z}(\mu, V, T) = \sum_i \exp(\alpha N_i - \beta E_i), \tag{6.21}$$

where the sum is over the microstates i of the system, $\alpha = \mu/T$ and $\beta = 1/T$. The average number of particles and average energy in the system are related to the partition function through the identities

$$\langle N\rangle = \sum_i N_i \frac{e^{\alpha N_i - \beta E_i}}{\mathcal{Z}} = \frac{1}{\mathcal{Z}}\frac{\partial \mathcal{Z}}{\partial \alpha} \qquad \text{and} \qquad \langle E\rangle = \sum_i E_i \frac{e^{\alpha N_i - \beta E_i}}{\mathcal{Z}} = -\frac{1}{\mathcal{Z}}\frac{\partial \mathcal{Z}}{\partial \beta}. \tag{6.22}$$

Taking another derivative with respect to α we have

$$\frac{\partial\langle N\rangle}{\partial\alpha} = \sum_i N_i \left(\frac{N_i e^{\alpha N_i - \beta E_i}}{\mathcal{Z}} - \frac{e^{\alpha N_i - \beta E_i}}{\mathcal{Z}^2} \frac{\partial \mathcal{Z}}{\partial \alpha} \right) = \langle N^2\rangle - \langle N\rangle^2, \tag{6.23}$$

and similarly

$$\frac{\partial\langle E\rangle}{\partial\alpha} = \sum_i E_i \left(\frac{N_i e^{\alpha N_i - \beta E_i}}{\mathcal{Z}} - \frac{e^{\alpha N_i - \beta E_i}}{\mathcal{Z}^2} \frac{\partial \mathcal{Z}}{\partial \alpha} \right) = \langle NE\rangle - \langle N\rangle\langle E\rangle = \frac{\partial\langle E\rangle}{\partial\langle N\rangle}\frac{\partial\langle N\rangle}{\partial\alpha}, \tag{6.24}$$

where the last equality follows by applying the chain rule to the left hand side of the equation. We recall that from Eq. (2.3) we can write the energy as $E = m_t \cosh y$. Near midrapidity $y \approx 0$ we have $\cosh y \approx 1$ and for particles with large momentum $p_t \gg m$ we have $m_t = \sqrt{m^2 + p_t^2} \approx p_t$. In this case we can identify the average energy of the system with the average of the total transverse momentum $\langle E\rangle \approx \langle P_t\rangle$. In particular we have $\frac{\partial\langle E\rangle}{\partial\langle N\rangle} = \frac{\partial\langle P_t\rangle}{\partial\langle N\rangle}$. Furthermore, it is often the case that over a wide range of centralities $\langle p_t\rangle$ is relatively constant (especially in the more central, more thermalized region) ([CCC] plot?). Thus, $\langle P_t\rangle = \langle p_t\rangle\langle N\rangle$ implies $\frac{\partial\langle P_t\rangle}{\partial\langle N\rangle} \approx \langle p_t\rangle$. Making these identifications in (6.24) and using (6.23) we find that in equilibrium

$$\langle NP_t\rangle - \langle N\rangle\langle P_t\rangle = \langle p_t\rangle \left(\langle N^2\rangle - \langle N\rangle^2\right). \tag{6.25}$$

Collision effects can introduce interesting and complicated correlations but we begin with a naive look at this equation. Certain effects, such as jets and minijets, create a large number of particles having a wide range of transverse momentum. Thus, the introduction of a jet into an event should result in a strong correlation between multiplicity and total transverse momentum which we expect to cause a greater increase to left side of (6.25) as opposed to the right. Other effects, namely transverse flow, work to increase p_t in an event but do little to change the multiplicity. In this case, we expect the right hand side of Eq. (6.25) to be larger than the left.

This motivates the introduction of a new observable similar to those above. Correlations between momentum and multiplicity can be characterized by the dynamic fluctuation observable

$$\mathcal{D} \equiv \frac{1}{\langle N\rangle^2}\left[\langle NP_t\rangle - \langle N\rangle\langle P_t\rangle - \langle p_t\rangle\left(\langle N^2\rangle - \langle N\rangle^2\right)\right] = \frac{1}{\langle N\rangle^2}\int \delta p_{t1} r(\mathbf{p}_1,\mathbf{p}_2) d^3p_1 d^3p_2. \tag{6.26}$$

To prove the last equality we first note that we can replace $r(\mathbf{p}_1,\mathbf{p}_2)$ with $\rho_2(\mathbf{p}_1,\mathbf{p}_2)$ as the integral over $\rho_1(\mathbf{p}_1)$ vanishes due to the factor δp_{t1}. Then

$$\begin{aligned}
\int \delta p_{t1}\rho_2 d^3p_1 d^3p_2 &= \left\langle \sum_{a\neq b} \delta p_{ta} \right\rangle \\
&= \left\langle \sum_{a} \delta p_{ta}(N-1) \right\rangle \\
&= \langle (P_t - N\langle p_t\rangle)(N-1)\rangle \\
&= \langle NP_t\rangle - \langle P_t\rangle - \langle N^2\rangle\langle p_t\rangle + \langle N\rangle\langle p_t\rangle \\
&= \langle N\rangle^2 \mathcal{D},
\end{aligned} \tag{6.27}$$

where the last equality follows by adding and subtracting $\langle N\rangle\langle P_t\rangle = \langle N\rangle^2\langle p_t\rangle$.

Based on their definitions, one can see that $\mathcal{D}$ is closely related to the other observables, however, it does have some nice properties to differentiate it from the pack. In principle, $\mathcal{D}$ can help to disentangle the jet-like and flow-like effects described above – something the others cannot see. Also, fluctuations in the collision volume from event to event can have an effect on $\mathcal{R}$, $\mathcal{C}$ and $\langle \delta p_{t1}\delta p_{t2}\rangle$, but not on $\mathcal{D}$ as we will see in the next section. Furthermore, $\mathcal{D}$ vanishes when integrated over the full range of momentum. First, note that when integrating ρ_2 over the full range of $\mathbf{p}_2$ the result must be proportional to the single particle distribution: $\int_{\text{all }\mathbf{p}_2} \rho_2 d^3p_2 \propto \rho_1$. Integrating this over $\mathbf{p}_1$ must give $\langle N(N-1)\rangle$ so that we have

$$\int_{\text{all }\mathbf{p}_2} \rho_2(\mathbf{p}_1,\mathbf{p}_2) d^3p_2 = \frac{\langle N(N-1)\rangle}{\langle N\rangle}\rho_1(\mathbf{p}_1). \tag{6.28}$$

The result then easily follows

$$\mathcal{D}_{\text{all }\mathbf{p}} = \frac{1}{\langle N\rangle^2}\int \delta p_{t1}\rho_2(\mathbf{p}_1,\mathbf{p}_2)d^3p_1 d^3p_2 \propto \int \delta p_{t1}\rho_1(\mathbf{p}_1)d^3p_1 = 0. \tag{6.29}$$

All together, $\mathcal{R}$, $\mathcal{C}$, $\mathcal{D}$ and $\langle \delta p_{t1}\delta p_{t2}\rangle$ form a suite of observables that can be used to study a wide range of collision features. While each is worthy of individual study they are not entirely independent. They are related via the "sum rule"

$$(1+\mathcal{R})\,\langle \delta p_{t1}\delta p_{t2}\rangle = \mathcal{C} - 2\langle p_t\rangle\mathcal{D} - \langle p_t\rangle^2\mathcal{R}. \tag{6.30}$$

We show this by noting that $\langle\sum_{a\neq b} p_{ta}\rangle = \langle\sum_{a\neq b} p_{tb}\rangle = \langle (N-1)P_t\rangle$ and that we can write $\langle N\rangle^2\mathcal{D} = \langle NP_t\rangle - \langle N^2\rangle\langle p_t\rangle$ since $\langle N\rangle\langle P_t\rangle = \langle N\rangle^2\langle p_t\rangle$. Then we have

$$\begin{aligned}
\langle N(N-1)\rangle\,\langle \delta p_{t1}\delta p_{t2}\rangle &= \left\langle \sum_{a\neq b}\delta p_{ta}\delta p_{tb}\right\rangle \\
&= \left\langle \sum_{a\neq b} p_{ta}p_{tb}\right\rangle + \left\langle \sum_{a\neq b}\langle p_t\rangle^2\right\rangle - 2\left\langle \sum_{a\neq b} p_{ta}\langle p_t\rangle\right\rangle \\
&= \left[\langle N\rangle^2\mathcal{C} + \langle N\rangle^2\langle p_t\rangle^2\right] + \langle N(N-1)\rangle\langle p_t\rangle^2 - 2\,\langle (N-1)P_t\rangle\,\langle p_t\rangle \\
&= \langle N\rangle^2\mathcal{C} + \langle N\rangle^2\langle p_t\rangle^2 - \langle N(N-1)\rangle\langle p_t\rangle^2 + 2\langle N(N-1)\rangle\langle p_t\rangle^2 \\
&\quad - 2\,\langle (N-1)P_t\rangle\,\langle p_t\rangle \\
&= \langle N\rangle^2\mathcal{C} - \langle N\rangle^2\langle p_t\rangle^2\mathcal{R} - 2\langle p_t\rangle\left[\langle (N-1)P_t\rangle - \langle N(N-1)\rangle\langle p_t\rangle\right] \\
&= \langle N\rangle^2\mathcal{C} - \langle N\rangle^2\langle p_t\rangle^2\mathcal{R} - 2\langle N\rangle^2\langle p_t\rangle\mathcal{D}.
\end{aligned} \tag{6.31}$$

Equation (6.30) then follows since $1+\mathcal{R} = \langle N(N-1)\rangle/\langle N\rangle^2$. This relation provides a useful "double check" for simulations and experiments worried about their calculations. Furthermore, we will find it useful in Sec. 7.1 when $\mathcal{C}$ turns out to be more difficult to work with than the others.

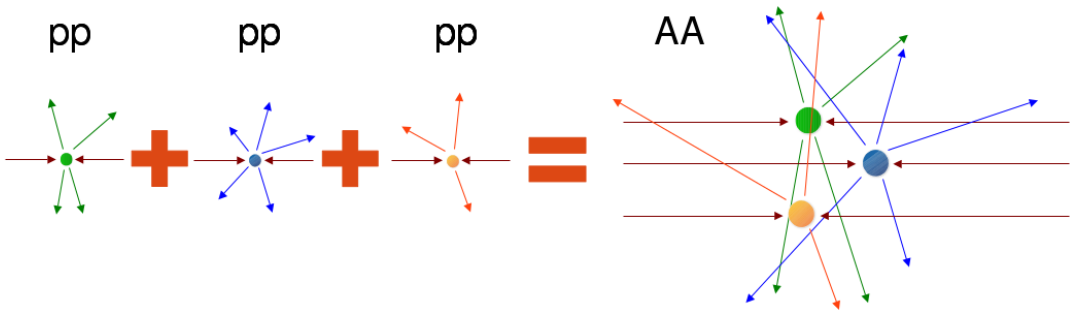

Figure 6.1: Depiction of the independent source model. Proton-proton collisions are superimposed to form a nucleus-nucleus collision.

6.2 Independent source model

In Chapter 7 we will want to study these observables in ion systems that feature very few collisions between the produced particles. Following [72], we model this for nucleus-nucleus collisions by representing each nucleon-nucleon subcollision as an independent source of particle production and assuming no interaction between sources. In this way, only particles that originate from the same source will be correlated. Then we can superimpose multiple sources – one for each nn sub-collision – to form the AA collision system. This is demonstrated in Fig. 6.1 where we identify each source as a single pp collision. The idea behind this is that we can use a scaled version of the simpler pp systems as a baseline for AA systems. The term "source" is left deliberately vague so as to maintain generality – in principle, you can picture your favorite type of source: flux tubes, wounded nucleons, etc.

Suppose there are M sources of particles in an event which fluctuates from event to event. Our purpose is to see how the observables are related to the number of sources. The single particle distribution in each event is M times the particle distribution per source. Assuming the distribution per source is independent of M we can write $\rho_1 = \langle M \rangle \hat{\rho}_1$ where we use hatted variables to represent per source quantities. Note that all of these quantities are now event averaged.

The total pair density ρ_2 must consider all possible pairs of particles. Pairs originating from the same source contribute through the term $\langle M \rangle \hat{\rho}_2$. It must also consider mixed pairs, where the second particle comes from a different source than the first. As there are $M(M-1)$

source pairs ρ_2 also includes the term $\langle M(M-1)\rangle\hat{\rho}_1\hat{\rho}_1$. Altogether we have

$$\rho_1 = \langle M\rangle\hat{\rho}_1 \qquad \text{and} \qquad \rho_2 = \langle M\rangle\hat{\rho}_2 + \langle M(M-1)\rangle\hat{\rho}_1\hat{\rho}_1 \tag{6.32}$$

Demonstrating the use of these distributions on the average multiplicity, we find

$$\langle N\rangle = \int \rho_1 d^3p = \langle M\rangle \int \hat{\rho}_1 d^3p = \langle M\rangle\mu \tag{6.33}$$

where we use $\mu = \int \hat{\rho}_1 d^3p$ for the average multiplicity per source rather than a more cumbersome hatted version. In words, the number of particles in an event is equal to the number of particle sources times the number of particles generated by a source. This would be the case if there were no interactions after the initial collision. We now use this model to study the observables we have been discussing.

We substitute these densities into the definition of $\mathcal{R}$ to find

$$\begin{aligned}
\mathcal{R} &= \frac{1}{\langle N\rangle^2}\int r(\mathbf{p}_1,\mathbf{p}_2)d^3p_1d^3p_2 \\
&= \frac{1}{\langle M\rangle^2\mu^2}\int \left[\langle M\rangle\hat{\rho}_2 + \langle M(M-1)\rangle\hat{\rho}_1\hat{\rho}_1 - \langle M\rangle^2\hat{\rho}_1\hat{\rho}_1\right] d^3p_1d^3p_2 \\
&= \frac{1}{\langle M\rangle^2\mu^2}\int \left[\langle M\rangle\hat{r} + \left(\langle M^2\rangle - \langle M\rangle^2\right)\hat{\rho}_1\hat{\rho}_1\right] d^3p_1d^3p_2 \\
&= \frac{1}{\langle M\rangle}\int \frac{\hat{r}}{\mu^2}d^3p_1d^3p_2 + \frac{\langle M^2\rangle - \langle M\rangle^2}{\langle M\rangle^2}\int \frac{\hat{\rho}_1\hat{\rho}_1}{\mu^2}d^3p_1d^3p_2 \\
&= \frac{\widehat{\mathcal{R}}}{\langle M\rangle} + \frac{\langle M^2\rangle - \langle M\rangle^2}{\langle M\rangle^2}
\end{aligned} \tag{6.34}$$

We see that $\mathcal{R}$ scales with the number of sources plus an additional term that accounts for fluctuations in the number of sources. The main purpose of this model is to use pp collisions to study the observables of interest. With this in mind we identify a source as a single pp collision[2]. Then, the per source quantities are equal to their values in a pp collision (e.g. $\widehat{\mathcal{R}} = \mathcal{R}_{pp}$) and the number of sources can be identified as the number of binary collisions

[2]Note that in this work we treat neutron sources as identical to proton sources.

between two participants $M = N_{\rm part}/2$ We find

$$\mathcal{R} = \frac{2\mathcal{R}_{pp}}{\langle N_{\rm part}\rangle} + \frac{\langle N_{\rm part}^2\rangle - \langle N_{\rm part}\rangle^2}{\langle N_{\rm part}\rangle^2}. \tag{6.35}$$

By making this identification we can view the second term as a measure of fluctuations in the initial collision volume. Thus, one can see that simply scaling $\mathcal{R}$ by the number of subcollisions is not sufficient, indeed, its value depends on geometric fluctuations of the system.

As another example, we now do the same for $\mathcal{D}$

$$\begin{aligned}
\mathcal{D} &= \frac{1}{\langle N\rangle^2}\int \rho_2 \delta p_{t1} d^3p_1 d^3p_2 \\
&= \frac{1}{\langle M\rangle^2\mu^2}\int \left(\langle M\rangle\hat{\rho}_2 + \langle M(M-1)\rangle\hat{\rho}_1\hat{\rho}_1\right)\delta p_{t1} d^3p_1 d^3p_2 \\
&= \frac{1}{\langle M\rangle\mu^2}\int \hat{\rho}_2 \delta p_{t1} d^3p_1 d^3p_2 \\
&= \frac{\widehat{\mathcal{D}}}{\langle M\rangle}.
\end{aligned} \tag{6.36}$$

Making the same identification as above we find

$$\mathcal{D} = \frac{2\mathcal{D}_{pp}}{\langle N_{\rm part}\rangle}. \tag{6.37}$$

In difference to $\mathcal{R}$ and as a point of sale, we see $\mathcal{D}$ scales very simply in the independent source model as it is immune to the initial volume fluctuations.

One can similarly calculate these quantities for $\mathcal{C}$ and $\langle \delta p_{t1}\delta p_{t2}\rangle$. Bypassing the details we find

$$\mathcal{C} = \frac{2\mathcal{C}_{pp}}{\langle N_{\rm part}\rangle} + \langle p_t\rangle^2 \frac{\langle N_{\rm part}^2\rangle - \langle N_{\rm part}\rangle^2}{\langle N_{\rm part}\rangle^2}, \tag{6.38}$$

$$\langle \delta p_{t1}\delta p_{t2}\rangle = \frac{2\langle \delta p_{t1}\delta p_{t2}\rangle_{pp}}{\langle N_{\rm part}\rangle}\left(\frac{1+\mathcal{R}_{pp}}{1+\mathcal{R}_{AA}}\right). \tag{6.39}$$

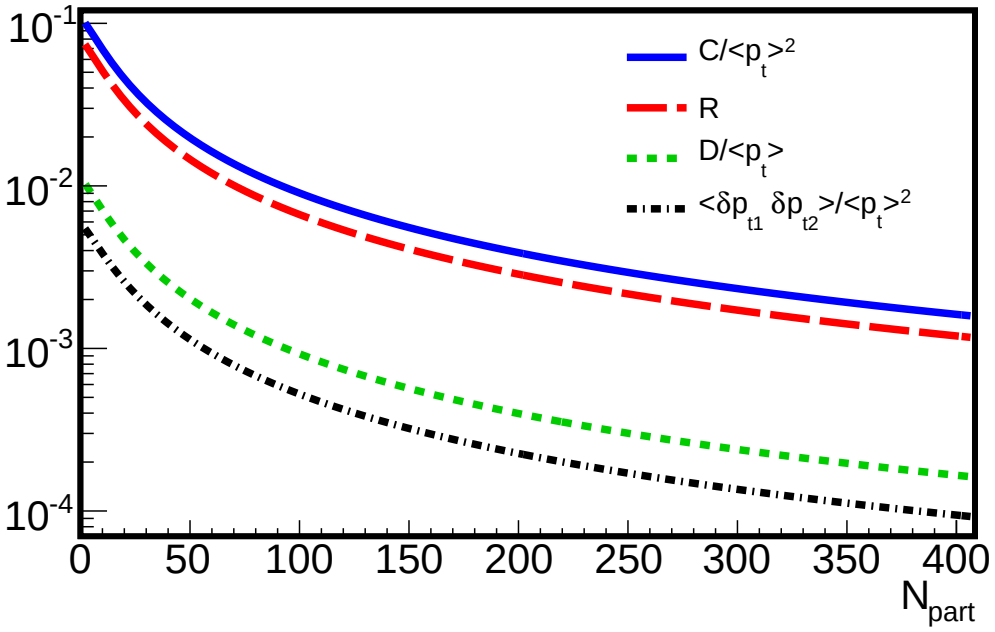

Figure 6.2: Independent source model curves for the observables in Eqs. (6.35), (6.37), (6.38) and (6.39) at an energy of $\sqrt{s} = 2760$ GeV. All of the observables share the same N_{part}^{-1} scaling.

We see that $\mathcal{C}$ shares the same scaling deficiency as $\mathcal{R}$, while $\langle \delta p_{t1} \delta p_{t2} \rangle$ only has a minor dependence on the volume fluctuations through the $\mathcal{R}_{AA}$ term in the denominator (the term in parentheses is entirely due to the different normalization between $\langle \delta p_{t1} \delta p_{t2} \rangle$ and the other observables). In Fig. 6.2 we plot these independent source observables as a function of N_{part}. Per source reference values are calculated using pp collisions in PYTHIA. We note that these theory curves have the benefit of minimized effect from the volume fluctuation terms as there is no fluctuation in the value of N_{part} when, e.g. $N_{part} = 50$. However, experiments do not benefit from this feature as many different N_{part} share the same centrality bin allowing for a variance. Nevertheless, we see that all of the observables have similar N_{part}^{-1} scaling behavior. We use these results in Sec. 7.2 when we study the extent of thermalization in a system. These curves correspond to a system which is completely unthermalized.

6.3 Connection to hydrodynamics

We will now connect the fluctuation observables introduced in this chapter with the correlation functions studied in previous chapters. Now is also the point that we will need to reconcile the difference between our two averages. We begin by showing that the covariance $\mathcal{C}_{ij}$ in a rapidity interval is related to the correlation function $\Delta r_{\mathcal{G}}^{ij}$ studied in Sec. 4.2 via

$$\mathcal{C}_{ij} = \frac{1}{\langle N \rangle^2} \int \langle \Delta r_{\mathcal{G}}^{ij}(\eta_r, \eta_a) \rangle d\eta_r d\eta_a \tag{6.40}$$

where we include brackets on $\langle \Delta r_{\mathcal{G}}^{ij} \rangle$ to indicate a full event average – i.e. $\Delta r_{\mathcal{G}}^{ij}$ is first averaged over noise as in Eq. (4.40) and then over initial conditions.

Consider $\delta f(\mathbf{x}, \mathbf{p}, t) = f(\mathbf{x}, \mathbf{p}, t) - \langle f(\mathbf{x}, \mathbf{p}, t) \rangle_n$, the deviation of the phase space distribution in an event from its noise averaged value. This is related to the momentum current by

$$M^i(\mathbf{x}) \equiv T^{0i} - \langle T^{0i} \rangle_n = \int \delta f(\mathbf{x}, \mathbf{p}) p^i d^3p. \tag{6.41}$$

The correlator $\langle M^i(\mathbf{x}_1) M^j(\mathbf{x}_2) \rangle_n = \langle M_1^i M_2^j \rangle_n$ then satisfies

$$\begin{aligned}
\int \langle M_1^i M_2^j \rangle_n d^3x_1 d^3x_2 &= \int \langle \delta f_1^i \delta f_2^j \rangle_n p_1^i p_2^j d^3p_1 d^3p_2 d^3x_1 d^3x_2 \\
&= \int \langle f_1^i f_2^j \rangle_n p_1^i p_2^j d^3p_1 d^3p_2 d^3x_1 d^3x_2 \\
&\quad - \int \langle f_1^i \rangle_n p_1^i d^3p_1 d^3x_1 \int \langle f_2^j \rangle_n p_2^j d^3p_2 d^3x_2 \\
&= \left\langle \sum_{a,b} p_a^i p_b^j \right\rangle_n - P^i P^j
\end{aligned} \tag{6.42}$$

Notice this summation is not restricted to distinct pairs, as in Eq. (6.9). Also note that we write $\langle P^i \rangle_n$ as P^i for brevity. Averaging this over initial conditions then yields

$$\left\langle \left\langle \sum_{a,b} p_a^i p_b^j \right\rangle_n \right\rangle = \langle P^i P^j \rangle + \int \langle \langle M_1^i M_2^j \rangle_n \rangle d^3x_1 d^3x_2. \tag{6.43}$$

It is convenient to change the integration measure in (6.43) to Milne coordinates via the transformation $dtdzd^2x_\perp = \tau d\tau d\eta d^2x_\perp$. We assume that freeze-out occurs at constant proper time and write

$$\int \langle\langle M_1^i M_2^j\rangle_n\rangle d^3x_1 d^3x_2 = \int \langle\langle M_1^i M_2^j\rangle_n\rangle \tau^2 d\eta_1 d\eta_2 d^2x_{1,\perp} d^2x_{2,\perp} = \int \langle\langle \mathcal{M}_1^i \mathcal{M}_2^j\rangle_n\rangle d\eta_r d\eta_a, \tag{6.44}$$

where for the last equality we define the rapidity density of transverse momentum $\mathcal{M}^i(\eta) \equiv \int M^i(\mathbf{x})\tau d^2x_\perp$ and change to the relative and average rapidities $\eta_r = \eta_2 - \eta_1$ and $\eta_a = (\eta_1 + \eta_2)/2$, respectively[3].

We wish to make the identification $\int\langle\langle \mathcal{M}_1^i \mathcal{M}_2^j\rangle_n\rangle d\eta_r d\eta_a = \int \langle r_{\mathcal{G}}^{ij}\rangle d\eta_r d\eta_a$. To do this, recall from Chapter 4 that $\mathcal{G}^i = \int g^i \tau d^2x_\perp$ and that g^i represents the shear modes of the system. Generally, $\mathbf{M}$ combines contributions from the shear modes and the curl-free longitudinal modes $\mathbf{g_l}$. Being curl-free means we can write $\mathbf{g_l} = \nabla\varphi$ for some potential φ. The rapidity density $\mathcal{M}^i$ is then proportional to $\int dx_i \partial\varphi/\partial x_i$ which is only dependent on the value of φ on the spatial part of the freeze-out surface, where interactions effectively cease. There is no restoring force for ripples in this surface as there would be for, e.g., ocean waves. The contribution from $\mathbf{g_l}$ to fluctuations at the freeze-out surface must therefore be along the normal direction so that the surface is an equipotential. Accordingly, $\partial\varphi/\partial x_i = 0$ and the contribution of $\mathbf{g_l}$ to $\mathcal{M}^i$ vanishes. We find that $\mathcal{M}^i$ depends only on the shear modes and, therefore, we have $\int\langle\langle \mathcal{M}_1^i \mathcal{M}_2^j\rangle_n\rangle d\eta_r d\eta_a = \int \langle r_{\mathcal{G}}^{ij}\rangle d\eta_r d\eta_a$. Note that $r_{\mathcal{G}}^{ij}$ is already averaged over noise.

Returning now to Eq. (6.43), we have

$$\left\langle \sum_{a,b} p_a^i p_b^j \right\rangle = \int \langle r_{\mathcal{G}}^{ij}\rangle d\eta_r d\eta_a + \langle P^i P^j\rangle. \tag{6.45}$$

In writing (6.45) we have moved to full event averages (noise + initial conditions) by equating $\langle\langle\cdots\rangle_n\rangle$ with $\langle\cdots\rangle$. For this derivation we are done distinguishing the averages although,

[3]The Jacobian of the rapidity transformation is $|\partial(\eta_r, \eta_a)/\partial(\eta_1, \eta_2)| = 1$

before completely throwing the distinction to the wayside, we revisit the concept in a moment to do a similar derivation with the Boltzmann solution (5.70). We use the definition of $\mathcal{C}_{ij}$ in (6.9) and the identity $\langle p^i \rangle = \langle P^i \rangle / \langle N \rangle$ to write the left-hand side of (6.45) as

$$\begin{aligned}\left\langle \sum_{a,b} p_a^i p_b^j \right\rangle &= \left\langle \sum_{a \neq b} p_a^i p_b^j \right\rangle + \left\langle \sum_a p_a^i p_a^j \right\rangle \\ &= \left\langle \sum_{a \neq b} p_a^i p_b^j \right\rangle - \langle N \rangle^2 \langle p^i \rangle \langle p^j \rangle + \left\langle \sum_a p_a^i p_a^j \right\rangle + \langle P^i \rangle \langle P^j \rangle \\ &= \langle N \rangle^2 \mathcal{C}_{ij} + \left\langle \sum_a p_a^i p_a^j \right\rangle + \langle P^i \rangle \langle P^j \rangle. \end{aligned} \tag{6.46}$$

Combining this with (6.45) we have

$$\langle N \rangle^2 \mathcal{C}_{ij} = \int \langle r_{\mathcal{G}}^{ij} \rangle d\eta_r d\eta_a - \left\langle \sum_a p_a^i p_a^j \right\rangle + \mathrm{cov}(P^i, P^j) \tag{6.47}$$

The price we paid for distinguishing between the two separate averages is in picking up the covariance term $\mathrm{cov}(P^i, P^j) = \langle P^i P^j \rangle - \langle P^i \rangle \langle P^j \rangle$. Consider Eq. (6.42) but with $\langle \cdots \rangle_n$ as the full event average. In this case, in the final line, the last term would read $\langle P^i \rangle \langle P^j \rangle$ and there would be no need to take a second average creating the momentum correlator. This term would then cancel exactly with the matching term in (6.47) and the covariance would vanish. This covariance represents fluctuations of the total momentum in a rapidity interval from event to event.

In local equilibrium $\mathcal{C}_{ij}$ vanishes and Eq. (6.47) becomes

$$\int \langle r_{\mathcal{G},le}^{ij} \rangle d\eta_r d\eta_a = \left\langle \sum_a p_a^i p_a^j \right\rangle - \mathrm{cov}(P^i, P^j). \tag{6.48}$$

Using this in Eq. (6.47) we find

$$\langle N \rangle^2 \mathcal{C}_{ij} = \int \langle r_{\mathcal{G}}^{ij} \rangle d\eta_r d\eta_a - \int \langle r_{\mathcal{G},le}^{ij} \rangle d\eta_r d\eta_a = \int \langle \Delta r_{\mathcal{G}}^{ij} \rangle d\eta_r d\eta_a. \tag{6.49}$$

Dividing this by $\langle N\rangle^2$ gives the desired result (6.40). Recall the result (6.10) for measurements encompassing all particles. Applying this to (6.40) we see that in the full range of rapidity $\int\langle\Delta r_{\mathcal{G}}^{ij}\rangle d\eta_r d\eta_a \to -\langle N\rangle\langle p_i^2\rangle\delta_{ij}$. Thus, the integral of $\langle\Delta r_{\mathcal{G}}^{ij}\rangle$ approaches a fixed, non-zero value, implying that systems constrained by momentum conservation cannot fully reach the uncorrelated local equilibrium state. Mathematically, this constraint constitutes a boundary condition for $\langle\Delta r_{\mathcal{G}}^{ij}\rangle$ that amounts to a rapidity independent shift in magnitude.

Experimental studies of momentum correlations have focused on p_t, rather than p_x and p_y. To obtain the transverse counterpart of $\mathcal{C}_{ij}$ we simply choose i and j to be the radial component. The correlation function becomes $\Delta r_{\mathcal{G}}$ for the momentum density $\mathcal{G} = \tau\int g_r r dr d\phi$ and the observable is

$$\mathcal{C} = \frac{1}{\langle N\rangle^2}\int\langle\Delta r_{\mathcal{G}}(\eta_r,\eta_a)\rangle d\eta_r d\eta_a. \tag{6.50}$$

This is the form we will use in Sec. 6.5 to study the qualitative behavior of $\mathcal{C}$.

6.4 Connection to kinetic theory

In a similar manner, we now show that $\langle\delta p_{t1}\delta p_{t2}\rangle$ is related to the correlation function $G_{12} = \langle f_1 f_2\rangle_n - \langle f_1\rangle_n\langle f_2\rangle_n - \langle f_1\rangle_n\delta(1-2)$ from Chapter 5 via the equation

$$\langle\delta p_{t1}\delta p_{t2}\rangle = \langle\delta p_{t1}\delta p_{t2}\rangle_e + \int\delta p_{t1}\delta p_{t2}\frac{\langle G_{12} - G_{12}^e\rangle}{\langle N(N-1)\rangle}d\omega_1 d\omega_2, \tag{6.51}$$

where $d\omega = d\mathbf{x}d\mathbf{p}$ and the spatial integral is taken over the Cooper-Frye freeze-out surface with $dx = p^\mu d\sigma_\mu/E$. The quantity $\langle\delta p_{t1}\delta p_{t2}\rangle_e$ represents the value of the observable for a system in local equilibrium, including both thermal and initial state fluctuations. For this derivation we assume the difference between the noise averaged phase-space distribution $\langle f\rangle_n$ and its equilibrium value f^e to be small enough that the linearized solution (5.40) is applicable. In particular, this means G_{12}^e, C_{12}^e and f^e are all constant along their characteristic curves and Eq. (5.70) holds.

We begin by writing the restricted sum in (6.14) as

$$\begin{aligned}\left\langle \sum_{i\neq j} \delta p_{t,i}\delta p_{t,j} \right\rangle_n &= \left\langle \sum_{i,j} \delta p_{t,i}\delta p_{t,j} \right\rangle_n - \left\langle \sum_i \delta p_{t,i}^2 \right\rangle_n \\ &= \int \delta p_{t1}\delta p_{t2} \left\langle f_1 f_2 \right\rangle_n d\omega_1 d\omega_2 - \int \delta p_{t1}\delta p_{t2} \left\langle f_1 \right\rangle_n \delta(1-2) d\omega_1 d\omega_2 \\ &= \int \delta p_{t1}\delta p_{t2} \left[\left\langle f_1 f_2 \right\rangle_n - \left\langle f_1 \right\rangle_n \delta(1-2) \right] d\omega_1 d\omega_2 \\ &= \int \delta p_{t1}\delta p_{t2} G_{12} d\omega_1 d\omega_2 + \int \delta p_{t1}\delta p_{t2} \left\langle f_1 \right\rangle_n \left\langle f_2 \right\rangle_n d\omega_1 d\omega_2, \end{aligned} \tag{6.52}$$

where in the last line we added and subtracted a $\langle f_1\rangle_n\langle f_2\rangle_n$ term. Averaging over initial conditions and dividing by the average number of pairs we find

$$\langle \delta p_{t1}\delta p_{t2} \rangle = \int \delta p_{t1}\delta p_{t2} \frac{\langle G_{12} \rangle}{\langle N(N-1) \rangle} d\omega_1 d\omega_2 + \int \delta p_{t1}\delta p_{t2} \frac{\langle \langle f_1 \rangle_n \langle f_2 \rangle_n \rangle}{\langle N(N-1) \rangle} d\omega_1 d\omega_2. \tag{6.53}$$

To identify the local equilibrium value $\langle \delta p_{t1}\delta p_{t2} \rangle_e$ we consider Eq. (6.53) in local equilibrium. The correlation function G_{12} assumes its value in equilibrium G_{12}^e. For the second term, we assume the departures of $\langle f \rangle_n$ from their event-wise values in local equilibrium are small enough so that they retain roughly the same values in equilibrium when integrated over the momentum weights . If p_t was a conserved quantity, this would hold exactly. Thus, we find

$$\langle \delta p_{t1}\delta p_{t2} \rangle_e = \int \delta p_{t1}\delta p_{t2} \frac{\langle G_{12}^e \rangle}{\langle N(N-1) \rangle} d\omega_1 d\omega_2 + \int \delta p_{t1}\delta p_{t2} \frac{\langle \langle f_1 \rangle_n \langle f_2 \rangle_n \rangle}{\langle N(N-1) \rangle} d\omega_1 d\omega_2. \tag{6.54}$$

By subtracting (6.54) from (6.53) we arrive at (6.51).

We understand the different terms in these equations as representing distinct physical contributions. The terms containing G_{12} on the right sides of (6.53) and (6.54) include all fluctuations within each event – initial-state and dynamic. The second terms in these equations give the contribution to $\langle \delta p_{t1}\delta p_{t2} \rangle$ from the variation of the average local equilibrium distribution from event to event. The first term in (6.54) is likely small and would vanish if the temperature and the transverse velocity were completely uniform on the freeze-out

surface. Furthermore, note that the integrals over $\delta p_t = p_t - \langle p_t \rangle$ need not vanish, as in the discussion after (6.14), because $\langle p_t \rangle$ is a full event average and not simply a noise average. In particular,

$$\langle P_t \rangle_n = \int p_t \langle f \rangle_n d\omega \neq \int p_t \langle f \rangle d\omega = \langle P_t \rangle, \tag{6.55}$$

since $\langle P_t \rangle_n$ can vary greatly from event to event.

All of the observables in this chapter have equivalent formulae which can be found by taking different moments of $\langle G_{12} - G_{12}^e \rangle$ with respect to the quantities 1, $\langle p_t \rangle$ and δp_t. We list the results here:

$$\mathcal{R} = \mathcal{R}_e + \frac{1}{\langle N \rangle^2} \int \langle G_{12} - G_{12}^e \rangle d\omega_1 d\omega_2, \tag{6.56}$$

$$\mathcal{C} = \mathcal{C}_e + \frac{1}{\langle N \rangle^2} \int p_{t1} p_{t2} \langle G_{12} - G_{12}^e \rangle d\omega_1 d\omega_2, \tag{6.57}$$

$$\mathcal{D} = \mathcal{D}_e + \frac{1}{\langle N \rangle^2} \int \delta p_{t1} \langle G_{12} - G_{12}^e \rangle d\omega_1 d\omega_2. \tag{6.58}$$

$$\langle \delta p_{t1} \delta p_{t2} \rangle = \langle \delta p_{t1} \delta p_{t2} \rangle_e + \int \delta p_{t1} \delta p_{t2} \frac{\langle G_{12} - G_{12}^e \rangle}{\langle N(N-1) \rangle} d\omega_1 d\omega_2, \tag{6.59}$$

In Chapter 7 we pair these results with those of Sec. 6.2 to study systems that are approaching, but not yet in, local equilibrium. Note that we are now done distinguishing between different types of averages and from this point forward $\langle \cdots \rangle$ will always indicate a full event average.

6.5 Diffusion vs. experiment

We now take a momentary aside to finish our discussion of the hydrodynamic equations developed in Chapter 4. We have already seen the difference between first and second order evolution using the rapidity width of $\Delta r_{\mathcal{G}}$. Here we solidify this behavior by examining the shape of $\mathcal{C}$ as a function of the relative rapidity[4]. Experimental results on the shape of $\mathcal{C}(\eta_r)$, defined by (6.13), where released by STAR for three centralities represented by open stars

[4]In an effort to maintain candor, I point out that the results in this section were obtained by the coauthors of [41]. However, I wanted to briefly include them in this work to show an application of the methods we developed in Chapters 3 and 4. See [41] for full details.

in Fig. 6.3 [7]. Additional centralities are shown as solid circles [8]. The percent centrality imprinted in each panel is characterized by the fraction of total cross section.

The correlation function $\Delta r_{\mathcal{G}}$ and its integral $\mathcal{C}(\eta_r)$ are computed by solving (4.41), assuming the initial transverse momentum correlation function to be Gaussian in both rapidities

$$\Delta r_{\mathcal{G}}(\eta_r, \eta_a, \tau_0) = A e^{-\eta_r^2/2\sigma_0^2} e^{-\eta_a^2/2\Sigma_0^2}. \tag{6.60}$$

This form is motivated by measurements of the rapidity dependence of correlation functions in pp collisions. The initial width σ_0 is chosen to fit the most peripheral curve in the lower right of Fig. 6.3. As indicated by the data, there seems to be no significant evolution in the three most peripheral panels and a consistent value of $\sigma_0 = 0.5$ can be chosen. The average rapidity width $\Sigma_0 \approx 5 - 6$ units is assumed to be "large" relative to the acceptance range of experiment. The interest of this analysis in mainly in the shape of $\mathcal{C}$ rather than the magnitude, and so, the value of A is set to fit the peak value of the measured covariance. The initial value of the first derivative is calculated as in (4.50).

For first order results, with $\tau_\pi^* = 0$, Eq. (4.41) reduces to (4.42). The dash-dotted curves in Fig. 6.3, with parameters adjusted to fit the rapidity width data in Fig. 4.1, generally fail to describe the data. This is particularly true once the peak begins to broaden in the more central bins. The dashed curves, representing a fit directly to the data in Fig. 6.3, share this same failure. Furthermore, the measurements in the top three panels show a small dip in the region of $\eta_r = 0$, suggesting a bimodal nature of the distributions. These shortcomings can be attributed directly to the nature of first order diffusion as it maintains the initial Gaussian shape (6.60) throughout evolution.

The flattening of the distribution in the central bins is enough reason to explain why first order diffusion fails. On the other hand, the dip and implied bimodal features display compelling evidence for second order diffusion. Causal diffusion broadens the rapidity distribution in the usual diffusion-like manner but also incorporates a wave-like propagation of the initial signal. Mathematically, the inclusion of the τ_π^* term in (4.41) changes the

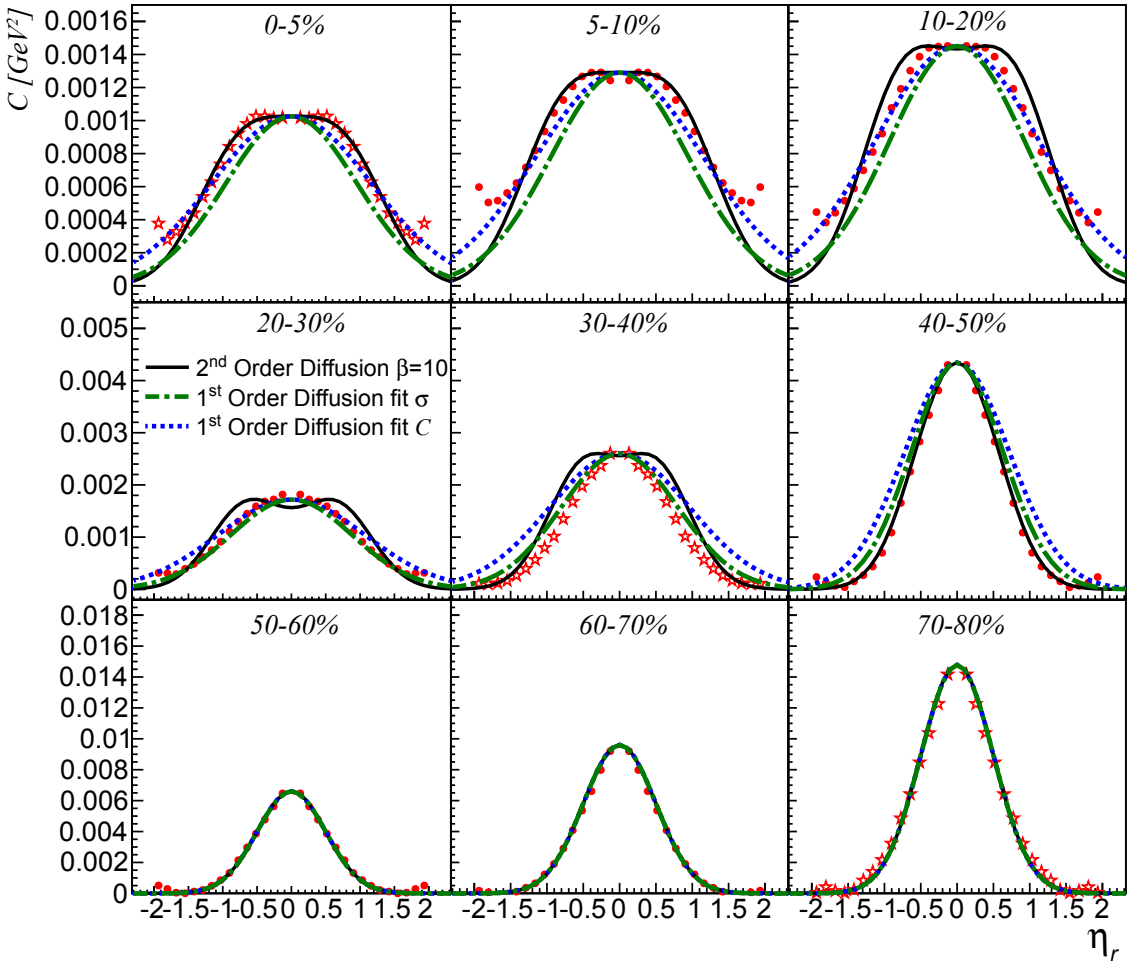

Figure 6.3: Second order momentum diffusion calculations (solid curve) compared to the rapidity dependence of the measured covariance (6.13). First order calculations are also compared for best fit to these data (dashed) and best fit to σ in Fig. 4.1 (dash-dotted curves). Data (open stars) are from [7] and (filled circles) from [8]. Percentages of the cross section indicate centrality, with each panel corresponding to a width measurement in Fig. 4.1.

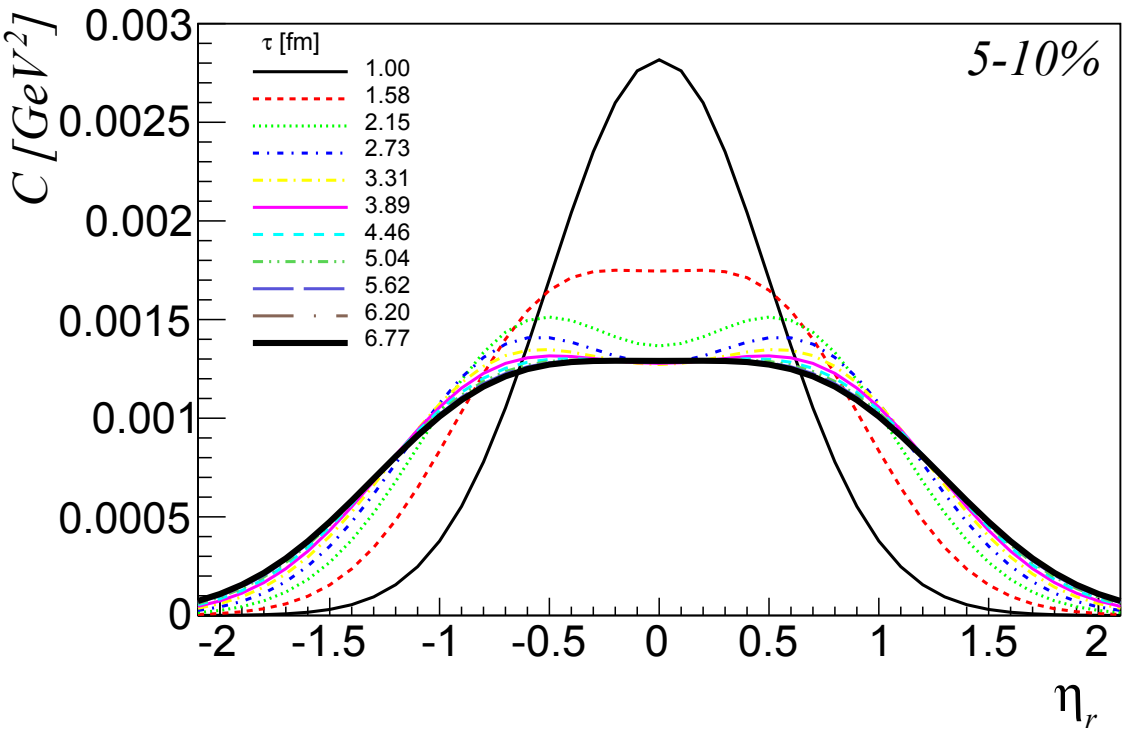

Figure 6.4: Time dependence of the rapidity covariance in second order diffusion.

parabolic (diffusion-like) equation into a hyperbolic (wave-like) equation. At early times wave-like evolution dominates, giving rise to left and right moving pulses. After a time $\sim \tau_\pi$ has elapsed, the first derivative in (4.41) becomes important and usual diffusion begins. As the distribution evolves, this fills the gap between the wave pulses and creates a single broad plateau. This time evolution of the rapidity profile is shown in Fig. 6.4 for parameter values used in Fig. 6.3.

The solution to the second order (4.41) gives the solid curves in Fig. 6.3. The evolution of the distribution when moving from peripheral to central bins reflects the time evolution shown in Fig. 6.4 due to the increase in τ_F for larger systems. For the central bins, the second order calculations describe the measured broadening quite well. With constant τ_π^* and ν^*, best fit to the data is obtained with $\beta = 10$, plotted in Fig. 6.3. Other values of β are tested in [41]. For the values of ν used in this analysis, τ_π is estimated in the range $1.0 - 1.1$ fm. By incorporating more realistic time and temperature dependent coefficients into future calculations, we expect this estimate to improve.

CHAPTER 7 PARTIALLY THERMALIZED SYSTEMS

Perfectly central nuclear collisions create a dense medium which quickly expands and coalesces into detectable particles. It is well known that the expansion of the medium can be treated using a hydrodynamic description of the underlying flow [16] . The hydrodynamic theory assumes the system is in local equilibrium during the entire lifetime of the expansion. Peripheral nuclear collision are more akin to pp collisions, containing far fewer particles and far less opportunity for scattering and equilibration. One should not expect a peripheral collision to equilibrate during its lifetime. An average collision exists somewhere between these two types of collisions. With this in mind, in this chapter we model nuclear collisions as a superposition of equilibrium expansion and the non-interacting evolution of an initial state.

In general, initial state partons are born correlated due to high energy kinematics and QCD dynamics. Scattering among these partons leads to dissipation that works to erase these correlations. If the system was contained inside a fixed volume, there would be enough time for scattering to bring about equilibration. However, the rapid expansion and short lifetime of the system prevents complete thermalization and freezes in certain correlations. Identifying such partially thermalized correlations can help to uncover the character of the thermalization process.

This is especially relevant to recent and upcoming experiments. Discovery of flow-like azimuthal correlations in pA and high-multiplicity pp collisions imply the existence of a fluid approaching a thermalized state [17–21]. Similar measurements for large systems have provided comprehensive evidence for a hydrodynamic description of heavy-ion collisions. However, finding this structure in smaller systems raises questions about the relation between the measured flow and hydrodynamics. In this chapter we attempt to rectify this seeming disparity by providing an illustrative way to study the approach to thermalization.

Our focus is on the transverse momentum observables defined in Chapter 6. Transverse momentum fluctuations have long been argued to be a probe of thermalization [22].

Furthermore, these fluctuations have been measured by LHC, RHIC and SPS experiments [9–12, 82–84] for a variety of reasons [85, 86]. Data have significant deviations from the expectation in equilibrium for peripheral heavy-ion collisions at LHC and RHIC [23]. We believe that measurements in pA collisions can demonstrate whether these systems are indeed thermal.

7.1 Observing thermalization

We begin by studying $\langle \delta p_{t1} \delta p_{t2} \rangle$ in the context of heavy-ion collisions. All quantities will assume to be fully event averaged so explicit average brackets may be suppressed, e.g. $\langle G_{12} \rangle = G_{12}$. The survival probability S is taken to be already averaged over an ensemble of events in order to simplify calculations. This need not be true in general, however, for this illustration we feel it appropriate. We combine the solution for G_{12} (5.70) with Eq. (6.59) to find

$$\langle \delta p_{t1} \delta p_{t2} \rangle - \langle \delta p_{t1} \delta p_{t2} \rangle_e = \int \delta p_{t1} \delta p_{t2} \frac{\Delta G^0_{12} S^2 + (X^0_{12} + X^0_{21}) S}{\langle N(N-1) \rangle} d\omega_1 d\omega_2 = aS^2 + bS \tag{7.1}$$

where S is given by (5.14),

$$a = \int \delta p_{t1} \delta p_{t2} \frac{\Delta G^0_{12}}{\langle N(N-1) \rangle} d\omega_1 d\omega_2 \tag{7.2}$$

and

$$b = \int \delta p_{t1} \delta p_{t2} \frac{X^0_{12} + X^0_{21}}{\langle N(N-1) \rangle} d\omega_1 d\omega_2 \tag{7.3}$$

We argue the term proportional to S^2 is the dominant contribution for $\langle \delta p_{t1} \delta p_{t2} \rangle$. In each event, the local equilibrium $\langle p_t \rangle$ corresponding to f^e is determined primarily by the parameter T, with small "blue-shift" corrections due to the radial component of $\mathbf{v}$. In equilibrium, the variation of these parameters on the freeze out surface is likely small and, thus, we expect

$p_t \approx \langle p_t \rangle$. We therefore approximate

$$\int dp_2 p_{t2} X^0_{12} = \int dp_2 p_{t2} (\langle \delta f^0_1 f^e_2 \rangle_n - \langle \delta f^0_1 \rangle_n f^e_2) \approx \langle p_t \rangle \int dp_2 X^0_{12}, \tag{7.4}$$

and similarly for $1 \leftrightarrow 2$. Since the integral in (7.3) depends on $\delta p_{ti} = p_{ti} - \langle p_t \rangle$ it follows that $b \approx 0$.

In the same vein, we can replace ΔG^0_{12} in (7.2) with $\Delta G^0_{12} + X^0_{12} + X^0_{12}$ and then use (5.67) to identify this quantity as $G^0_{12} - G^e_{12}$. We can then simplify to find

$$a = \int \delta p_{t1} \delta p_{t2} \frac{G^0_{12} - G^e_{12}}{\langle N(N-1) \rangle} d\omega_1 d\omega_2 = \langle \delta p_{t1} \delta p_{t2} \rangle_0 - \langle \delta p_{t1} \delta p_{t2} \rangle_e , \tag{7.5}$$

where the second equality follows from (6.53), (6.54) and the discussion surrounding these equations. Using this in (7.1) and rearranging we find

$$\langle \delta p_{t1} \delta p_{t2} \rangle = \langle \delta p_{t1} \delta p_{t2} \rangle_0 S^2 + \langle \delta p_{t1} \delta p_{t2} \rangle_e (1 - S^2). \tag{7.6}$$

Loosely speaking we can interpret this result as follows. The final correlations $\langle \delta p_{t1} \delta p_{t2} \rangle$ are due to a combination of initial correlations $\langle \delta p_{t1} \delta p_{t2} \rangle_0$ and equilibrium correlations $\langle \delta p_{t1} \delta p_{t2} \rangle_e$. The initial correlations are due to particles from the initial state that reach the detector without scattering, thus the term is proportional to the survival probability. The equilibrium correlations are from particles that have scattered and thermalized, thus the term is proportional to $1 - S^2$.

More accurately, we can say that fluctuations start from an initial value $\langle \delta p_{t1} \delta p_{t2} \rangle_0$ at the formation time τ_0 and evolve toward the equilibrium value $\langle \delta p_{t1} \delta p_{t2} \rangle_e$. The evolution ends at freeze-out and the detected fluctuations $\langle \delta p_{t1} \delta p_{t2} \rangle$ are a function of the freeze-out time through S. If freeze-out is soon after formation then $\tau_F \approx \tau_0$ and there is little time for scattering. Therefore, $S \approx 1$ and $\langle \delta p_{t1} \delta p_{t2} \rangle$ is dominated by the initial value $\langle \delta p_{t1} \delta p_{t2} \rangle_0$. If freeze-out is long after formation then $\tau_F \to \infty$ so that all particles have time to scatter and

completely thermalize. As a result, $S \approx 0$ and $\langle \delta p_{t1} \delta p_{t2} \rangle$ essentially takes on the equilibrium value $\langle \delta p_{t1} \delta p_{t2} \rangle_e$.

We now repeat this calculation for $\mathcal{D}$ by combining (5.70) with Eq. (6.58) to obtain

$$\mathcal{D} - \mathcal{D}_e = \frac{1}{\langle N \rangle^2} \int \delta p_{t1} \left[\Delta G_{12}^0 S^2 + (X_{12}^0 + X_{21}^0) S \right] d\omega_1 d\omega_2 = cS^2 + dS \tag{7.7}$$

where the coefficients are now given by

$$c = \frac{1}{\langle N \rangle^2} \int \delta p_{t1} \Delta G_{12}^0 d\omega_1 d\omega_2 \tag{7.8}$$

and

$$d = \frac{1}{\langle N \rangle^2} \int \delta p_{t1} (X_{12}^0 + X_{21}^0) d\omega_1 d\omega_2. \tag{7.9}$$

The above argument for neglecting the term X_{21}^0 still holds for $\mathcal{D}$. However, without δp_{t2} present inside the integral in (7.9) we cannot neglect the X_{12}^0 term. On the other hand, without δp_{t2} inside the integral in (7.8) the coefficient c vanishes. As in Sec. 5.5, we write the non-equilibrium contribution to correlations as $\Delta G_{12}^0 = \langle \delta f_1 \delta f_2 \rangle_n - \langle \delta f_1 \rangle_n \langle \delta f_2 \rangle_n - \langle \delta f_1 \rangle_n \delta(1-2)$. Without the transverse momentum weight on the second particle, the integral of this function over $d\omega_2$ equals zero due to number conservation.

Therefore, we find

$$\begin{aligned} \mathcal{D} - \mathcal{D}_e &= S \frac{1}{\langle N \rangle^2} \int \delta p_{t1} X_{12}^0 d\omega_1 d\omega_2 \\ &= S \frac{1}{\langle N \rangle^2} \int \delta p_{t1} \left[X_{12}^0 + X_{21}^0 + \Delta G_{12}^0 \right] d\omega_1 d\omega_2 \\ &= S \frac{1}{\langle N \rangle^2} \int \delta p_{t1} \left[G_{12}^0 - G_{12}^e \right] d\omega_1 d\omega_2 \\ &= S(\mathcal{D}_0 - \mathcal{D}_e), \end{aligned} \tag{7.10}$$

where we use the same trick as in (7.5) to replace X_{12}^0 with $G_{12}^0 - G_{12}^e$ inside the integral.

Rearranging this equation we finally obtain

$$\mathcal{D} = \mathcal{D}_0 S + \mathcal{D}_e(1 - S). \tag{7.11}$$

We interpret this result similarly to (7.6). Fluctuations start from an initial value $\mathcal{D}_0$ and evolve toward the equilibrium value $\mathcal{D}_e$. That the terms in (7.11) only have one power of S is directly a result of integrating over the momentum of only one of the particles. In principle, elastic scattering affects the momentum of particles, but not the number, and with only one momentum under consideration we only receive one power of the survival probability.

In line with the previous sentence, we should expect that the final equation for $\mathcal{R}$ contains no powers of S. This turns out to be the case as we can see by rewriting (6.56)

$$\mathcal{R} - \mathcal{R}_e = \frac{1}{\langle N \rangle^2} \int (G_{12} - G_{12}^e)\, d\omega_1 d\omega_2. \tag{7.12}$$

The above arguments still hold and we see the right-hand side of this equation vanishes. Therefore, we find

$$\mathcal{R} = \mathcal{R}_e. \tag{7.13}$$

That is, number conservation implies that event-by-event multiplicity fluctuations are identical in and out of equilibrium. We stress that this need not be the case in general. In these derivations we have made strong assumptions about the linearity of the equations and many simplifying assumptions about the character of the system. Nevertheless, we believe this illustrative example can help provide insight into the thermalization process.

Continuing on, we can now apply the sum rule to find an equation for $\mathcal{C}$. Having found

equations for the other observables we use (6.30) to obtain

$$\begin{aligned}
\mathcal{C} &= (1+\mathcal{R})\,\langle \delta p_{t1}\delta p_{t2}\rangle + 2\langle p_t\rangle\mathcal{D} + \langle p_t\rangle^2\mathcal{R} \\
&= (1+\mathcal{R})[\langle \delta p_{t1}\delta p_{t2}\rangle_0\, S^2 + \langle \delta p_{t1}\delta p_{t2}\rangle_e\,(1-S^2)] + 2\langle p_t\rangle[\mathcal{D}_0 S + \mathcal{D}_e(1-S)] + \langle p_t\rangle^2\mathcal{R}_e \\
&= (1+\mathcal{R})[\langle \delta p_{t1}\delta p_{t2}\rangle_0 + 2\langle p_t\rangle\mathcal{D}_0 + \langle p_t\rangle^2\mathcal{R}_0]S^2 - 2\langle p_t\rangle\mathcal{D}_0 S^2 - \langle p_t\rangle^2\mathcal{R}_0 S^2 \\
&\quad + 2\langle p_t\rangle[\mathcal{D}_0 S - \mathcal{D}_e S] \\
&\quad + (1+\mathcal{R})[\langle \delta p_{t1}\delta p_{t2}\rangle_e + 2\langle p_t\rangle\mathcal{D}_e + \langle p_t\rangle^2\mathcal{R}_e](1-S^2) + 2\langle p_t\rangle\mathcal{D}_e S^2 + \langle p_t\rangle^2\mathcal{R}_e S^2 \\
&= \mathcal{C}_0 S^2 + 2\langle p_t\rangle(\mathcal{D}_0 - \mathcal{D}_e)S(1-S) + \mathcal{C}_e(1-S^2). \qquad (7.14)
\end{aligned}$$

From lines 2 to 3 we add and subtract $\mathcal{D}$ and $\mathcal{R}$ terms. We also separate the initial and equilibrium terms to try and maintain clarity. In the end we find that $\mathcal{C}$ has a more complex relation to S than the other observables. This is a result of $\mathcal{C}$ being weighted by p_t rather than the deviation δp_t. The dependence of $\mathcal{C}$ on $\mathcal{D}$ is particularly curious. ([CCC] Could put a plot of x^2, $1-x^2$ and $x(1-x)$ to show the relative contributions... meh...). As S decreases from 1, the relative contribution of this middle term grows from 0. However, the contribution from the equilibrium term $\mathcal{C}_e$ grows faster. By the time the middle term reaches its maximum, at $S = 1/2$, the $\mathcal{C}_e$ term has fully eclipsed it. As such, we expect the contribution to $\mathcal{C}$ from $\mathcal{D}$ to be minimal but not insignificant.

For completeness, we write the equations for all the observables below:

$$\mathcal{R} = \mathcal{R}_e \qquad (7.15)$$

$$\mathcal{C} = \mathcal{C}_0 S^2 + 2\langle p_t\rangle(\mathcal{D}_0 - \mathcal{D}_e)S(1-S) + \mathcal{C}_e(1-S^2) \qquad (7.16)$$

$$\mathcal{D} = \mathcal{D}_0 S + \mathcal{D}_e(1-S) \qquad (7.17)$$

$$\langle \delta p_{t1}\delta p_{t2}\rangle = \langle \delta p_{t1}\delta p_{t2}\rangle_0\, S^2 + \langle \delta p_{t1}\delta p_{t2}\rangle_e\,(1-S^2). \qquad (7.18)$$

With this, we round out an assortment of observables suitable for studying the degree to which a system has thermalized. In the next section we demonstrate how they may be used

for such a task.

7.2 Comparing with experiment

To compare our results with experiment, we choose to work with $\langle \delta p_{t1} \delta p_{t2} \rangle$ as this data is most readily available at different collisional energies. Rather than directly computing the values $\langle \delta p_{t1} \delta p_{t2} \rangle_0$ and $\langle \delta p_{t1} \delta p_{t2} \rangle_e$ from (6.54) and (7.2), we will estimate them as follows. The local equilibrium value $\langle \delta p_{t1} \delta p_{t2} \rangle_e$ is determined by fluctuations from event to event of the initial participant geometry. We estimate these fluctuations using the blast wave model from Ref. [23]. This model provides excellent phenomenological agreement with a wide range of fluctuation and correlation measurements [87–89].

We mention that practicality drives our use of the blast wave model. We would prefer to compute $\langle \delta p_{t1} \delta p_{t2} \rangle_e$ using dissipation-free hydrodynamics with initial-state fluctuations. However, the statistics must be adequate to distinguish the solid and dashed curves at a range of energies as in Fig. 7.1. Reference [90] is a good example of a preferable model but there are insufficient statistics to address the answers we seek. Experience suggests that this would take millions of events per beam energy.

The initial p_t fluctuations are generated by the particle production mechanism. We approximate this using the independent source model from Sec. 6.2. Specifically, we approximate the early collision as a superposition of independent pp sources. Each source contributes both p_t and multiplicity fluctuations. For $\langle \delta p_{t1} \delta p_{t2} \rangle$ the scaling from proton to ion collisions is given by (6.39):

$$\langle \delta p_{t1} \delta p_{t2} \rangle_0 = \frac{2 \langle \delta p_{t1} \delta p_{t2} \rangle_{pp}}{\langle N_{\rm part} \rangle} \left(\frac{1 + \mathcal{R}_{pp}}{1 + \mathcal{R}_{AA}} \right). \tag{7.19}$$

We fix the coefficient $\langle \delta p_{t1} \delta p_{t2} \rangle_0$ at each beam energy using PYTHIA to calculate $\langle \delta p_{t1} \delta p_{t2} \rangle_{pp}$ and $\mathcal{R}_{pp}$ for proton collisions. We take $\mathcal{R} \propto (dN/dy)^{-1}$ and fix the proportionality constants to be consistent with the blast wave calculation. We do this to ensure that $\langle \delta p_{t1} \delta p_{t2} \rangle_e$ and $\langle \delta p_{t1} \delta p_{t2} \rangle_0$ describe events with the same numbers of particles.

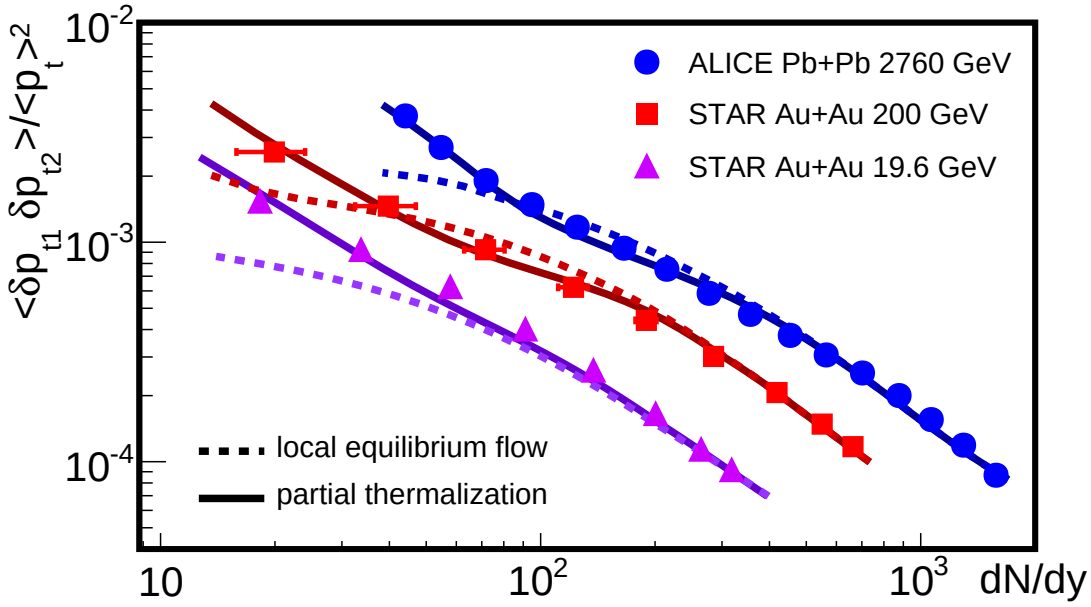

Figure 7.1: Transverse momentum fluctuations as a function of the charged particle rapidity density dN/dy for partial thermalization (solid curves) and local equilibrium flow (dashed curves). Data (circles, squares and triangles) are from Refs. [9], [10] and [11,12], respectively.

Experimental results for $\langle \delta p_{t1} \delta p_{t2} \rangle$ are shown in Fig. 7.1 at three beam energies [9–12]. We plot against the rapidity density dN/dy to allow for eventual comparison to pp or pA collisions [91]. In Pb+Pb and Au+Au systems, dN/dy is highly correlated with impact parameter b. We convert between dN/dy and the number of participants $N_p(b)$ using data from Refs. [92–95]. We mention that the measured $\langle \delta p_{t1} \delta p_{t2} \rangle / \langle p_t \rangle^2$ for different energies lie on top of each other when plotted as functions of N_p. Using dN/dy separates the energies for clarity. All data points in the figure include statistical error bars. Those not visible lie beneath the icons.

To investigate whether the data in Fig. 7.1 shows signs of partial thermalization, we compare with the blast wave model of the event-wise fluctuations of thermalized expansion. The dashed curves in Fig. 7.1 show that blast wave results agree well with data for most of the centrality range, continuing the trend noted in Ref. [23]. However, this comparison shows a significant systematic deviation from the data in the most peripheral region. Events in this

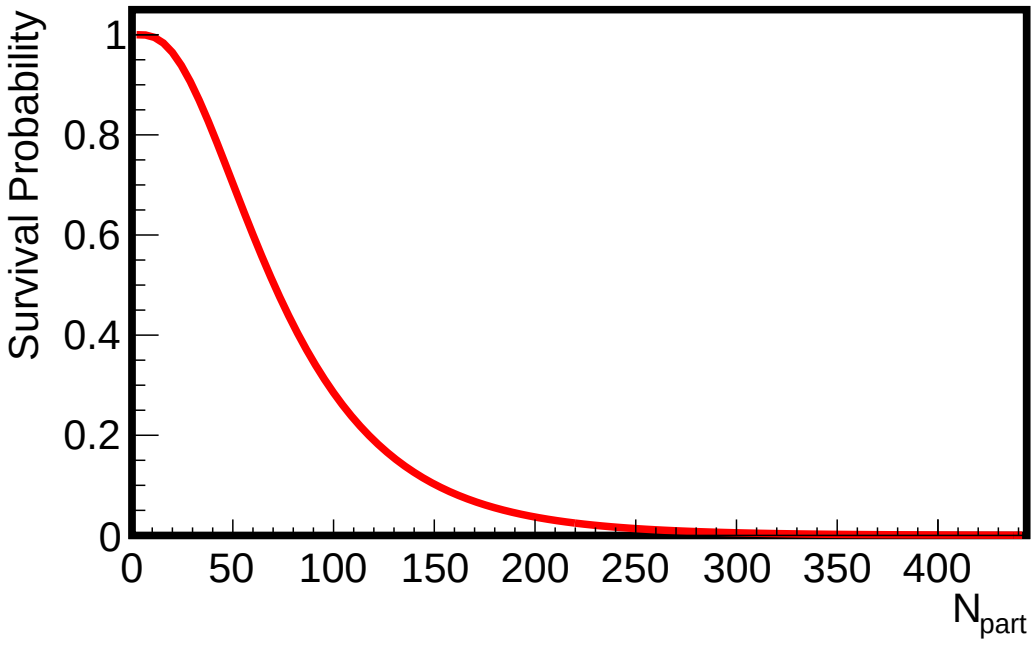

Figure 7.2: Extracted value of the survival probability S as a function of N_{part}. Values are extracted from a fit of $\langle \delta p_{t1} \delta p_{t2} \rangle$ to ALICE data [9] in accord with Eq. (7.18). Peripheral collisions ($N_{part} \approx 0$) are short-lived with low multiplicity so produced particles have a high change to survive. Central collisions ($N_{part} \approx 400$) are long-lived with high multiplicity and produced particles will likely scatter before freeze out.

region correspond to collisions with fewer than ~ 50 participants, compared to the maximum of ~ 400 in central collisions. If thermalization in these small systems is incomplete then this is exactly the type of deviation we should expect.

To see the degree of thermalization in heavy ion collisions that lie in the peripheral region, we compute the initial quantity $\langle \delta p_{t1} \delta p_{t2} \rangle_0$ using Eq. (7.19) and use the blast wave model to determine the equilibrium value $\langle \delta p_{t1} \delta p_{t2} \rangle_e$. We note that the blast wave model we employ uses an $\langle p_t \rangle$ that agrees with measured values at each energy within experimental uncertainties, so that partial thermalization does not appreciably alter $\langle p_t \rangle$ as in [22]. We then use (7.18) to extract S from the ALICE data. The extracted survival probability is shown in Fig. 7.2. We apply this same S to the other energies, neglecting any possible beam dependence for this simple model. The resulting solid curves in Fig. 7.1 agree well with data, giving support to the possibility that these data are indeed measuring thermalization.

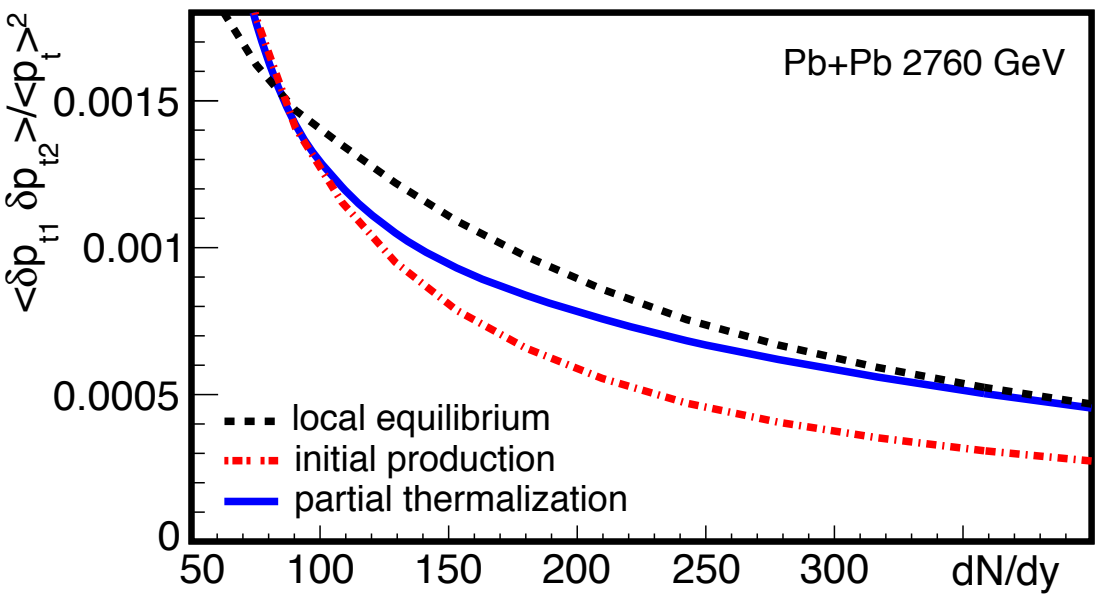

Figure 7.3: Pb+Pb fluctuations as a function of the charged particle rapidity density dN/dy in the peripheral region where partial thermalization (solid curve) drives systems of increasing lifetime from the initial state (dash-dotted curve) to local equilibrium flow (dashed curve).

We emphasize that our model makes a number of simplifying assumptions and more work needs to be done before drawing quantitative conclusions.

To highlight the effect of partial thermalization described by (7.18), we zoom to the peripheral region shown in Fig. 7.3. The dashed and solid curves in this figure represent the same calculations as the corresponding curves in Fig. 7.1. Additionally shown is the dash-dotted initial production curve given by (7.19). In this region the extracted S drops from 1 (for the most peripheral collisions) to 0 (for the most central collisions). Events producing the lowest dN/dy have fluctuations closest to the initial distribution. We expect higher multiplicity events to produce a larger collision volume that is more dense and longer lived. Consequently, the probability that a particle survives the collision without scattering S should be smaller. The values of S we extracted from Fig. 7.1 agree with these expectations as seen in Fig. 7.2. Figure 7.3 shows that the fluctuations given by (7.18) approach locally thermalized behavior $\langle \delta p_{t1} \delta p_{t2} \rangle_e$ above $dN/dy \approx 400$.

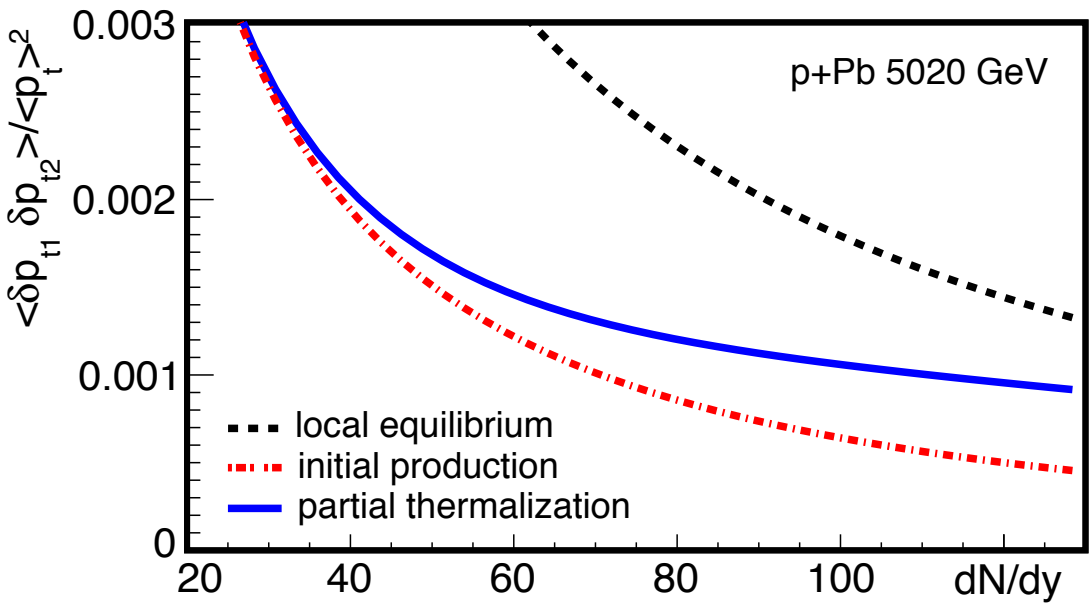

Figure 7.4: In p+Pb collisions partial thermalization becomes more prominent with higher multiplicity dN/dy. Extrapolated fluctuations for partial thermalization (solid curve) are compared to the initial particle production (dash-dotted curve) and local equilibrium flow (dashed curve).

7.3 Predictions

We believe that pA collisions are ideal to search for signs of partial thermalization. The survival probability in these collisions should start at 1 in the most peripheral region, as is the case in heavy ion collisions. Since we do not expect a fully equilibrated system, even in the most central collisions, it should be that S never fully drops to 0. We demonstrate this idea in Fig. 7.4, where we extrapolate our heavy ion estimate to a pA system. We use the appropriate initial values from (7.19) and fit the blast wave parameters to pA data [96]. Our partial thermalization result is obtained using the same S extracted from Fig. 7.1 but in the appropriate dN/dy range. This extrapolation overlooks the fact that the dynamic evolution that determines S in a pA collision is likely very different than that in the larger, longer lived and more dense Pb+Pb system. Nevertheless, the solid curve agrees with our intuition and excites future possibilities.

Using the extracted S we can make a rough prediction of the overall equilibration time

scale ν^{-1}. Kinetic theory implies $\nu \sim \sigma v_{rel} n$, see Eq. (A.18), where the scattering cross section is σ and v_{ref} is the relative velocity. If we take ν to be constant in proper time then the survival probability (5.14) is given by $S \approx \exp\{-\nu(\tau_F - \tau_0)\}$. We estimate $S \approx 0.00435$ for the most central Pb+Pb collisions at 2.76 TeV. For a formation time $\tau_0 = 0.6$ fm and a freeze out time $\tau_F = 10$ fm, we find $\nu^{-1} = 1.7$ fm for the most central Pb+Pb collisions. More realistically, if we take the density $n \propto \tau^{-1}$ – see Eq. (2.19) – to account for longitudinal expansion, but assume σv_{rel} to be constant, then $S \approx (\tau_0/\tau_F)^{\alpha}$, see Eq. (A.19), where $\alpha = \nu_0 \tau_0$ and ν_0 is the initial value of $\nu(\tau)$. We then estimate the initial value $\nu_0^{-1} \sim 0.31$ fm, with a ten-fold increase as the system evolves. These values are consistent with the rapid thermalization required, e.g., by hydrodynamic analyses of flow harmonics.

Figure 7.5 shows a prediction for the value of $\mathcal{D}$ in Pb+Pb collisions at a center of mass energy of $\sqrt{s} = 2760$ GeV. The initial production curve was plotted according to Eq. (6.37) with the pp reference value calculated in PYTHIA. The local equilibrium value of $\mathcal{D}$ was calculated in the blast wave model. A curious feature of the blast wave curve for $\mathcal{D}$ is that it lies entirely below the x-axis. Following our discussion of $\mathcal{D}$ after Eq. (6.25), this could be due to: 1. flow in the blast wave model causing a decrease in $\mathcal{D}$, and 2. a lack of jets in the blast wave, which would cause a rise in $\mathcal{D}$ if present. We are currently investigating this feature to see if this is truly the case. The partial thermalization curve is calculated with (7.17) using the same extracted S shown in Fig. 7.2. As with $\langle \delta p_{t1} \delta p_{t2} \rangle$ we scale both $\mathcal{D}_e$ and $\mathcal{D}_0$ by factors of $\mathcal{R}$ to ensure we describe events with the same number of particles. This curve shows exactly the behavior we expect, shifting from the initial production curve to the local equilibrium curve with increasing centrality.

In Fig. 7.6 we focus on the peripheral region to more closely examine the partial thermalization curve. At $N_{part} \approx 150$ we see a compelling change of sign in $\mathcal{D}$ not present in the other observables. The crossover from positive to negative values could signify the point when the flow-like effects of the more thermalized central collisions begin to dominate the jet-like effects that prevail in peripheral AA and pp collisions. If this feature holds in exper-

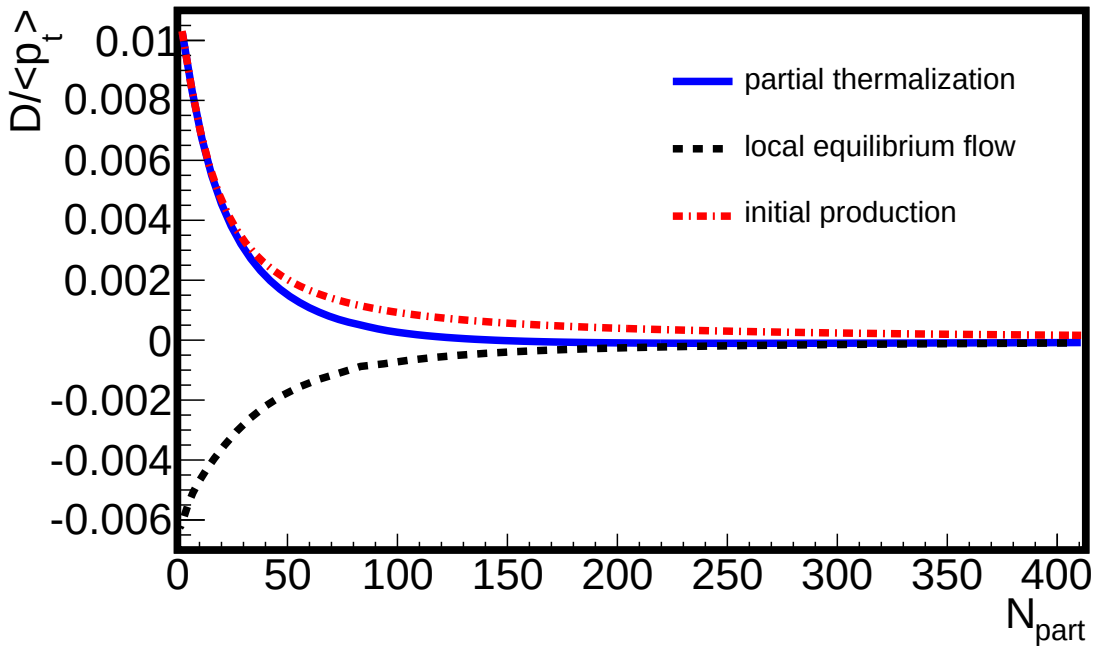

Figure 7.5: Momentum-multiplicity fluctuation prediction for Pb+Pb systems at $\sqrt{s} = 2760$ GeV as a function of number of participants. Partial thermalization, again, drives the system from the initial state to local equilibrium flow. Significantly, local equilibrium flow lies entirely below the x-axis.

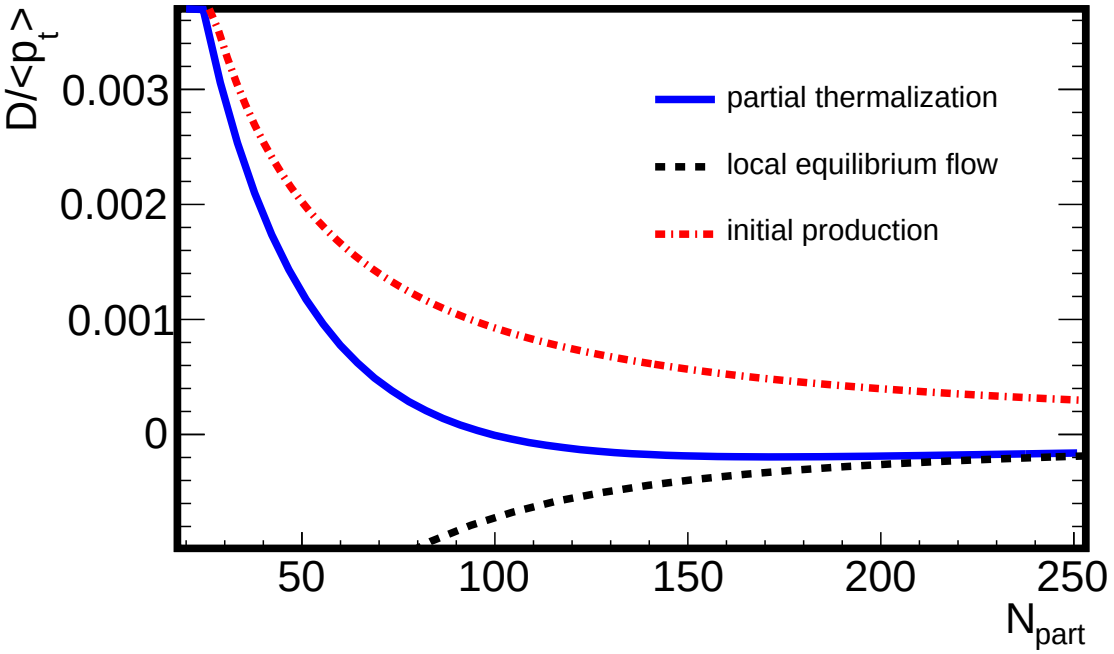

Figure 7.6: The same curves shown in Fig. 7.5, focused on the peripheral region. As the system is propelled from the initial state toward local equilibrium we see a clear crossover from positive to negative values at $N_{part} \approx 150$, a potentially striking sign of thermalization.

iment, we feel that $\mathcal{D}$ could prove to be an invaluable tool in measuring thermalization. We mention two caveats with this result. First, it must be verified that $\mathcal{D}$ is indeed negative for local equilibrium flow and not simply a feature of the blast wave model. Second, the shape of S plays a large role in the crossing. If, for example, S did not drop from 1 as sharply, then it may be that the partial thermalization curve can maintain positive values. More work must be done to investigate both of these possibilities.

Figure 7.7 shows the prediction curves of $\mathcal{C}$ in Pb+Pb collisions at $\sqrt{s} = 2760$ GeV plotted against number of participants. The initial production curve is calculated using the independent source model Eq. (6.38). The pp reference value is calculated in PYTHIA. For local equilibrium flow we again use the blast wave model. The partial thermalization curve is calculated using (7.16) using the extracted value of S from Fig. 7.2. Values of $\mathcal{C}_e$ and $\mathcal{C}_0$ are scaled by factors of $\mathcal{R}$ to, again, ensure we are describing events with the same multiplicity. In the most peripheral and most central regions, $\mathcal{C}$ behaves as expected, respectively matching the initial and local equilibrium curves. With current model parameters, the value of the initial production curve does not differ appreciably from that of equilibrium flow. Due to this we do not expect $\mathcal{C}$ to give us much information in regards to thermalization of the system in the most extreme regions. However, $\mathcal{C}$ does have a unique feature around $N_{part} \approx 30 - 200$. In this range $\mathcal{C}$ distinctly deviates from both the initial and equilibrium curves.

In Fig. 7.8 we multiply $\mathcal{C}/\langle p_t \rangle^2$ by the multiplicity to get a better look at the deviation. The initial production curve is perfectly flat, as to be expected since $\mathcal{C}_0 \propto \langle N_{part} \rangle^{-1}$. The local equilibrium curve also shows this except in the peripheral region where the blast wave does a poor job of describing non-thermalized behavior. The partial thermalization curve exhibits a clear peak around $N_{part} \approx 70$, another potentially striking signature of thermalization. The origin of this effect is entirely due to the term in (7.16) proportional to $S(1 - S)$ and its causes are two-fold. First, $S(1 - S)$ has a maximum at $S = 1/2$, which is around the same location as the peak, as seen in Fig. 7.2. Second, the quantity $\mathcal{D}_0 - \mathcal{D}_e$ is guaranteed to be positive since $\mathcal{D}_0 > 0$ is invariably true and since $\mathcal{D}_e$ is always negative for the blast wave.

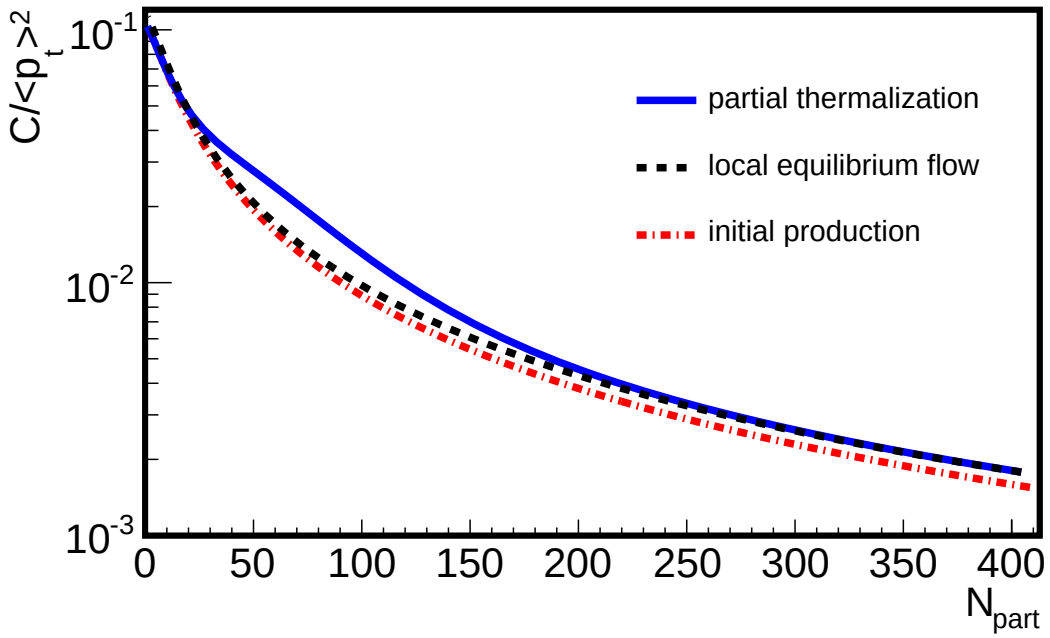

Figure 7.7: Prediction curves for $\mathcal{C}$ in Pb+Pb collisions at $\sqrt{s} = 2760$ GeV. Behavior is as expected in the most peripheral and central regions, with the mid-peripheral deviation being due to the middle term in (7.16).

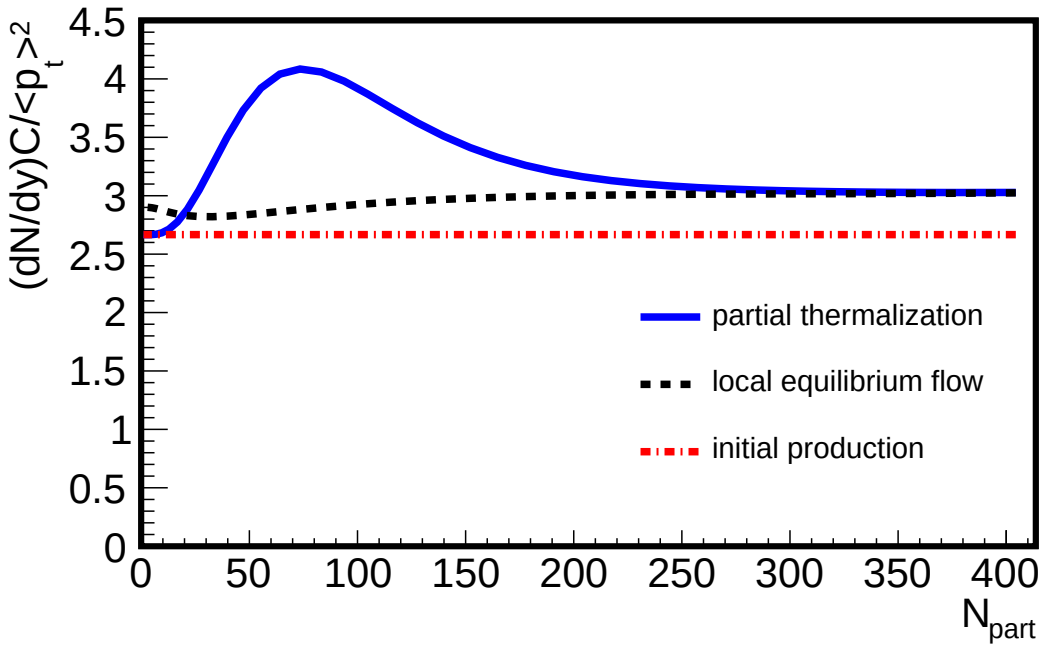

Figure 7.8: Curves in Fig. 7.7 multiplied by dN/dy to emphasize the deviation of the partial thermalization curve. Initial production and local equilibrium curves are relatively flat in centrality while we see a clear peak at $N_{part} \approx 70$ in the partial thermalization curve.

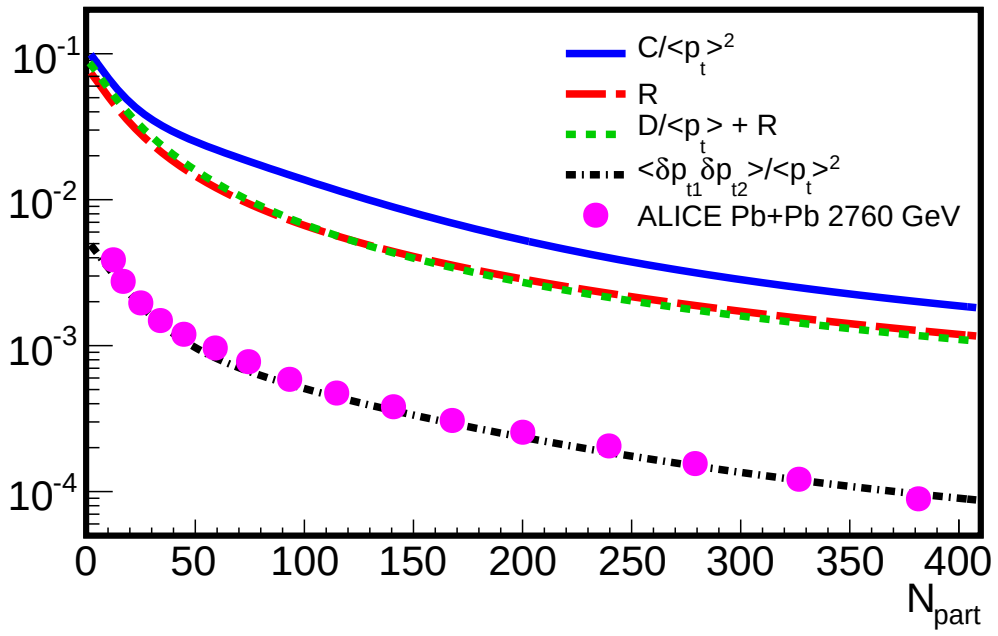

Figure 7.9: All of the observables plotted together. All show correlations diminishing in central collisions. We see that $\mathcal{C}$ and $\mathcal{D}$ each offer unique features in studying thermalization. Data is the same as in Fig. 7.1.

Together, these two cooperating causes promise a positive contribution from the middle term in (7.16), forming the distinct peak.

For completeness we plot all of the observables together in Fig. 7.9. In order to show the character of the curves on a log-plot we replace[1] the sometimes negative $\mathcal{D}/\langle p_t\rangle$ with the always positive $\mathcal{D}/\langle p_t\rangle + \mathcal{R}$. That $\mathcal{R}$ and $\mathcal{D}/\langle p_t\rangle$ overlap is due to $\mathcal{R}$ being an order of magnitude larger. All of the observables show the same behavior with rising centrality. As the system size and lifetime increases, correlations are gradually washed out by progressively increasing equilibration. This figure draws attention to two important aspects of our previous discussions. First, $\mathcal{D}$ is the only observable in our collection that crosses the x-axis. Second, $\mathcal{C}$ is the only observable that exhibits the conspicuous deviation in the mid-centrality range. We believe these two traits are compelling enough to show that $\mathcal{C}$ and $\mathcal{D}$ are two of the most potent tools available to study thermalization in ion collisions.

We emphasize that the results in this section are heavily dependent on the assumptions

[1]The motivation here is that making this replacement only changes the sign on $\mathcal{D}$ in the sum rule.

from previous chapters. Furthermore, in accordance with the blast wave model, we have used an $\langle p_t \rangle$ in all of our calculations that is independent of S. This scenario need not be true in experiment. We have scaled our initial conditions to be consistent with blast wave model calculations. While this seems reasonable, there may be unintended side effects when altering values from well established models (i.e. PYTHIA and the blast wave). However, we note that we do take care to manage consistency by, e.g. making sure the sum rule (6.30) holds. Our expectation is that these results serve as a decent approximation to reality. That is, we expect $\mathcal{C}$ and $\mathcal{D}$ to each give us a unique and meaningful look into the equilibration process. It may be that these observables provide us with the best opportunity to learn new physics but we can state nothing conclusive at this point. Many assumptions can be improved upon and we leave this avenue open for future work. Nevertheless, we are optimistic that more realistic assumptions will provide us with more refined results strengthening these methods.

CHAPTER 8 SUMMARY AND DISCUSSION

8.1 Summary

The principal goal of this thesis is to develop a theoretical and phenomenological toolkit for studying nonequilibrium features of correlation measurements. By injecting Langevin noise into kinetic and hydrodynamic theory, we obtain differential equations that can be used to study the evolution of correlations and other aspects of ion collisions. We point to specific observables that can highlight the features that we find most interesting.

In chapter 2, we introduce some of the concepts we will use throughout the rest of the work. The kinematic variables and Bjorken model discussed will be familiar to any researcher in the field but serve as a basis for our discussion. To complement the Bjorken model of longitudinal expansion, we also review the blast wave model of transverse expansion. This model acts as our local equilibrium baseline for studying unthermalized systems.

Chapter 3 is where we begin to detail the essence of this work. We open with examples of Langevin noise as applied to the problems of Brownian motion and particle number diffusion. This highlights the aspects of stochastic noise that we use in later sections, namely the manner in which we use noise to introduce correlations to a system. Our first main result, Eq. (3.59), is a novel way to describe correlations in second order hydrodynamics.

In chapter 4 we discuss dissipative relativistic hydrodynamics in both first and second order theory. The discussion of first order theory points out the acausal nature of the Navier-Stokes equation. This motivates the move to second order so as to restore causality. We also discuss the importance of shear modes in studying transverse momentum correlations. We demonstrate a method of applying our approach, to linear order, to a fluid undergoing Bjorken expansion. We conclude this chapter with an application to heavy ion collisions by studying the width in rapidity of transverse momentum correlations.

Chapter 5 is devoted to applying Langevin noise to kinetic theory. We begin with a general discussion of the Boltzmann equation and the relaxation time approximation, as well their linearized versions. We stress the importance of the microscopic conservation laws

and introduce projection operators, derived from the linearized equation, to enforce these laws. Formal solutions to the equations are obtained using the method of characteristics. In order to describe nonequilibrium correlations we introduce Langevin fluctuations to the Boltzmann equation. Our main result is Eq. (5.60), an evolution equation for the two-particle phase space correlation function. Finally, we construct a formal solution to this equation as a first step in analyzing transverse momentum correlations in ion collisions.

In chapter 6 we discuss the observables that are relevant to our work. Multiplicity fluctuations are a useful measure of the deviation from statistical behavior and, furthermore, are helpful in comparing different types of measurements. Transverse momentum fluctuations have twofold importance to our work. The observable $\mathcal{C}$ is sensitive to shear viscosity and is used to study transport coefficients of the collision system. We use the covariance $\langle \delta p_{t1} \delta p_{t2} \rangle$ to study the onset of thermalization in ion collisions. We also introduce a new observable $\mathcal{D}$ to study the interplay between momentum and multiplicity. This rounds out our set of observables in the sense of Eq. (6.30), the sum rule. Also in this chapter, we connect the correlation functions from previous chapters to these observables. We round out the chapter by comparing $\mathcal{C}$ to experiment and demonstrate that second order hydrodynamics describes heavy ion collisions better than first order diffusion.

In chapter 7 we put our results from chapter 5 to use by studying the approach nonequilibrium systems take toward equilibration. We find that each of our observables offers a unique look into the process. Using $\langle \delta p_{t1} \delta p_{t2} \rangle$ we compare to available data in order to demonstrate the promise of our methods. We make a prediction for pA collisions that shows the importance these small systems may hold in regards to learning about nonequilibrium behavior. Finally, we make further predictions for $\mathcal{C}$ and $\mathcal{D}$, both of which indicate potentially striking signals of partial thermalization.

8.2 Discussion

This work represents our first step toward building a theoretical description of fluctuations and correlations in the pre-equilibrium fluid. While our results indicate that our method

provides a good schematic understanding of the problems we address, it is important to understand the limitations of this approach as well as to draw a road map for future work.

Our kinetic theory scheme only considers dynamic fluctuations due to the actual collisions of partons. These fluctuations result in a locally correlated Langevin noise described by (5.43) with (5.56). Additionally present, for example, are stochastic quantum fields as discussed in Ref. [97]. These fields introduce momentum gradients to the left hand side of the Boltzmann equation. This can be incorporated into our framework by generalizing the method of characteristics. The locality of the noise can also be extended to finite-size by such fields, the importance of which is discussed in [98]. Meanwhile, overpopulation in regions of phase space can result in occupation numbers large enough so that quantum statistics, Bose-Einstein condensation and other quantum effects can become important [99]. These effects can eventually be included in our framework.

We reiterate that many of our results rely on assumptions and procedures that can be improved upon. Refinement of our theoretical techniques should result in more quantitative conclusions. Furthermore, future experimental measurements, pA in particular, will help guide our understanding. In the meantime, we can work to improve our partial thermalization model by incorporating a three-dimensional hydrodynamic code with more realistic initial conditions. More immediate, we can improve on the value of the survival probability S. For one, by accounting for the likelihood that S is dependent on collisional energy, but even more so we would prefer to calculate S from theory in order to solidify our model. While this is not necessarily a difficult task, it is relegated to future work. Finally, as an interesting aside, we have ideas of using our evolution equation to test simulation codes for accuracy in regions where the answers are expected to overlap. Specifically, our solution (5.70) can be compared to fluctuating hydrodynamics in the low density regime where both the Boltzmann equation and hydrodynamics generally give the same answers [38–41, 45, 100–102].

In regards to our hydrodynamic results, we are currently working to incorporate time and temperature dependent coefficients τ_π^* and ν^*. We are also intrigued by the possibility

of studying these coefficients in pA systems. This is a nontrivial extension of our current methods, however, as it involves solving the coupled equations (3.56) and (3.57). We have plans to extend our approach to other modes in order to address a wider range of observables. In particular, diffusion of net charge and baryon number can be addressed and these have been studied by a number of authors [103–108].

In conclusion, we are optimistic about our current approach. Perhaps the most exciting potential resides in small systems. It is well accepted that central collisions of large nuclei exhibit hydrodynamic flow. While data in Fig. 7.1 agree with this viewpoint, we also see a systematic discrepancy from local equilibrium flow in the peripheral region. This indicates that the first traces of thermalization should emerge in peripheral collisions and become more significant with increasing centrality as the system lifetime increases. Our partial thermalization model is in excellent agreement with data over a range of energies. For this reason we are excited by the possibility of future pA measurements. Our extrapolation to these shorter lived systems in Fig. 7.4 suggests that full equilibration never occurs, making the study of partial thermalization all the more important.

APPENDIX

A.1 Wiener Process

In this section we will develop some concepts from stochastic calculus needed for the main text. This is not meant to make the work self-contained but only to shine a light on the ideas we will use. One of our goals is to study how heavy ion collision systems diffuse stochastically in a manner similar to Brownian motion. The physical process of Brownian motion is described mathematically by the Wiener process[1].

To keep the discussion simple we will start by assuming we are working with a one-dimensional, classical system. The Wiener process $W(t)$ is a random variable described by the probability density function $p(x,t)$ which solves the diffusion equation

$$\frac{\partial p}{\partial t} = \frac{\Gamma}{2}\frac{\partial^2 p}{\partial x^2}. \tag{A.1}$$

where the coefficient Γ governs the strength with which p evolves and the factor of $1/2$ is for convenience. As an initial condition, we assume a spike in probability at the origin. The Wiener process then describes the spreading of this localized perturbation – see Fig. A.1. Thus, given the initial condition $p(x,0) = \delta(x)$, one can work out the solution

$$p(x,t) = \frac{1}{\sqrt{2\pi\Gamma t}} e^{-\frac{x^2}{2\Gamma t}}, \tag{A.2}$$

which is simply a Gaussian distribution with mean 0 and variance Γt. The Wiener process $W(t)$ is then defined via $P[a \leq W(t) \leq b] = \int_a^b p(x,t)dx$. Based on the Gaussian form of p one can easily find the first two moments:

$$\langle W(t) \rangle = 0 \qquad \text{and} \qquad \langle W^2(t) \rangle = \Gamma t. \tag{A.3}$$

Due to the relation between W and the Gaussian distribution, the Wiener process is some-

[1]The Wiener process is an example of a continuous-time stochastic process. It is named in honor of Norbert Wiener whose early work on stochastic processes and noise was influential to the field.

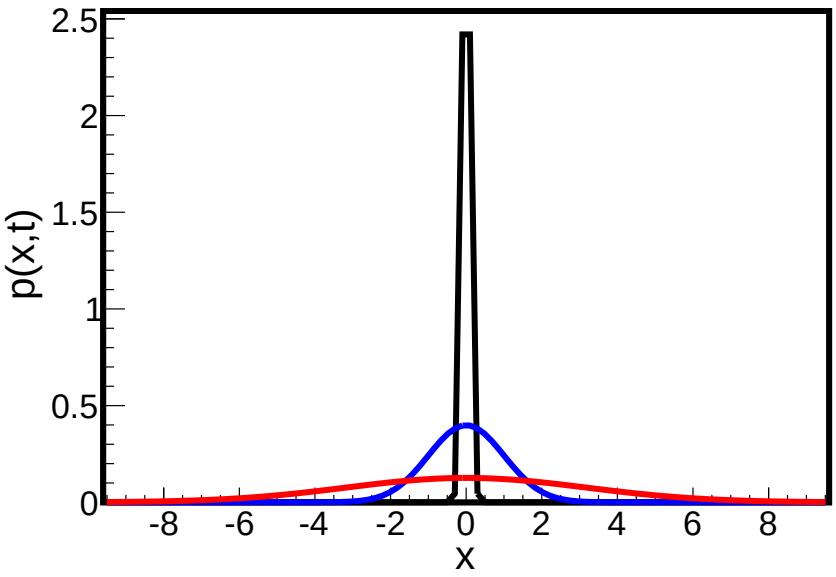

Figure A.1: Plots of the Gaussian $p(x,t)$ at different times. The initial δ-function undergoes diffusion, spreading out at later times. For this example we choose $\Gamma = 1$ and the times shown are $t = 0.1$ s (black), $t = 1$ s (blue), $t = 10$ s (red).

times referred to as Gaussian (white) noise.

It is worth taking a moment to discuss the meaning of these average brackets as they are not an average over time nor do they have the same meaning as is traditional in the field of heavy ion physics. Rather, we will be using $W(t)$ to model random "kicks" a system receives due to internal stochastic processes. In this sense, the $\langle \cdots \rangle$ represents an average over an ensemble of systems that have evolved stochastically from the same initial condition, i.e. systems that have received all different manner of kicks. We refer to this as a "thermal" or "noise" average.

An event average in heavy ion physics, say $\langle N \rangle$, represents the number of particles in an event averaged over an ensemble of different events. This ensemble is meant to represent all possible collisions, in particular it encompasses events that have different initial conditions as well as events that evolve differently from the same initial conditions. A full event average needs to consider both of these situations. The average brackets used in this section only consider the stochastic evolution of a system from a particular initial condition. To reconcile

this with a full event average we will also have to average over initial conditions. In the text there is little chance for confusion so we will simply use $\langle \cdots \rangle$ in the majority of this work. In Sec. 6.1 where we must make a distinction, we will use $\langle \cdots \rangle_n$ to represent the noise average.

An important assumption we must make for Wiener processes is the property of independent increments, where an increment is defined as $\Delta W(t) \equiv W(t + \Delta t) - W(t)$ for the time step Δt. Mathematically this means $\Delta W(t)$ and $\Delta W(s)$ are statistically independent so long as $t \neq s$, and we can write

$$\langle \Delta W(t) \Delta W(s) \rangle = \langle \Delta W(t) \rangle \langle \Delta W(s) \rangle = 0, \tag{A.4}$$

where the last step follows clearly from Eq. (A.3)[2]. An example is the random walk process: knowing the motion of the first few steps gives no information on the motion of the next few steps. Brownian motion is another example if we assume the collisions are sufficiently random, which is the position we take in the text.

Our next step is to find the covariance $\langle W(s)W(t) \rangle$. First, note that for $t < s$, $W(s) - W(t)$ forms an increment which must be independent from the increment $W(t) - W(0) = W(t)$. Then we have

$$\begin{aligned} \langle W(s)W(t) \rangle &= \langle (W(s) - W(t))W(t) + W^2(t) \rangle \\ &= \langle (W(s) - W(t))W(t) \rangle + \langle W^2(t) \rangle \\ &= 0 + \Gamma t \\ &= \Gamma \min(t, s) \end{aligned} \tag{A.5}$$

where the last line simply removes the restriction $t < s$. Finally, we use this to calculate

[2]A more formal treatment of the subject would be careful to define a sequence $t_1 < t_2 < \ldots < t_n$ rather than use a generic time step Δt. For the sake of simplicity and notation we will avoid this and assume our time step behaves properly, i.e. $t \neq s$ implies the intervals $[t, t + \Delta t]$ and $[s, s + \Delta s]$ do not overlap.

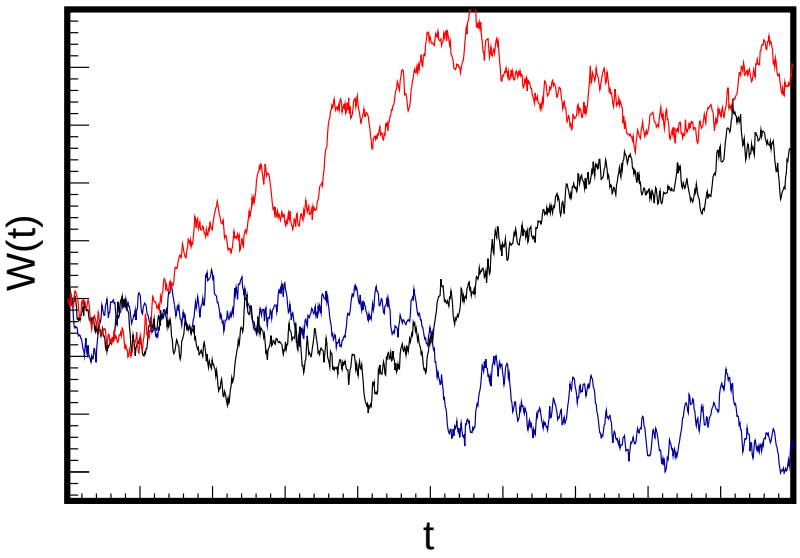

Figure A.2: Sample paths taken by $W(t)$. Paths starting from the same point can vary wildly, demonstrating the effect noise can have on a system over time. The jaggedness of the lines represents the variability in the increments $\Delta W(t)$.

$\langle \Delta W^2 \rangle$:

$$\begin{aligned}
\langle \Delta W^2 \rangle &= \langle [W(t+\Delta t) - W(t)]^2 \rangle \\
&= \langle W^2(t+\Delta t) \rangle + \langle W^2(t) \rangle - 2\langle W(t+\Delta t) W(t) \rangle \\
&= \Gamma(t+\Delta t) + \Gamma t - 2\Gamma t \\
&= \Gamma \Delta t. \qquad \text{(A.6)}
\end{aligned}$$

The two most important equations to take away from this section are

$$\langle \Delta W \rangle = 0 \qquad \text{and} \qquad \langle \Delta W^2 \rangle = \Gamma \Delta t. \qquad \text{(A.7)}$$

We use these extensively in the text and they form a basis for our incorporation of stochastic processes into heavy ion collisions.

Equation (A.6) marks one of the major differences between regular calculus and stochastic calculus. The relation $\Delta W^2 \propto \Delta t$ indicates that ΔW is an increment (or differential if we

were to formally define dW) on the order of one-half Δt. Then, terms of order one-half or three-halves Δt vanish due to the first equation in (A.7) and terms of higher order vanish as in regular calculus. In practice, one can use this rule to simplify many problems in stochastic calculus, including the Itô product rule in the next section.

An interesting quirk of the Wiener process is its lack of differentiability, as one can infer from Fig. A.2. Thus, while dW is often used in stochastic differential equations (or ΔW in our equations), the derivative dW/dt does not exist. We work around this by eliminating ΔW before writing complete equations – i.e. dividing by Δt and taking its limit to zero. One can develop other methods to deal with this seemingly inconsistent differential, including actual methods of integration. These can be found in the numerous texts written on the subject – e.g. [34, 109–112].

Finally, we will briefly mention a multivariate extension of the Wiener process as it will be used in the text. In systems more complicated than the one-dimensional example used above, we may wish to affix noise to several different compenents x_i. As such, each component of noise will acquire a new subscript ΔW_i. The rules for ΔW_i remain the same as those listed above. In addition we need another rule for the interaction between the different components. The simplest way to accomplish this is to assume there is no interaction – i.e. $\langle \Delta W_i \Delta W_j \rangle = 0$ for $i \neq j$. Therefore, for the multivariate extension we employ, we simply modify Eq. (A.7) by including a delta-function:

$$\langle \Delta W_i \rangle = 0 \qquad \text{and} \qquad \langle \Delta W_i \Delta W_j \rangle = \delta_{ij} \Gamma_i \Delta t. \tag{A.8}$$

A.2 Ito product rule

Now that we have incorporated new differentials into our toolbox, the product rule of regular calculus will no longer suffice. We need a more general product rule that realizes the product of two half-order differentials is of order Δt. For this we look to the calculus of finite differences. Similar to increments above, for the time step Δt, we define the finite difference

of a function $f(t)$ as $\Delta f \equiv f(t+\Delta t) - f(t)$ which we can also write as $f(t+\Delta t) = f(t) + \Delta f$. Now, consider two arbitrary functions of t, $x(t)$ and $y(t)$. For the product $x(t)y(t)$ we have

$$\begin{aligned}\Delta[x(t)y(t)] &= x(t+\Delta t)y(t+\Delta t) - x(t)y(t) \\ &= [x(t)+\Delta x][y(t)+\Delta y] - x(t)y(t) \\ &= x(t)\Delta y + y(t)\Delta x + \Delta x \Delta y. \end{aligned} \tag{A.9}$$

In ordinary calculus, functions $f(t)$ satisfy the differential equation $df(t)/dt = A(t)$, where $A(t)$ is another function – i.e. the derivative. Writing this as a difference equation we have $\Delta f = A(t)\Delta t$, implying that the difference Δf is of order Δt. Products such as $\Delta x \Delta y$ in Eq. (A.9) are then of order Δt^2 and vanish much faster than the lower order terms as t approaches 0. Therefore, with the understanding that a limit will eventually be taken, we drop them from the equation and write the product rule as $\Delta(xy) = x\Delta y + y\Delta x$.

As an analogue to the above, in stochastic calculus, functions satisfy the difference equation $\Delta f(t) = A(t)\Delta t + B(t)\Delta W(t)$, where one can think of the function $B(t)$ as a stochastic counterpart of a derivative. Note that $B(t)$ need not have any relation to the regular derivative $A(t)$. Now, for the product $\Delta x \Delta y$ we have

$$\begin{aligned}\Delta x \Delta y &= [A_x \Delta t + B_x \Delta W_x][A_y \Delta t + B_y \Delta W_y] \\ &= [B_x B_y]\Delta W_x \Delta W_y + A_x B_y \Delta t \Delta W_y + B_x A_y \Delta t \Delta W_x + A_x A_y \Delta t^2. \end{aligned} \tag{A.10}$$

As in ordinary calculus, we can safely drop order Δt^2 terms. In stochastic calculus, due to Eq. (A.7) we can also drop terms proportional to ΔW knowing that we will eventually take an average. The first term in Eq. (A.10) is proportional to ΔW^2 so is of order Δt and it must remain. Therefore, we can write the product rule as

$$\Delta(xy) = [xA_y + yA_x]\Delta t + B_x B_y \Delta W_x \Delta W_y \tag{A.11}$$

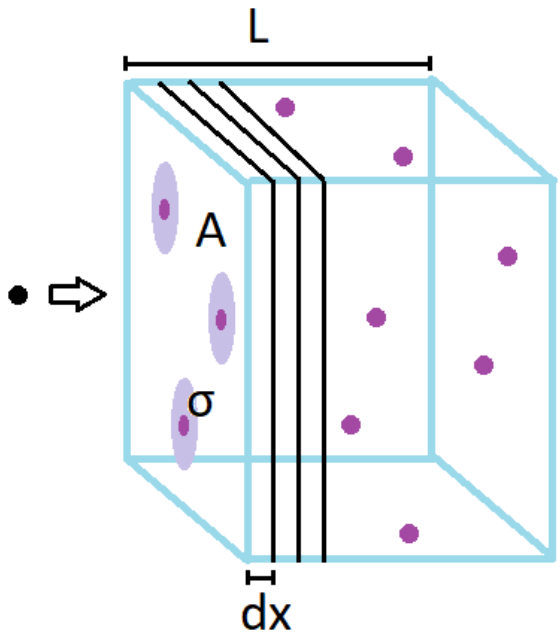

Figure A.3: A particle traveling toward a fluid, divided into equal slices of volume Adx. As it approaches the first volume slice it sees only a single layer of fluid particles. The fluid particles have a collision cross section σ, depicted as a large disk surrounding the particles.

This equation – or simply Eq. (A.9) – is known in stochastic calculus as the Itô product rule.

A.3 Survival probability

The survival probability S is the probability that a particle escapes a fluid without suffering any collisions. It plays a major role in much of this work so it is worth discussing briefly. In general, we can write $S = e^{-\mathcal{N}}$ where $\mathcal{N}$ is the number of collisions between fluid particles. Now we quickly outline why this is true and why it takes the form given in Eq. (5.14).

Imagine a particle traveling toward a fluid as shown in Fig. A.3. The length of the fluid parallel to the velocity of the particle is L. The area of the fluid perpendicular to the velocity is A. The volume of the fluid is then given by $V = AL$. We divide the length L into M segments, each of length dx so that $Mdx = L$. This also subdivides the volume so that each new volume segment has volume $dV = Adx$. We assume dx to be small enough so that

two particles in the same volume slice cannot overlap, from the viewpoint of the traveling particle.

The probability that the traveling particle collides with one of the fluid particles in the first volume segment equals the number of particles in that volume slice times the proportion of transverse area taken up by a particle. Symbolically we have, for the cross sectional area σ and particle density n:

$$\begin{aligned}\text{Probability of colliding} &= (\text{Number of particles in volume slice}) \cdot \frac{\sigma}{A} \\ &= n \cdot dV \cdot \frac{\sigma}{dV/dx} \\ &= \sigma \cdot n \cdot dx. \end{aligned} \tag{A.12}$$

Therefore, the probability of surviving the first slice unscathed is given by $1 - \sigma n dx$. If the traveling particle survives the first slice, then it has the same probability of surviving the second slice and so on. In total, the probability of surviving all of the slices is given by

$$S_M = (1 - \sigma n dx)^M = \left(1 - \frac{\sigma n L}{M}\right)^M. \tag{A.13}$$

Taking the limit $dx \to 0$ or, equivalently, $M \to \infty$ gives the survival probability

$$S = e^{-\sigma n L}, \tag{A.14}$$

where we use the exponential function identity $\lim_{t\to\infty}(1 - x/t)^t = \exp\{-x\}$.

Now we show the quantity $\sigma n L$ is equal to the number of collisions between the fluid particles during the time the traveling particle takes to move through the fluid. The distance traveled by a fluid particle before colliding with another is the mean free path of the fluid, given by $\lambda = 1/\sigma n$. Therefore, we have

$$\sigma n = \frac{1}{\lambda} = \frac{\text{Number of collisions}}{\text{Unit distance}} = \frac{\text{Number of collisions}}{L}. \tag{A.15}$$

giving us the desired result.

More generally, the number of collisions during the time interval dt is given by

$$(\text{Collision rate}) \cdot dt = \nu dt, \tag{A.16}$$

where $\nu = \nu(t)$ can depend on t. The total number of collisions during the time interval $t - t_0$ that it takes for the traveling particle to pass through the fluid is then $\int_{t_0}^{t} \nu(t)dt$. Putting everything together we find the survival probability is given by

$$S(t, t_0) = e^{-\int_{t_0}^{t} \nu(t')dt'}, \tag{A.17}$$

which matches Eq. (5.14).

As a sidenote, we mention an approximate form of S used in the text. We can write

$$\nu \Delta t = \sigma \cdot n \cdot \Delta L \qquad \Rightarrow \qquad \nu = \sigma \cdot n \cdot \frac{\Delta L}{\Delta t} = \sigma v_{rel} n. \tag{A.18}$$

where v_{rel} is the velocity of the traveling particle relative to the fluid particles. Bjorken expansion implies that $n \propto \tau^{-1}$ (see Eq. (2.19)) where we switch to the proper time τ, more appropriate for ion collisions. We can write $\nu = \sigma v_{rel} \beta / \tau = \alpha / \tau$ where $\alpha = \nu_0 \tau_0$. The survival probability is then

$$S(\tau_F, \tau_0) = e^{-\int_{\tau_0}^{\tau_F} \alpha/\tau d\tau} = e^{-\alpha \ln(\tau_F/\tau_0)} = \left(\frac{\tau_0}{\tau_F}\right)^{\alpha} \tag{A.19}$$

We use these approximations briefly to discuss results in Sec. 7.2.

BIBLIOGRAPHY

[1] K Aamodt et al. Elliptic flow of charged particles in Pb-Pb collisions at 2.76 TeV. *Phys. Rev. Lett.*, 105:252302, 2010.

[2] Raimond Snellings. Elliptic Flow: A Brief Review. *New J. Phys.*, 13:055008, 2011.

[3] J. Velkovska. P(t) distributions of identified charged hadrons measured with the PHENIX experiment at RHIC. *Nucl. Phys.*, A698:507–510, 2002.

[4] C. Adler et al. Measurement of inclusive anti-protons from Au+Au collisions at (s(NN))**(1/2) = 130-GeV. *Phys. Rev. Lett.*, 87:262302, 2001.

[5] Ulrich W. Heinz and Peter F. Kolb. Two RHIC puzzles: Early thermalization and the HBT problem. In *18th Winter Workshop on Nuclear Dynamics (WWND 2002) Nassau, Bahamas, January 20-22, 2002*, pages 205–216, 2002.

[6] Betty Bezverkhny Abelev et al. Multiparticle azimuthal correlations in p -Pb and Pb-Pb collisions at the CERN Large Hadron Collider. *Phys. Rev.*, C90(5):054901, 2014.

[7] H. Agakishiev et al. Evolution of the differential transverse momentum correlation function with centrality in Au+Au collisions at $\sqrt{s_{NN}}$ = 200 GeV. *Phys.Lett.*, B704:467–473, 2011.

[8] *M. Sharma and C. Pruneau (private communication, 2010).*

[9] Betty Bezverkhny Abelev et al. Event-by-event mean $p_{\mathbf{T}}$ fluctuations in pp and Pb-Pb collisions at the LHC. *Eur. Phys. J.*, C74(10):3077, 2014.

[10] John Adams et al. Incident energy dependence of p(t) correlations at RHIC. *Phys. Rev.*, C72:044902, 2005.

[11] J. Novak et al. Searching for the QCD Critical Point with the Energy Dependence of p_t Fluctuations. http://meetings.aps.org/link/BAPS.2013.DNP.JG.2, 2013.

[12] John Novak. *Energy dependence of fluctuation and correlation observables of transverse momentum in heavy-ion collisions.* PhD thesis, 2013.

[13] John Adams et al. Experimental and theoretical challenges in the search for the quark gluon plasma: The STAR Collaboration's critical assessment of the evidence from RHIC collisions. *Nucl. Phys.*, A757:102–183, 2005.

[14] K. Adcox et al. Formation of dense partonic matter in relativistic nucleus-nucleus collisions at RHIC: Experimental evaluation by the PHENIX collaboration. *Nucl. Phys.*, A757:184–283, 2005.

[15] B. B. Back et al. The PHOBOS perspective on discoveries at RHIC. *Nucl. Phys.*, A757:28–101, 2005.

[16] Chun Shen and Ulrich Heinz. The road to precision: Extraction of the specific shear viscosity of the quark-gluon plasma. 2015.

[17] Vardan Khachatryan et al. Observation of Long-Range Near-Side Angular Correlations in Proton-Proton Collisions at the LHC. *JHEP*, 09:091, 2010.

[18] Serguei Chatrchyan et al. Multiplicity and transverse momentum dependence of two- and four-particle correlations in pPb and PbPb collisions. *Phys. Lett.*, B724:213–240, 2013.

[19] Georges Aad et al. Measurement with the ATLAS detector of multi-particle azimuthal correlations in p+Pb collisions at $\sqrt{s_{NN}} = 5.02$ TeV. *Phys. Lett.*, B725:60–78, 2013.

[20] Betty Abelev et al. Long-range angular correlations on the near and away side in p-Pb collisions at $\sqrt{s_{NN}} = 5.02$ TeV. *Phys. Lett.*, B719:29–41, 2013.

[21] A. Adare et al. Quadrupole Anisotropy in Dihadron Azimuthal Correlations in Central d+Au Collisions at $\sqrt{s_{_{NN}}}$=200 GeV. *Phys. Rev. Lett.*, 111(21):212301, 2013.

[22] Sean Gavin. Traces of thermalization from transverse momentum fluctuations in nuclear collisions. *Phys. Rev. Lett.*, 92:162301, 2004.

[23] Sean Gavin and George Moschelli. Fluctuation Probes of Early-Time Correlations in Nuclear Collisions. *Phys. Rev.*, C85:014905, 2012.

[24] K. Alpgard et al. UA5 collaboration. First results on complete events from pp collisions at the cm energy of 540 GeV. *Phys. Lett.*, 107B:310, 1981.

[25] K. Alpgard et al. UA5 collaboration. Charged particle multiplicities at the CERN SPS collider. *Phys. Lett.*, 107B:315, 1981.

[26] J. D. Bjorken. Highly Relativistic Nucleus-Nucleus Collisions: The Central Rapidity Region. *Phys. Rev.*, D27:140–151, 1983.

[27] Olga Yu. Barannikova. Probing collision dynamics at RHIC. In *Ultra-relativistic nucleus-nucleus collisions. Proceedings, 17th International Conference, Quark Matter 2004, Oakland, USA, January 11-17, 2004*, 2004.

[28] Fabrice Retiere and Michael Annan Lisa. Observable implications of geometrical and dynamical aspects of freeze out in heavy ion collisions. *Phys. Rev.*, C70:044907, 2004.

[29] Fred Cooper and Graham Frye. Comment on the Single Particle Distribution in the Hydrodynamic and Statistical Thermodynamic Models of Multiparticle Production. *Phys. Rev.*, D10:186, 1974.

[30] Ekkard Schnedermann, Josef Sollfrank, and Ulrich W. Heinz. Thermal phenomenology of hadrons from 200-A/GeV S+S collisions. *Phys. Rev.*, C48:2462–2475, 1993.

[31] Wojciech Broniowski, Anna Baran, and Wojciech Florkowski. Thermal approach to RHIC. *Acta Phys. Polon.*, B33:4235–4258, 2002.

[32] Wojciech Florkowski, Wojciech Broniowski, and Mariusz Michalec. Thermal analysis of particle ratios and p(t) spectra at RHIC. *Acta Phys. Polon.*, B33:761–769, 2002.

[33] George Moschelli. *Two-particle correlations and the ridge in relativistic heavy ion collisions*. PhD thesis, 2010.

[34] C.W. Gardiner. *Handbook of Stochastic Methods for Physics, Chemistry, and the Natural Sciences*. Springer complexity. Springer, 2004.

[35] Guy D. Moore and Derek Teaney. How much do heavy quarks thermalize in a heavy ion collision? *Phys. Rev.*, C71:064904, 2005.

[36] Yukinao Akamatsu. Langevin dynamics and decoherence of heavy quarks at high temperatures. *Phys. Rev.*, C92(4):044911, 2015.

[37] Taesoo Song and Thomas Epelbaum. Heavy quark diffusion from coherent color fields in relativistic heavy-ion collisions. 2015.

[38] Esteban Calzetta. Relativistic fluctuating hydrodynamics. *Class. Quant. Grav.*, 15:653–667, 1998.

[39] J. I. Kapusta, B. Muller, and M. Stephanov. Relativistic Theory of Hydrodynamic Fluctuations with Applications to Heavy Ion Collisions. *Phys. Rev.*, C85:054906, 2012.

[40] Avdhesh Kumar, Jitesh R. Bhatt, and Ananta P. Mishra. Fluctuations in Relativistic Causal Hydrodynamics. *Nucl. Phys.*, A925:199–217, 2014.

[41] Sean Gavin, George Moschelli, and Christopher Zin. Rapidity correlation structure in nuclear collisions. *Phys. Rev. C*, 94:024921, 2016.

[42] P.M. Chaikin and T.C. Lubensky. *Principles of Condensed Matter Physics*. Cambridge University Press, 2000.

[43] E.M. Lifshitz and L.P. Pitaevskiĭ. *Statistical Physics: Theory of the condensed state*. Course of theoretical physics. Pergamon Press, 1980.

[44] Paul Romatschke. New Developments in Relativistic Viscous Hydrodynamics. *Int. J. Mod. Phys.*, E19:1–53, 2010.

[45] C. Young, J. I. Kapusta, C. Gale, S. Jeon, and B. Schenke. Thermally Fluctuating Second-Order Viscous Hydrodynamics and Heavy-Ion Collisions. *Phys. Rev.*, C91(4):044901, 2015.

[46] Sean Gavin and Mohamed Abdel-Aziz. Measuring Shear Viscosity Using Transverse Momentum Correlations in Relativistic Nuclear Collisions. *Phys.Rev.Lett.*, 97:162302, 2006.

[47] D. Teaney, J. Lauret, and E. V. Shuryak. A Hydrodynamic description of heavy ion collisions at the SPS and RHIC. 2001.

[48] G. Baym. Thermal equilibration in ultrarelativistic heavy ion collisions. *Phys. Lett.*, B138:18–22, 1984.

[49] B. Banerjee, R. S. Bhalerao, and V. Ravishankar. Equilibration of the Quark - Gluon Plasma Produced in Relativistic Heavy Ion Collisions. *Phys. Lett.*, B224:16–20, 1989.

[50] Sean Gavin. Partial thermalization in ultrarelativistic heavy ion collisions. *Nucl. Phys.*, B351:561–578, 1991.

[51] H. Heiselberg and Xin-Nian Wang. Expansion, thermalization and entropy production in high-energy nuclear collisions. *Phys. Rev.*, C53:1892–1902, 1996.

[52] S. M. H. Wong. Thermal and chemical equilibration in relativistic heavy ion collisions. *Phys. Rev.*, C54:2588–2599, 1996.

[53] Gouranga C. Nayak and V. Ravishankar. Preequilibrium evolution of nonAbelian plasma. *Phys. Rev.*, D55:6877–6886, 1997.

[54] Miklos Gyulassy, Yang Pang, and Bin Zhang. Transverse energy evolution as a test of parton cascade models. *Nucl. Phys.*, A626:999–1018, 1997.

[55] Gouranga C. Nayak and V. Ravishankar. Preequilibrium evolution of quark - gluon plasma. *Phys. Rev.*, C58:356–364, 1998.

[56] Adrian Dumitru and Miklos Gyulassy. The Transverse energy as a barometer of a saturated plasma. *Nucl. Phys.*, A698:471–474, 2002.

[57] Zhe Xu and Carsten Greiner. Thermalization of gluons in ultrarelativistic heavy ion collisions by including three-body interactions in a parton cascade. *Phys. Rev.*, C71:064901, 2005.

[58] Zhe Xu and Carsten Greiner. Transport rates and momentum isotropization of gluon matter in ultrarelativistic heavy-ion collisions. *Phys. Rev.*, C76:024911, 2007.

[59] Wojciech Florkowski and Radoslaw Ryblewski. Separation of elastic and inelastic processes in the relaxation-time approximation for the collision integral. *Phys. Rev.*, C93(6):064903, 2016.

[60] Yoshitaka Hatta, Mauricio Martinez, and Bo-Wen Xiao. Analytic solutions of the relativistic Boltzmann equation. *Phys. Rev.*, D91(8):085024, 2015.

[61] U. Heinz, D. Bazow, G. S. Denicol, M. Martinez, M. Nopoush, J. Noronha, R. Ryblewski, and M. Strickland. Exact solutions of the Boltzmann equation and optimized hydrodynamic approaches for relativistic heavy-ion collisions. In *Proceedings, 7th International Conference on Hard and Electromagnetic Probes of High-Energy Nuclear Collisions (Hard Probes 2015): Montral, Qubec, Canada, June 29-July 3, 2015*, 2016.

[62] Mohammad Nopoush, Michael Strickland, Radoslaw Ryblewski, Dennis Bazow, Ulrich Heinz, and Mauricio Martinez. Leading-order anisotropic hydrodynamics for central collisions. *Phys. Rev.*, C92(4):044912, 2015.

[63] Ronald Forrest Fox and George E. Uhlenbeck. Contributions to non-equilibrium thermodynamics. i. theory of hydrodynamical fluctuations. *Physics of Fluids*, 13(8):1893–1902, 1970.

[64] Ronald Forrest Fox and George E Uhlenbeck. Contributions to nonequilibrium thermodynamics. ii. fluctuation theory for the boltzmann equation. *Physics of Fluids (1958-1988)*, 13(12):2881–2890, 1970.

[65] Mordechai Bixon and Robert Zwanzig. Boltzmann-langevin equation and hydrodynamic fluctuations. *Phys. Rev.*, 187:267–272, Nov 1969.

[66] F. Reif. *Fundamentals of Statistical and Thermal Physics:*. Waveland Press, 2009.

[67] M. Stone and P. Goldbart. *Mathematics for Physics: A Guided Tour for Graduate Students*. Cambridge University Press, 2009.

[68] C.G. van Weert S.R. deGroot, W.A. van Leeuwen. *Relativistic Kinetic Theory: Principles and Applications*. North-Holland, Amsterdam, 1980.

[69] James W. Dufty, Mirim Lee, and J. Javier Brey. Kinetic model for pair correlations. *Phys. Rev. E*, 51:297–309, Jan 1995.

[70] Esteban Calzetta and B. L. Hu. Stochastic dynamics of correlations in quantum field theory: From Schwinger-Dyson to Boltzmann-Langevin equation. *Phys. Rev.*, D61:025012, 2000.

[71] M. A. Stephanov. Evolution of fluctuations near QCD critical point. *Phys. Rev.*, D81:054012, 2010.

[72] C. Pruneau, S. Gavin, and S. Voloshin. Methods for the study of particle production fluctuations. *Phys. Rev.*, C66:044904, 2002.

[73] S. Jeon and V. Koch. Charged particle ratio fluctuation as a signal for QGP. *Phys. Rev. Lett.*, 85:2076–2079, 2000.

[74] Arthur M. Poskanzer and S. A. Voloshin. Methods for analyzing anisotropic flow in relativistic nuclear collisions. *Phys. Rev.*, C58:1671–1678, 1998.

[75] B. Alver and G. Roland. Collision geometry fluctuations and triangular flow in heavy-ion collisions. *Phys. Rev.*, C81:054905, 2010. [Erratum: Phys. Rev.C82,039903(2010)].

[76] Vardan Khachatryan et al. Charged-particle nuclear modification factors in PbPb and pPb collisions at $\sqrt{s_{\mathrm{N\,N}}} = 5.02$ TeV. *JHEP*, 04:039, 2017.

[77] Sangyong Jeon and Volker Koch. Event by event fluctuations. 2003.

[78] A. Adare et al. Charged hadron multiplicity fluctuations in Au+Au and Cu+Cu collisions from $\sqrt{s_{NN}} = 22.5$ to 200 GeV. *Phys. Rev.*, C78:044902, 2008.

[79] Scott Pratt, Soeren Schlichting, and Sean Gavin. Effects of Momentum Conservation and Flow on Angular Correlations at RHIC. *Phys. Rev.*, C84:024909, 2011.

[80] Sergei A. Voloshin. Multiplicity and mean transverse momentum fluctuations in Au+Au collisions at RHIC. pages 591–596, 2001. [AIP Conf. Proc.610,591(2002)].

[81] Stefan Heckel. Event-by-event mean fluctuations in pp and Pb-Pb collisions measured by the ALICE experiment at the LHC. *J. Phys.*, G38:124095, 2011.

[82] John Adams et al. Minijet deformation and charge-independent angular correlations on momentum subspace (eta, phi) in Au-Au collisions at $\sqrt{s_{NN}}$ = 130-GeV. *Phys. Rev.*, C73:064907, 2006.

[83] John Adams et al. Transverse-momentum p_t correlations on (eta,Phi) from mean-p(t) fluctuations in Au - Au collisions at $\sqrt{s_{NN}}$ = 200-GeV. *J. Phys.*, G32:L37–L48, 2006.

[84] D. Adamova et al. Scale-dependence of transverse momentum correlations in Pb-Au collisions at 158A GeV/c. *Nucl. Phys.*, A811:179–196, 2008.

[85] Stanislaw Mrowczynski. Transverse momentum and energy correlations in the equilibrium system from high-energy nuclear collisions. *Phys. Lett.*, B439:6–11, 1998.

[86] Misha A. Stephanov, K. Rajagopal, and Edward V. Shuryak. Event-by-event fluctuations in heavy ion collisions and the QCD critical point. *Phys. Rev.*, D60:114028, 1999.

[87] Sean Gavin, Larry McLerran, and George Moschelli. Long Range Correlations and the Soft Ridge in Relativistic Nuclear Collisions. *Phys. Rev.*, C79:051902, 2009.

[88] George Moschelli and Sean Gavin. Soft Contribution to the Hard Ridge in Relativistic Nuclear Collisions. *Nucl. Phys.*, A836:43–58, 2010.

[89] Sean Gavin and George Moschelli. Flow Fluctuations from Early-Time Correlations in Nuclear Collisions. *Phys. Rev.*, C86:034902, 2012.

[90] Piotr Bozek and Wojciech Broniowski. Transverse-momentum fluctuations in relativistic heavy-ion collisions from event-by-event viscous hydrodynamics. *Phys. Rev.*, C85:044910, 2012.

[91] Betty Abelev et al. Pseudorapidity density of charged particles in p + Pb collisions at $\sqrt{s_{NN}} = 5.02$ TeV. *Phys. Rev. Lett.*, 110(3):032301, 2013.

[92] B. I. Abelev et al. Systematic Measurements of Identified Particle Spectra in pp, d^+ Au and Au+Au Collisions from STAR. *Phys. Rev.*, C79:034909, 2009.

[93] Jurgen Schukraft. First Results from the ALICE experiment at the LHC. *Nucl. Phys.*, A862-863:78–84, 2011.

[94] Kenneth Aamodt et al. Centrality dependence of the charged-particle multiplicity density at mid-rapidity in Pb-Pb collisions at $\sqrt{s_{NN}} = 2.76$ TeV. *Phys. Rev. Lett.*, 106:032301, 2011.

[95] B. Alver et al. Phobos results on charged particle multiplicity and pseudorapidity distributions in Au+Au, Cu+Cu, d+Au, and p+p collisions at ultra-relativistic energies. *Phys. Rev.*, C83:024913, 2011.

[96] Roberto Preghenella. Transverse momentum distribution of charged particles and identied hadrons in pPb collisions at the LHC with ALICE. *PoS*, EPS-HEP2013:188, 2013.

[97] Radoslaw Ryblewski and Wojciech Florkowski. Equilibration of anisotropic quark-gluon plasma produced by decays of color flux tubes. *Phys. Rev.*, D88:034028, 2013.

[98] Scott Pratt and Clint Young. Relating Measurable Correlations in Heavy Ion Collisions to Bulk Properties of Equilibrated QCD Matter. *Phys. Rev.*, C95(5):054901, 2017.

[99] Shoichiro Tsutsui, Jean-Paul Blaizot, and Yoshitaka Hatta. Thermalization of overpopulated systems in the 2PI formalism. 2017.

[100] Li Yan and Hanna Grönqvist. Hydrodynamical noise and Gubser flow. *JHEP*, 03:121, 2016.

[101] Kenichi Nagai, Ryuichi Kurita, Koichi Murase, and Tetsufumi Hirano. Causal hydrodynamic fluctuation in Bjorken expansion. 2016.

[102] Yukinao Akamatsu, Aleksas Mazeliauskas, and Derek Teaney. A kinetic regime of hydrodynamic fluctuations and long time tails for a Bjorken expansion. 2016.

[103] Mohamed Abdel Aziz and Sean Gavin. Causal diffusion and the survival of charge fluctuations in nuclear collisions. *Phys. Rev.*, C70:034905, 2004.

[104] Stefan Floerchinger and Mauricio Martinez. Fluid dynamic propagation of initial baryon number perturbations on a Bjorken flow background. *Phys. Rev.*, C92(6):064906, 2015.

[105] J. I. Kapusta and C. Young. Causal Baryon Diffusion and Colored Noise for Heavy Ion Collisions. *Nucl. Phys.*, A931:1051–1055, 2014.

[106] J. I. Kapusta and C. Young. Causal Baryon Diffusion and Colored Noise. *Phys. Rev.*, C90(4):044902, 2014.

[107] Bo Ling, Todd Springer, and Mikhail Stephanov. Hydrodynamics of charge fluctuations and balance functions. *Phys. Rev.*, C89(6):064901, 2014.

[108] Masayuki Asakawa and Masakiyo Kitazawa. Fluctuations of conserved charges in relativistic heavy ion collisions: An introduction. 2015.

[109] N.G. Van Kampen. *Stochastic Processes in Physics and Chemistry*. North-Holland Personal Library. Elsevier Science, 2011.

[110] H. Risken and T. Frank. *The Fokker-Planck Equation - Methods of Solution and Applications*. Springer Series in Synergetics. Springer-Verlag, 1996.

[111] J. L. Garcia-Palacios. Introduction to the theory of stochastic processes and Brownian motion problems. 2007.

[112] Z. Brzezniak and T. Zastawniak. *Basic Stochastic Processes*. Springer Undergraduate Mathematic Series. Springer-Verlag, 1999.

ABSTRACT

DYNAMIC FLUCTUATIONS FROM HYDRODYNAMICS AND KINETIC THEORY IN HIGH ENERGY COLLISIONS

by

CHRISTOPHER ZIN

December 2017

Advisor: Dr. Sean Gavin

Major: Physics

Degree: Doctor of Philosophy

It is well accepted that heavy ion collisions can be described using hydrodynamic theory, implying these systems are large enough and long lived enough to reach local equilibrium. Recent measurements of correlations in pA and high multiplicity pp collisions at the Relativistic Heavy Ion Collider and Large Hadron Collider have shown that these systems also exhibit signs of thermalization, unexpected in the smaller, shorter lived systems. Studying this behavior can give insight into the thermalization process and help clarify the relationship between flow in large systems and hydrodynamics. In an effort to understand these measurements we use the Boltzmann equation, in conjunction with a dynamic description of Langevin noise, to study the approach nonequilibrium systems take toward thermalization. We use this equation and its solution to identify observables sensitive to the thermalization process. We also apply Langevin noise to the equations of second-order hydrodynamics in order to derive equations for dynamic two-particle transverse momentum correlations. We demonstrate the use of these equations by computing transport coefficients of the quark-gluon plasma.

AUTOBIOGRAPHICAL STATEMENT

Name: Christopher Zin

Education:
B.S. Mathematics, Wayne State University, Detroit, MI, 2005
M.S. Mathematics, Michigan State University, East Lansing, MI, 2008

Publications:
S. Gavin, G. Moschelli, and C. Zin, *Rapidity Correlation Structure in Nuclear Collisions*. Phys. Rev. C 94, 024921 (2016).
S. Gavin, G. Moschelli, and C. Zin, *Boltzmann-Langevin Approach to Pre-equilibrium Correlations in Nuclear Collisions*. Phys. Rev. C 95 064901 (2017).

Canadian born and American raised, Chris started attending Wayne State University in the fall of 2001. As an undergraduate he struggled to choose between a degree in mathematics and a degree in physics, eventually compromising by first doing one and then the other. After completing a B.S. degree in math at Wayne State University and then an M.S. degree in math at Michigan State University, he returned to Wayne State in an effort to receive his master's in physics. Growing attached to the subject, he decided to push onward, pursuing a PhD in the field. While his time spent at university has been rather long-winded, he notes that the knowledge gained and the people met have made it an invaluable experience.